1. Introduction

Liquid crystals built of banana-shaped molecules are new interesting and original liquid crystals class. Investigations of this group provide us with new interesting results and give a contribution to liquid crystals science. Smectic B phases of banana-shaped systems differ from typical ferroelectric and antiferroelectric smectic phases studied so far. They form new kinds of smectics and two-dimensional phases, so unlike to those obtained for calamitic LCs. These new materials attract our attention because of unexpected electrooptic properties.

The aim of present PhD Thesis was to investigate electrooptic and dielectric properties and conductivity of B phases of banana-shaped homologues nOSOR (n = 9, 12, 14) and a mixture of 12OSOR and MHPSBO9 (in short 12R9AF). nOSOR compounds are built of achiral banana-shaped molecules, however MHPSBO9 is built of chiral calamitic molecules. 9OSOR compound shows banana-shaped ferroelectric B_1 phase, however 12OSOR, 14OSOR and 12R9AF mixture show antiferroelectric B_2 phase. All materials studied were synthesized by Mrs. Dr. hab. Mirosława Ossowska-Chruściel from Institute of Chemistry, University of Podlasie.

To determine temperatures, enthalpy and entropy changes of phase transitions differential scanning calorimetry (DSC) was used (section 3.2.). To identify phases polarization microscopy was used described in section 3.1.1.

Spontaneous polarization versus temperature measurements were performed using reversal current method (section 3.1.3.). Using this method, polarization dependence on electric field was also investigated.

In present dissertation dielectric relaxation processes and ionic conductivity were measured in frequency range from 40 Hz to 10 MHz for B_1 and B_2 phases. Dielectric investigations were performed using Frequency Domain Dielectric Spectroscopy method (in short FDDS) (section 3.4.).

All measurements were done in New Materials Engineering Department, Institute of Physics, Jagiellonian University in Cracow.

2. Theory

2.1. Basic Information About Banana-Shaped Liquid Crystals

For a long time polar ordering was associated with chiral symmetry breaking [1]. In 1996 Niori and his co-workers found ferroelectric switching of polar smectic phase for a compound built of banana-shaped achiral molecules. Dipolar ordering was a result of rotational restrictions due to steric interactions between the molecules. Polar order phenomena and chiral properties of B phases allow one to observe ferro- or antiferroelectric behavior as well as electroopitc switching despite the lack of chirality of the molecules [2, 3, 4].

Liquid crystals built of banana-shaped molecules are very good materials to apply in large flat displays for computers and color TV's – they characterize with fast antiferroelectric switching. Thin liquid crystal layers having banana-shaped molecules in tilted smectic layer show electrooptic switching after applying electric voltage without earlier polarization and without highlight, the order of magnitude of switching time is 100 microseconds. One of the promising features to apply these materials is their non-linear optical response, they are the most efficient liquid crystal materials to non-linear optic application. Large spontaneous polarization made them interesting as ferroelectrics and pyro- and piezoelectric materials. Displays built of banana-shaped liquid crystals has better angle of view and what is more important, they are energy-saving.

In 1997 the first conference devoted to these phases took place in Berlin. During this conference different structures of them were named from B_1 to B_7.

The B_1 phase structure is a fluid-like smectic giving a mosaic texture. This phase has been observed in higher temperatures than B_2 phase, but lower than B_6 phase [5].

Also the B_2 phase is a fluid smectic like. This phase shows usually antiferroelectric switching behavior and its texture can be focal-conic-like, but also fan-like [5].

The B_3 phase is a higher ordered smectic or soft crystal phase and usually is observed below the B_2 phase but its nature and structure is not quite known yet [5].

The B_4 phase belongs to soft crystal phases and it is observed below B_2 and B_3 phase. Its texture has characteristic features - weak birefringence and intensive blue color. The B_4 phase different domains show optical activity of opposite sign [5]. The most seldom observed B phase is B_5 phase appearing below B_2 phase and is very difficult to recognize because the

changes in texture are very subtle. The electrooptic behavior of this phase is analogous to that of B_2 phase, but the viscosity is higher for B_5 phase [5].

The B_6 phase is an intercalated tilted smectic phase. The intercalation can be a result of core-chain interaction smaller than for B_1 phase but with larger entropy [6]. The B_6 phase does not have any order in-plane and exhibits a fan-shaped texture [5].

The B_7 phase is very easy to identify because of its complex texture, it forms a helical superstructure. Its spiral and double spiral lancets can be left- or right-handed. The steric packing of the molecules causes a polar order in smectic layer. The B_7 phase has the ability to switch just like the B_2 phase, but at larger electric field applied [5].

The B phases are formed when the bending angle between molecule branches is 120 – 130°. For this phases there are three independent order parameters: density modulation, tilt angle and layer polarization. These phases show at least one-dimensional positional order. Rotational restriction of banana-shaped molecules results from the long range order of their transverse axes and in consequence – the dipole moments (Fig. 2.1) [7, 8]. Ferro- or antiferroelectric switching show B_2 and B_5 phases and also two-dimensional B_7 phases.

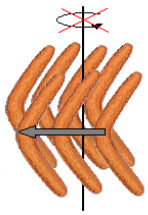

Fig. 2.1. Rotational restriction around the long molecular axis

2.2. Structure and Properties of B_1 and B_2 Phase

The structure of B_1 phase is shown in Fig. 2.2. The rectangular lattice is described by two parameters: **a** - describes the in-plane periodicity of the modulated phase and **c** - corresponds to the layer thickness. Side chains of the molecule in one layer overlap the cores of molecules in neighboring layers. The structure is stabilized by the core-core attraction and the core-chain segregation at these interfaces [7, 9].

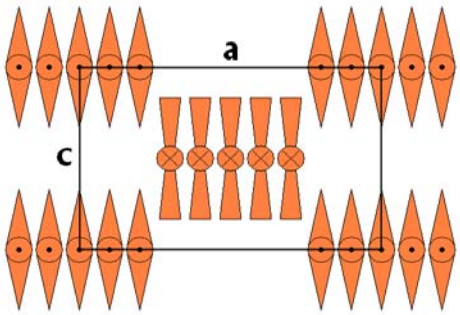

Fig. 2.2. Alignment of molecules in B_1 phase

The most intensively investigated is B_2 phase, in which the molecular long axes is tilted with respect to the layer normal.

The most attractive aspect of tilted smectic phases built of bent-core molecules is their mezoscopic chirality of the layer despite the lack of chiral centers of molecules [2, 3]. This is connected with polar packaging of molecules and the tilt of optical axis $\vec{n}$ with respect to the smectic layer normal. These layers are biaxial and acquire second optical axis parallel to the smectic layer to describe their electrooptic and dielectric properties. Molecular reorientation of bent-core molecules in the B_2 phase is strongly restricted due to high molecule packaging density in the smectic layer. Thanks to this, the order parameter is almost temperature independent, which stands for good stability of these phases, unlike liquid crystals built of rod-like and discotic molecules [10, 11].

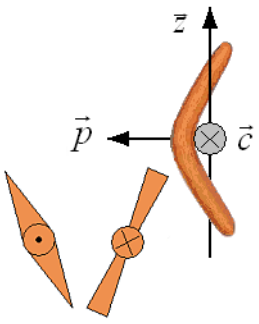 (a)	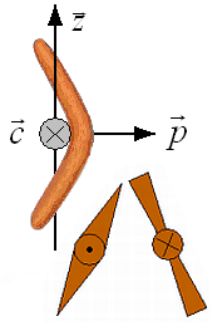 (b)
$(\hat{z},\hat{c},\hat{p})$ $\vec{z}\times\vec{c}=\vec{p}$	$(\hat{c},\hat{z},\hat{p})$ $\vec{c}\times\vec{z}=-\vec{p}$

Fig. 2.3. (a) and (b) Coordinate systems and structures built on them

In order to describe the orientation of banana-shaped molecule in a single smectic layer of B_2 phase three unit vectors are introduced: normal to the layer (***z***), polarization vector (***p***) and projection of the ***n*** director on the smectic layer (***c***). In tilted smectics these vectors can form two coordinate systems: $(\hat{z},\hat{c},\hat{p})$ or $(\hat{c},\hat{z},\hat{p})$ – right- or left-handed, respectively. Smectic structures [8] built on them bear opposite chiralities (Fig. 2.3.(a) and (b)).

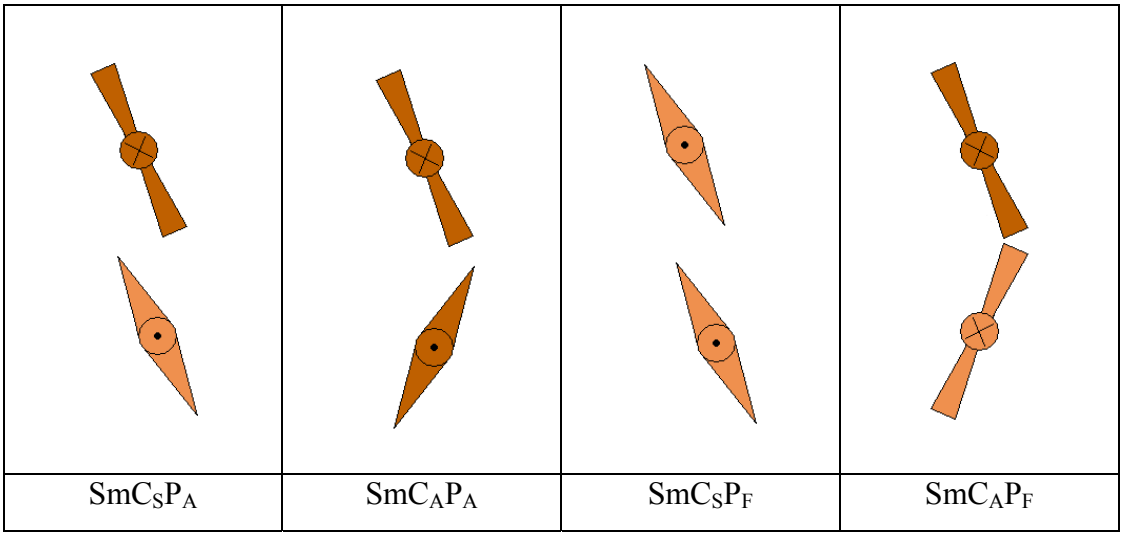

Fig. 2.4. Theoretically predicted structures of B_2 phase

These chiral layers can be arranged in different ways. The B_2 phase can have four possible structures (Fig. 2.4.) from the left: synclinic – antiferroelectric, antyclinic – antiferroelectric, synclinic – ferroelectric and antyclinic – ferroelectric [12]. Two antiferroelectric states usually appear as ground state and two ferroelectric states can be obtained by applying an external electric field [13]. Different types of B_2 phases can be distinguished by using complimentary methods: texture observation, electrooptic response and X-ray diffraction.

2.3. The Switching Mechanism in Anticlinic - Antiferroelectric B_2 Phase (SmC_AP_A)

As it was mentioned before, polar order phenomena and chiral properties of B phases allow one to observe ferro- or antiferroelectric behavior as well as electroopitc switching despite the lack of chirality of the molecules [2, 3]. In banana-shaped liquid crystals there is no correlations between the direction of the tilt and the direction of the polarization in difference to ordinary chiral ferroelectric SmC and chiral antiferroelectric SmC_A.

The switching process of SmC_AP_A phase is tristable because there are three distinct states: SmC_SP_F, SmC_AP_A and SmC_SP_F. This switching process between antiferro- and ferroelectric states occurs by fast rotation of molecules around a tilt cone (Fig. 2.5. (a)), during rotation polar direction reverses as well as tilt direction.

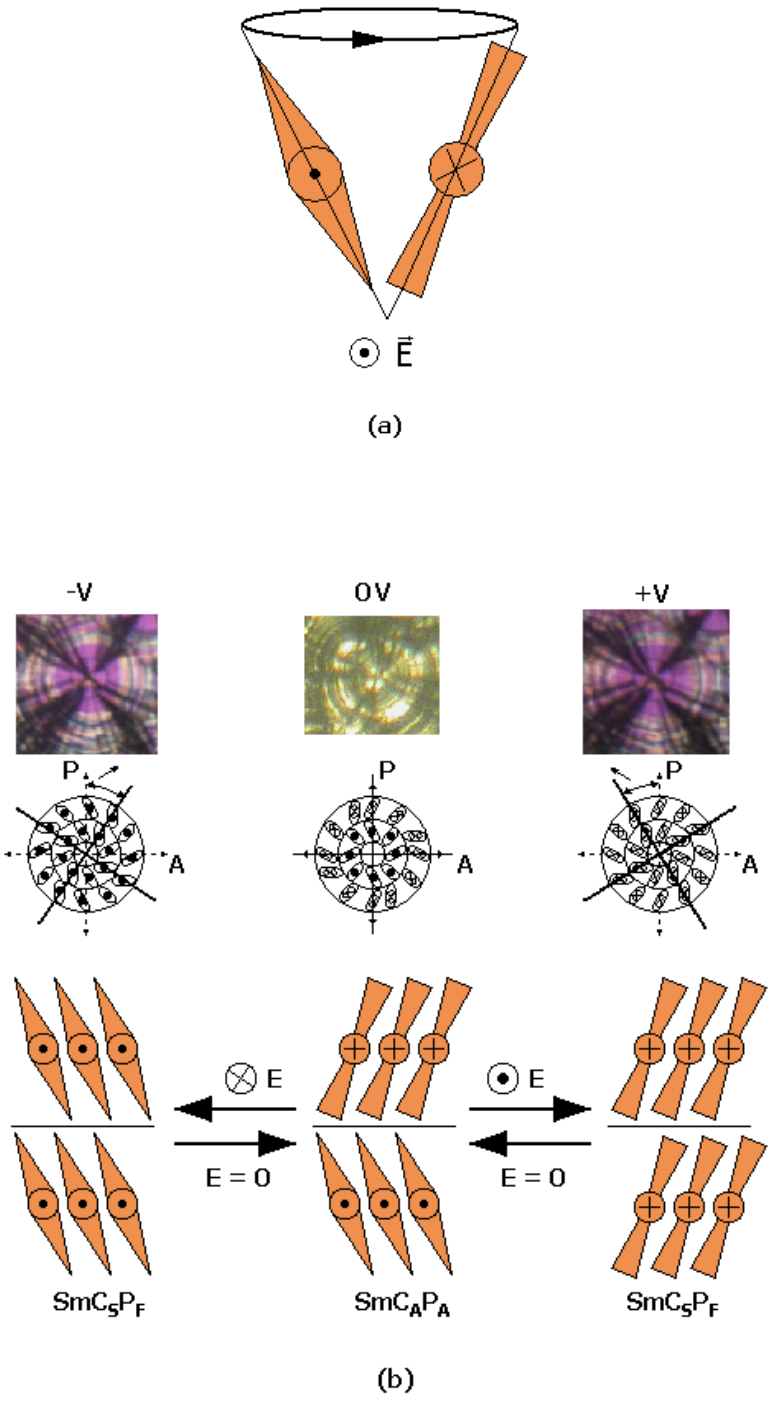

Fig.2.5. (a) Rotation of molecules around a tilt cone and **(b)** tristable switching process of SmC_AP_A phase

Change of the tilt direction can be seen by the rotation of the dark extinction brushes occurring in circular domains. In this domains the molecules lay predominantly parallel to the surfaces and the layers are rolled up (see Fig. 2.5. (b)). The dark brushes occur due to the tilt of the molecules and are parallel and perpendicular to the molecular long axes. In SmC_AP_A state (when $E = 0$) the average optical axes is parallel to polarizers that is why the dark brushes occur parallel to the direction of the polarizers [14].

2.4. Dielectric Relaxation

External electric field applied to the dielectric material causes slow increase of its orientational polarization to a specific value, the removal of this electric field leads to disappearance of orientation but it is not sudden effect, it is very slow. The phenomena of slow increasing and disappearance of polarization is called a dielectric relaxation. The speed of polarization disappearance is characterized by a relaxation function [15, 16]:

$$\phi(t) = \phi_0 exp\left(-\frac{t}{\tau}\right), \tag{2.1}$$

where τ constant is the dielectric relaxation time correlated with critical frequency: $\tau = \frac{1}{2\pi f_C}$.
Complex electric permittivity for dielectric material has a form [16]:

$$\varepsilon^*(\omega) = \varepsilon'(\omega) - i\varepsilon''(\omega), \tag{2.2}$$

where: $\varepsilon'(\omega)$ is dispersion and $\varepsilon''(\omega)$ is absorption.
The dielectric spectrum can be presented by the Debye'a – Pellat equation [15]:

$$\varepsilon^*(\omega) = \varepsilon(\infty) + \frac{\varepsilon(0)-\varepsilon(\infty)}{1+i\omega\tau}, \tag{2.3}$$

One can split this equation to real and imaginary part and get an expression of dispersion and absorption [16]:

$$\frac{\varepsilon'-\varepsilon(\infty)}{\varepsilon(0)-\varepsilon(\infty)}=\frac{1}{1+(\omega\tau)^2},$$

$$\frac{\varepsilon''}{\varepsilon(0)-\varepsilon(\infty)}=\frac{\omega\tau}{1+(\omega\tau)^2}. \tag{2.4}$$

When: $\omega \to 0$: $\varepsilon'(0)=\varepsilon(0)$, $\varepsilon''(0)=0$, $\omega \to \infty$: $\varepsilon'(0)=\varepsilon(\infty)$, $\varepsilon''(0)=0$. The difference: $\varepsilon(0)-\varepsilon(\infty)=\Delta\varepsilon$ is called a dielectric increment. Theoretical dispersion and absorption curves are presented in Fig. 2.6. From these curves one can determine a critical frequency [15].

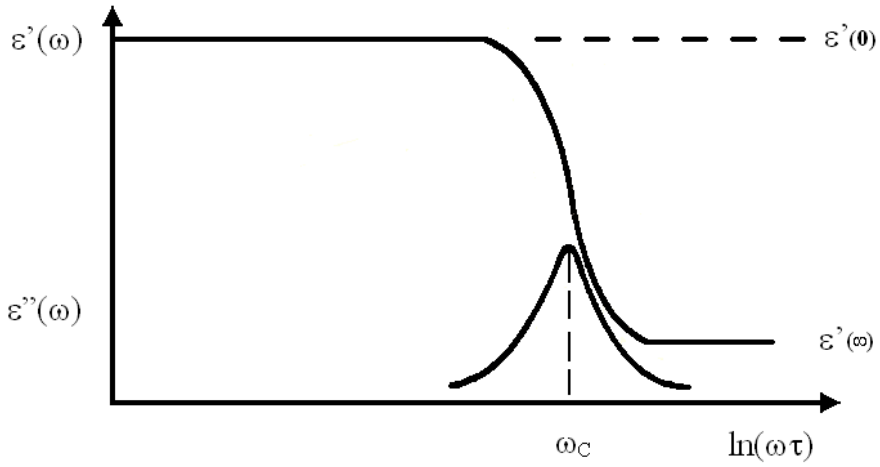

Fig. 2.6. Theoretical dispersion and absorption curves [17]

To describe the relaxation processes of liquid crystals more general form of 2.3 function is used [15]:

$$\varepsilon^*(\nu)=\varepsilon(\infty)+\frac{\varepsilon(0)-\varepsilon(\infty)}{1+(i2\pi\nu\tau_0)^{1-\alpha}}, \tag{2.5}$$

where $\varepsilon(\infty)$ is a high frequency electric permittivity, $\varepsilon(0)$ – static electric permittivity, τ – relaxation time, α – distribution parameter of relaxation times ($0 \le \alpha \le 1$), ν is a frequency. This function is called Cole – Cole function. Theoretical Cole – Cole graph for pure Debye process ($\alpha = 0$) is presented in Fig. 2.7.

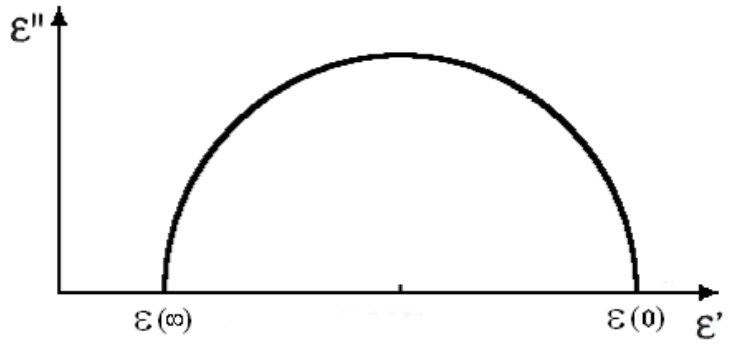

Fig. 2.7. Cole – Cole graph for $\alpha = 0$. Debye type relaxation [17]

When $\alpha \neq 0$ the relaxation process is not Debye type and the shape of Cole – Cole graph is not a semicircle but a circle arc centre of which lies below the ε' axis [16] (Fig. 2.8.).

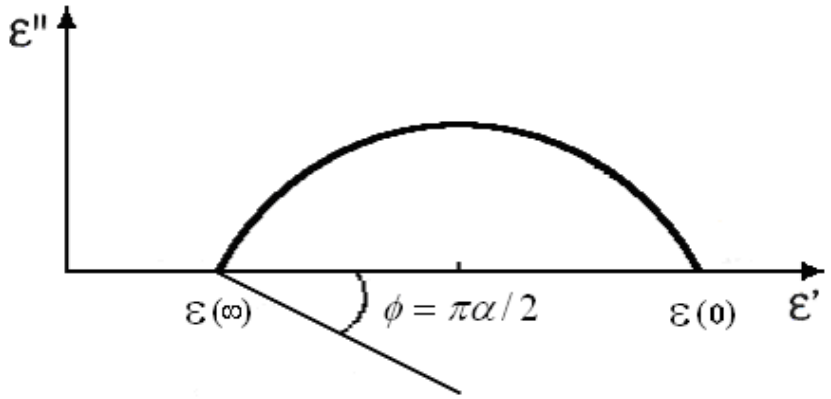

Fig. 2.8. Cole – Cole graph for $\alpha \neq 0$. Complex relaxation process [17]

For banana-shaped liquid crystals at low frequencies the dispersion behaves rather unusual – it is linear on the logarithmic scale for the investigated compound there is an electrode polarization contribution to the dielectric permittivity. For the dielectric loss however, at low frequencies there is the electrical ionic conductivity contribution. The best fitting function occurred to be a Cole – Cole function with extra parameters [13, 18]:

$$\varepsilon^*(\nu) = \varepsilon(\infty) + \frac{\varepsilon(0)-\varepsilon(\infty)}{1+(i2\pi\nu\tau)^{1-\alpha}} - \frac{iA}{\epsilon_0 \nu^M} + \frac{B}{\nu^N}, \tag{2.6}$$

where $\varepsilon(\infty)$ is a high frequency electric permittivity, ϵ_0 – electric permittivity of the free space, $\varepsilon(0)$ – static electric permittivity, τ – relaxation time, α – distribution parameter of

relaxation times ($0 \leq \alpha \leq 1$), $\sigma(\nu)$ – ionic conductivity, ν is a frequency and A, B, M, N – phenomenological fitting parameters, where $A = \frac{\sigma(\nu)}{(2\pi)^M}$.

3. Experimental Methods

In present PhD Thesis to determine phase diagrams for investigated materials, Differential Scanning Calorimetry was used. Polarization microscopy allowed to identify these phases. To measure spontaneous polarization reversal current method was used. Dielectric measurements with FDDS method were also performed.

3.1. Electrooptic Methods in Investigating Liquid Crystals

3.1.1. Polarization microscopy

Birefringence or double refraction is a feature of liquid crystals that allows investigating them by polarization microscopy. Double refraction is a phenomenon of the splitting of a ray of light into two rays when it passes through certain types of materials – the ordinary ray and the extraordinary ray. This effect can occur only if the structure of the material is anisotropic and liquid crystals fulfill this condition. The birefringence magnitude is: $\Delta n = n_e - n_o$, where n_e is the extraordinary ray and n_o is the ordinary ray.

To electrooptic measurements and texture observations Nikon Eclipse Polarizing Microscope LV100POL and INSTEC temperature controller were used. Texture observations and studies of electrooptic switching between the planar and homeotropic textures for 12OSOR were done at LEMCEL using Olympus Polarizing Microscope BX60 and LINCAM temperature controller. Both microscopes have accessory allowing doing pictures. The principle of operation of polarizing microscope and a picture of Nikon Eclipse Polarizing Microscope are presented in fig. 3.1. Polarizer and analyzer in polarizing microscope are identical polarizers giving linearly polarized light. Polarizer and analyzer are crossed; their polarization planes form an angle of 90 degrees. If there is no substance showing double refraction between polarizer and analyzer the image observed will be black because the ray of light will not get to the eyepiece, it will be extinguished. Otherwise, if we put birefringence substance between polarizers we will see brightening of the image (Fig. 3.1.).

The image of observed liquid crystal under polarizing microscope is called the texture. It arises due to interaction between the polarized light and liquid crystal order [19]. An appearance of the texture is influenced by a few factors like: quality of the surface of glass plates, which delimit liquid crystal, defects appearing in the liquid crystal structure, and also

the influence of electric and magnetic fields, temperature gradients and the mechanical stresses.

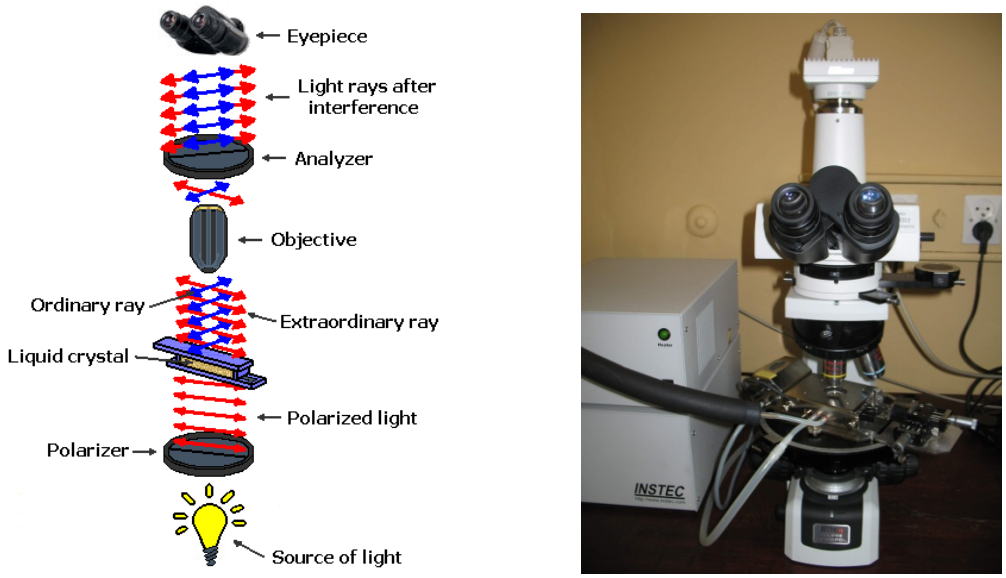

Fig. 3.1. The principle of operation of polarization microscopy [20] and a picture of Nikon Eclipse Polarizing Microscope

These factors cause local changes of ϕ angle and also birefringence, what leads to changes in the texture. Intensity of the light going through the liquid crystal layer can be introduced by Fresnel equation [21]:

$$I(\lambda) = I_0 sin^2(2\phi) sin^2(\frac{\pi d \Delta n}{\lambda}), \tag{3.1}$$

where: I_0 – intensity of the polarized light entering the liquid crystal,

ϕ – the angle between the director and the polarization plane of the polarizer,

d – the sample thickness,

Δn – optical anisotropy ($\Delta n = n_e - n_o$),

λ – the wavelength of light passing through.

For every liquid crystal phase there are characteristic textures. Texture observations during temperature changes allow determining phase diagram and identifying single phases comparing observed images with adequate texture models. Sometimes it can be difficult because not always observed image is identical with the model.

3.1.2. Electrooptic measurements

To observe textures of liquid crystals it can be put on a glass plate, but then we will have thick layer with not known thickness. It is more convenient to put the liquid crystal into the electrooptic cell, which allows observing thin layer of liquid crystal with constant thickness as a function of temperature and electric field. Electrooptic cell is built of two glass plates with properly prepared surfaces, plates are separated by spacers and glued together so that the cell and what comes next – liquid crystal – has strictly fixed thickness (from few to few dozen micrometers). To the inner surfaces of glass plates electrodes with indium – tin oxide (ITO) are put. ITO is light transparent. This type of electrooptic cells are called in short ITO cells. Electric wires are stacked to the electrodes by silver paste. Scheme of this kind of electrooptic cell is presented in Fig. 3.2.

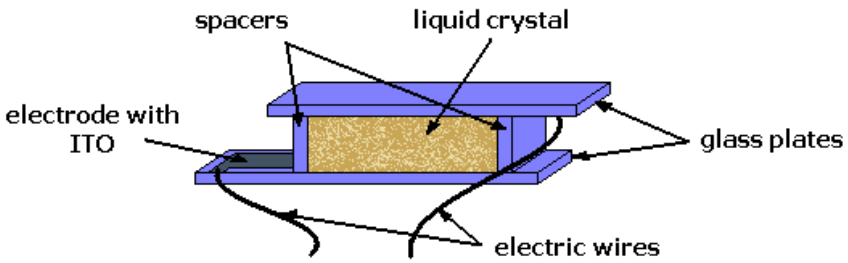

Fig. 3.2. Electrooptic cell

Liquid crystal is put into the electrooptic cell by means of capillary effect. To do this the electrooptic cell has to be heated to the temperature of isotropic phase of the substance investigated. Small amount of the sample is put near capillary slot between the glass plates, after heating to the clarification point temperature the sample fills entire cell due to capillary effect [17]. Electrooptic cells allow controlling order of samples putted into them by polymer layer placed on electrodes surfaces. This properly prepared polymer layer makes easier to orientate long molecule axes parallel to this layer [21].

In present dissertation electrooptic measurements were done using HG electrooptic cells (giving homogeneous orientation) with ITO electrodes made by AWAT Company. Dielectric measurements were done also using HG electrooptic cells made by AWAT Company but with gold electrodes.

Texture observations and electrooptic measurements were done using Nikon Eclipse Polarizing Microscope LV100POL. Electrooptic cell was put in heating accessory controlled

by INSTEC temperature controller. To observe textures in electrooptic field high voltage was put to the electrooptic cell from Agilent 33120A wave form generator amplified by F20A amplifier.

3.1.3. Spontaneous polarization measurements by reversal current method

Reversal current method is also known as triangular wave method. The measurements of spontaneous polarization were done using Agilent 33120A wave form generator and F20A amplifier. Both the driving voltage and the response current spectra of the samples were recorded on the Agilent DSO6102A digital scope and transferred by LAN connection to the computer. Temperature of the sample was controlled by means of INSTEC hot stage driven by the computer. Scheme of measurement equipment is presented in Fig. 3.3. [17].

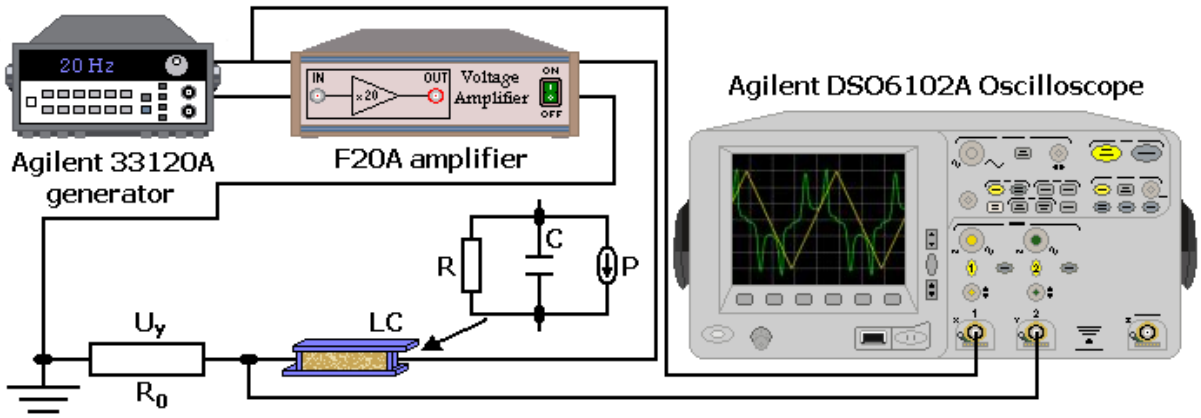

Fig. 3.3. Scheme of spontaneous polarization measurements equipment

Electrooptic cell with liquid crystal is connected with model resistor R_0 by series connection. Measuring voltage drop on R_0 resistor one can determine response current $I(t)$ flowing through the sample. Electrooptic cell with liquid crystal can be treated as parallel connection of resistor R, capacity C and current source P, then response current of the sample consist of three contributions [22]:

$$I(t) = I_R(t) + I_C(t) + I_P(t) = \frac{U(t)}{R} + C\frac{dU(t)}{dt} + \frac{dQ_P(t)}{dt}, \qquad (3.2)$$

where: $I_R(t)$ – ionic flow current,

$I_C(t)$ – charging capacitor current,

$I_P(t)$ – polarization reorientation current,

$Q_P(t)$ – electric charge quantity, induced by reorientation of macroscopic polarization of the sample.

If one take $I_P(t)$ contribution from total signal than it will be possible to calculate spontaneous polarization by integrating area under the peak. Spontaneous polarization is connected with area under the peak [23, 24]:

$$P_S = \frac{A}{2RS}, \tag{3.3}$$

where: A – area under the current peak ($A = \int_a^b \frac{U_y(t)}{R_0} dt$),

R – resistance,

S – area of electrodes of measuring cell.

Exemplary response of the sample on the electric voltage with triangular wave shape is presented in Fig. 3.4.

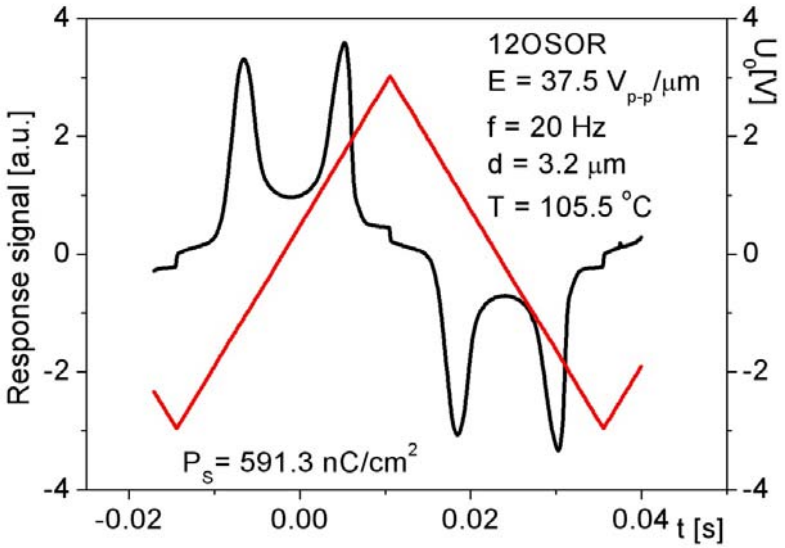

Fig. 3.4. Triangular driving voltage (right-hand side scale) applied and reversal current spectrum (left-hand side scale) for antiferroelectric B_2 phase in 12OSOR

3.2. DSC Scanning Calorimetry

Thermal properties of investigated materials have been studied by Pyris1 DSC scanning calorimeter made by Perkin Elmer Company. Transition temperatures, enthalpies and entropies of the transitions have been computed based on DSC heating and cooling runs. Calorimeter head chart is presented in Fig. 3.5 [25]:

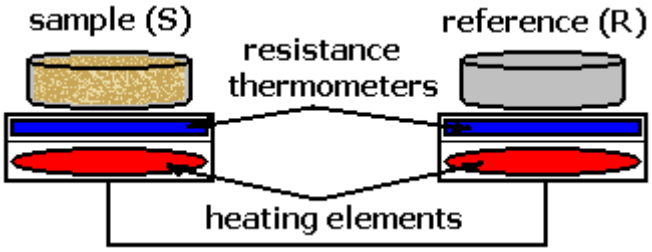

Fig. 3.5. Calorimeter head chart

The calorimeter is composed of two identical heating systems equipped with platinum resistance thermometer and heater. The container on the left – hand side contains an aluminum vessel filled with investigated sample (S), the right – hand side however contains empty aluminum vessel named the reference sample (R). Both containers are heated by their individual heater and kept in the same temperature during entire scanning. Heat capacity versus temperature for the investigated sample is different than for the reference sample, and then heating power supplied to both heaters is different. Now the DSC curve – the difference in power ΔP versus temperature can be plotted. Until the phase transition occurs in the investigated sample (S) there is no difference in power taken by this sample and by the reference sample (R). When the phase transition occurs, the power taken by the investigated sample will be different from the power taken by the reference sample. This difference in power supplied to both heaters is registered by the computer. In endothermic process the heat is taken by the sample (S) so it is heated stronger than the reference sample (R): $\Delta T = T_S - T_R < 0$, in exothermic process the sample (S) is giving back the heat thus it is less heated than the reference sample (R): $\Delta T = T_S - T_R > 0$. The reference sample is assorted so it does not show any phase transition, in the vicinity of the phase transition of the investigated sample the difference in power shows as an anomaly of the curve – as maximum in endothermic processes and as minimum in exothermic processes [15, 25]. The Exemplary DSC curve is presented in Fig. 3.6.

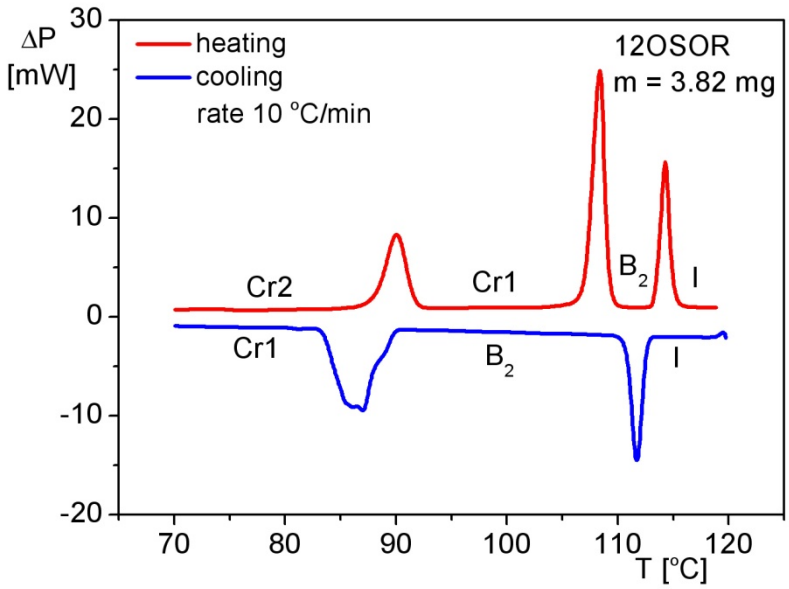

Fig. 3.6. DSC results obtained for 12OSOR compound on cooling and heating by using Pyris1 DSC scanning calorimeter

Using this method one can obtain the transition temperatures, enthalpies and entropies of the transitions but it is not possible to determine the kind of the phase transition because anomalies look the same for phase transitions of the first kind as well as for the second kind. Also it is not possible to specify what kind of phases one is dealing with, that is why the electrooptic measurements are important.

3.3. Dielectric Spectroscopy, FDDS Method

Every ordering gives a restriction of the dynamics and dielectric methods allow to see it. FDDS method (Frequency Domain Dielectric Spectroscopy) consists in measuring complex dielectric permittivity in frequency domain applying various kinds of impedance analyzers [16].

Dielectric studies have been performed by using a dielectric spectrometer based on Agilent 4294A impedance analyzer controlled by PC. The sample was put into the capacitor consisting of two glass plates covered with gold layer separated by 5 μm mica spacers (AWAT HG cells). The cell was calibrated by using standard liquids. The substances being in isotropic phase were introduced into cells by means of capillary effect. This electrooptic cell

filled with liquid crystal is put between two metal plates and placed into metal heating block (see Fig. 3.7).

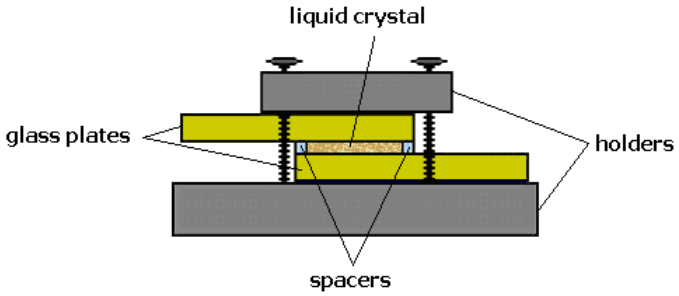

Fig. 3.7. Dielectric measurement cell with gold electrodes put between metal plates [17, 21]

This metal heating block is connected with temperature regulator Euroterm 2604 which allows to change the temperature of liquid crystal. The scheme of measurements equipment is presented in Fig. 3.8. Thermocouple and 197A multimeter made by Keithley Company are used to measure the temperature inside the sample.

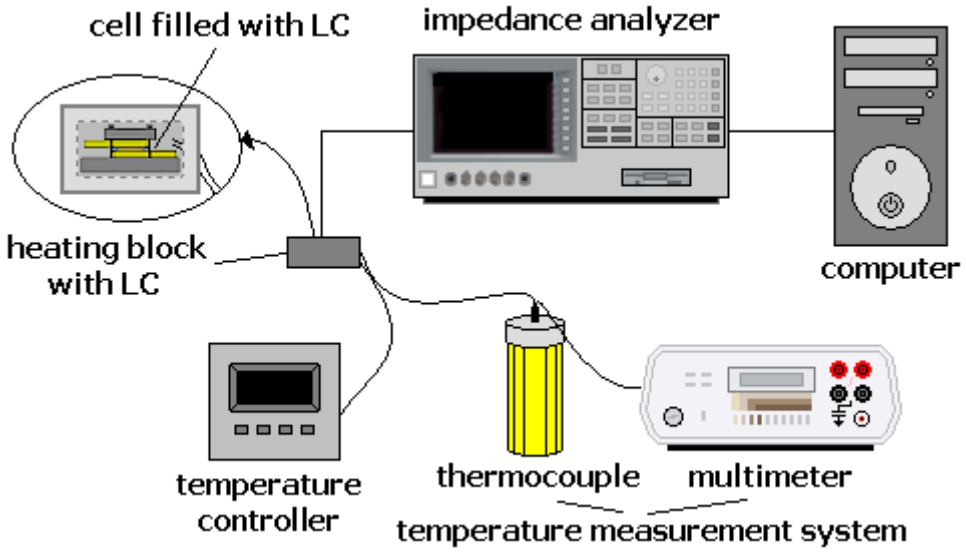

Fig. 3.8. Scheme of dielectric spectrometer [17]

Complex dielectric permittivity measurements can be done for two orientations of the molecules in electrooptic cell: homeotropic – when the transverse optical axes of molecules is parallel to the measuring electric field $\overrightarrow{E_m}$ and planar – when the optical axes of molecules is perpendicular to the measuring electric field. In the first case parallel component of complex dielectric permittivity is measured $\varepsilon_{\parallel}^{*}$ and in second case – perpendicular component is

measured $\varepsilon_{\perp}^{*}$ [23]. The B_2 is a biaxial phase having the dielectric permittivity tensor of the form:

$$\varepsilon^{*}(\nu) = \begin{pmatrix} \varepsilon_{\perp 1}^{*}(\nu) & 0 & 0 \\ 0 & \varepsilon_{\perp 2}^{*}(\nu) & 0 \\ 0 & 0 & \varepsilon_{\parallel}^{*}(\nu) \end{pmatrix}, \tag{3.4}$$

In this study it was possible to measure two principal components of this tensor, namely $\varepsilon_{\perp 1}^{*}(\nu)$ and $\varepsilon_{\perp 2}^{*}(\nu)$.

Exemplary dielectric spectrum of B_2 phase and Cole – Cole plot of dielectric spectrum received by FDDS method is presented in Fig. 3.9. (a) and (b).

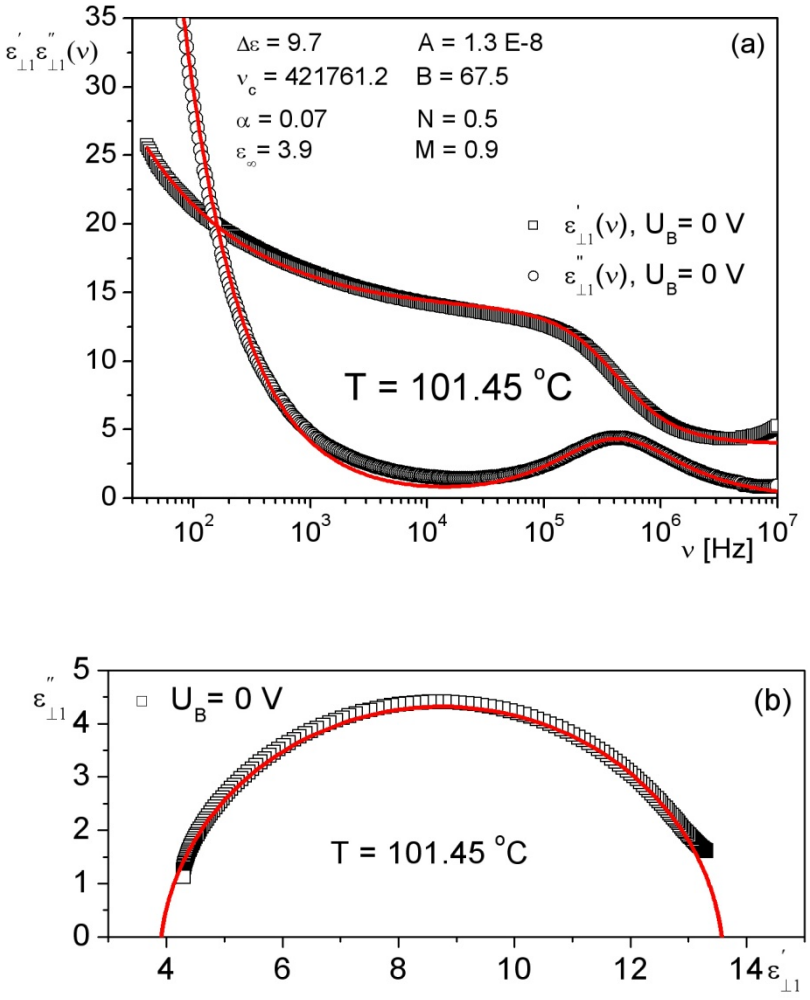

Fig. 3.9. (a) Exemplary dielectric spectrum of B_2 phase and (b) Cole – Cole plot of dielectric spectrum

The following complex function was fit to the experimental points measured without bias field:

$$\varepsilon^*(\nu) = \varepsilon(\infty) + \frac{\varepsilon(0)-\varepsilon(\infty)}{1+(i2\pi\nu\tau)^{1-\alpha}} - \frac{iA}{\epsilon_0 \nu^M} + \frac{B}{\nu^N}, \tag{3.5}$$

where $\varepsilon(\infty)$ is a high frequency electric permittivity, ϵ_0 – electric permittivity of the free space, $\varepsilon(0)$ – static electric permittivity, τ – relaxation time, α – distribution parameter of relaxation times ($0 \leq \alpha \leq 1$), $\sigma(\nu)$ – ionic conductivity, ν is a frequency and A, B, M, N – phenomenological fitting parameters, where $A = \frac{\sigma(\nu)}{(2\pi)^M}$. Solid lines in Fig. 3.9. (a) and (b) are theoretical fit curves of Eq. (3.5) to the experimental points.

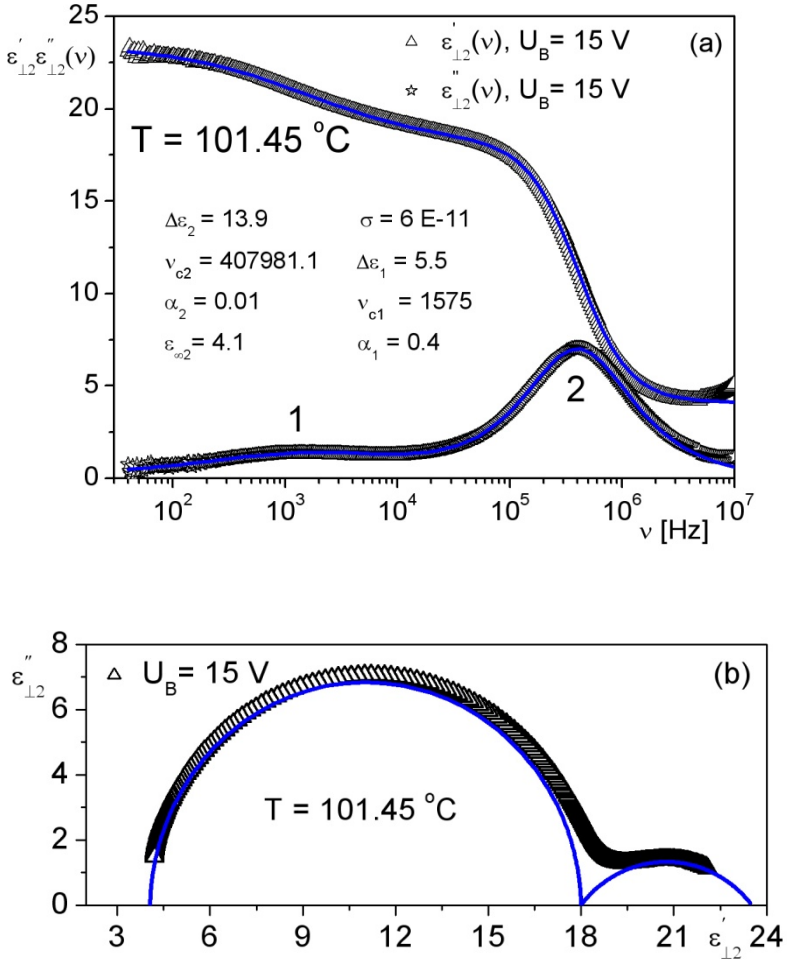

Fig. 3.10. (a) Exemplary dielectric spectrum of B_2 phase and (b) Cole – Cole plot of dielectric spectrum with bias voltage U_B = 15 V

To the experimental points obtained under the bias field Fig. 3.10. (a) and (b) the following complex fitting function was used:

$$\varepsilon^*(\nu) = \varepsilon(\infty) + \frac{\varepsilon_1(0)-\varepsilon(\infty)}{1+(i2\pi\nu\tau_1)^{1-\alpha_1}} + \frac{\varepsilon(0)-\varepsilon_1(0)}{1+(i2\pi\nu\tau_2)^{1-\alpha_2}}, \quad (3.6)$$

where $\varepsilon(\infty)$ is a high frequency electric permittivity, ϵ_0 – electric permittivity of the free space, $\varepsilon(0)$ – static electric permittivity, $\varepsilon_1(0)$ – quasi-static electric permittivity, τ_1 and τ_2- are relaxation times, α_1 and α_2 – distribution parameters of relaxation times ($0 \leq \alpha_i \leq 1$) and ν is a frequency.

The dielectric spectra were acquired in the frequency range from 40 Hz to 10 MHz. The dielectric spectra acquired incorporate about 80 points pear decade.

4. Experimental Results and Discussion

4.1. Investigated Materials – Molecular Structure and Phase Diagrams

Like it was mentioned ealier, in present dissertation the measurements were done for B phases of three banana-shaped homologues nOSOR (n = 9, 12, 14) and a mixture of 12OSOR and MHPSBO9 (in short 12R9AF).

nOSOR compounds are built of achiral banana-shaped molecules. The core of nOSOR molecule consists of five phenyl rings interconnected by either ester or thiobenzoate groups as illustrated in Fig. 4.1. [9]. The alkoxy $OC_{12}H_{25}$ end chains play an important role in smectic polymorphism. nOSOR molecules are polar having effective dipole moment ($\vec{\mu}$) along the symmetry axis.

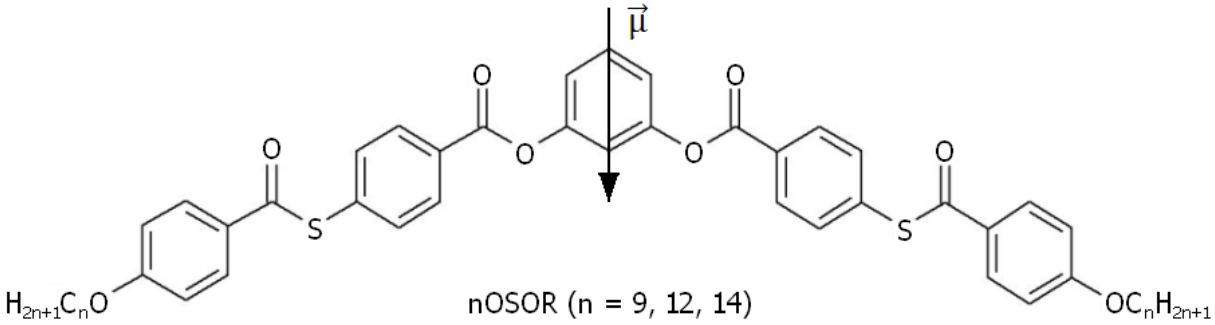

Fig. 4.1. Molecular structure of nOSOR compounds

9OSOR compound shows banana-shaped ferroelectric B_1 phase, however 12OSOR, 14OSOR and 12R9AF mixture show antiferroelectric B_2 phase. Names and phase diagrams of individual nOSOR compounds are shown below.

1. 9OSOR

1,3-phenylene bis{4-[(4-nonyloxybenzoyl)sulfanyl]benzoate

Heating: Cr 103.4 [°C] → X 112.5 [°C] → B_1 123 [°C] → I

Cooling: I 123.4 [°C] → B_1 82.6 [°C] → Cr

2. 12OSOR

1,3-phenylene bis{4-[(4-dodecyloxybenzoyl)sulfanyl]benzoate

Heating: Cr2 88.9 [°C] → Cr1 107.1 [°C] → B_2 113.4 [°C] → I

Cooling: I 112.6 [°C] → B_2 88.6 [°C] → Cr1

3. 14OSOR

1,3-phenylene bis{4-[(4-tetradecyloxybenzoyl)sulfanyl]benzoate

Heating: Cr 102.3 °C → X 104.8 °C → B_2 114.5 °C → I

Cooling: I 114.6 °C → B_2 87.2 °C → Cr

12R9AF is a mixture of 12OSOR and MHPSBO9. MHPSBO9 is built of chiral calamitic molecules (see Fig. 4.2.).

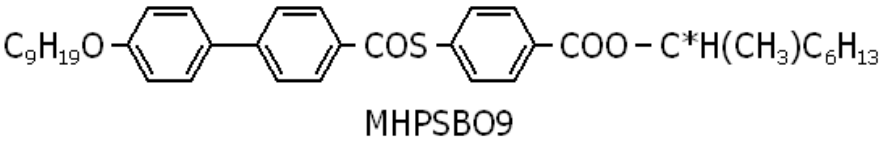

MHPSBO9

Fig. 4.2. Molecular structure of MHPSBO9

Phase diagram of 12R9AF:

Heating: Cr2 91 °C → Cr1 106.1 °C → B_2 109.8 °C → I

Cooling: I 105.6 °C → B_2 82.5 °C → Cr1

4.2. Phase Transitions Measurements by DSC Method

DSC measurements were carried out during heating (ENDO) and cooling (EXO) with the rate of 10 °C/min for all investigated materials. Comparing DSC results with texture observations it was possible to identify almost all phases occurring in studied materials. DSC curves for 9OSOR, 12OSOR, 12R9AF and 14OSOR are introduced below.

DSC results and texture observations of 9OSOR compound show that during heating apart from B_1 phase there are four more phases: probably glassy phase, crystal, a phase that is not identified yet (X) and the isotropic phase. The B_1 phase is enantiotropic one and shows up

during heating in the temperature range of ten degrees however during cooling it lasts for forty degrees (see Fig. 4.3.).

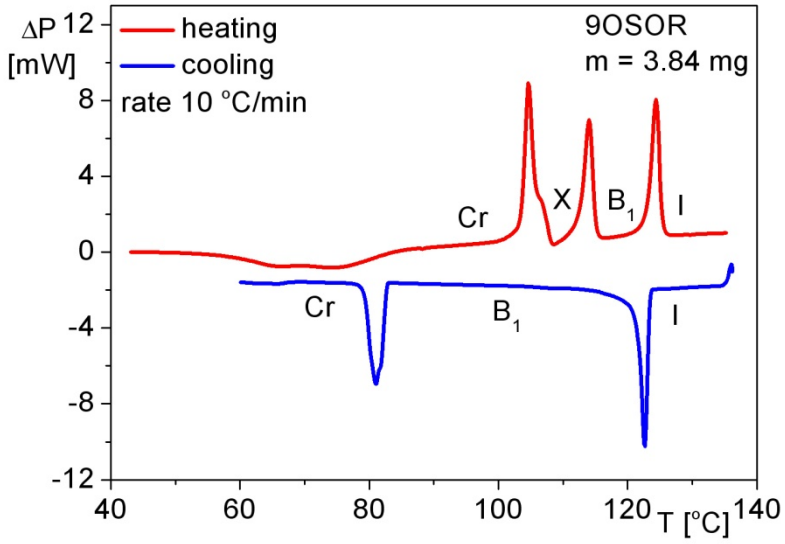

Fig. 4.3. DSC heating and cooling runs for 9OSOR

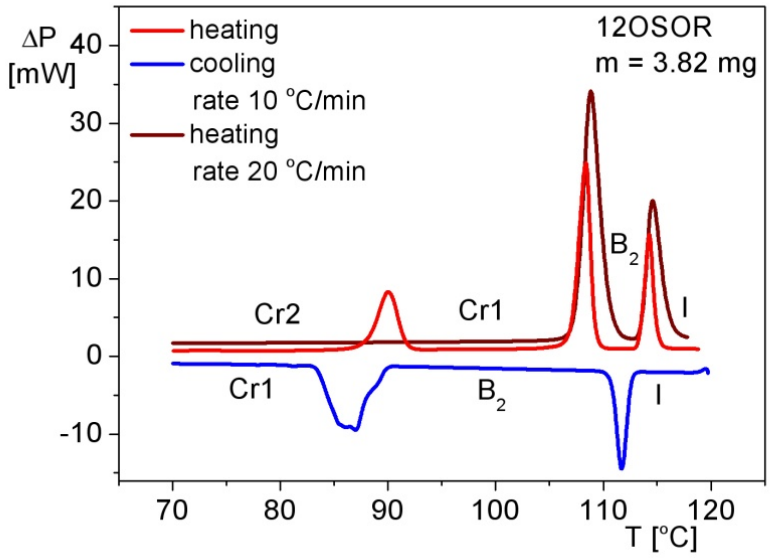

Fig. 4.4. DSC heating and cooling runs for 12OSOR

DSC curve for 12OSOR compound (Fig. 4.4.) shows four phases during the first heating run. Texture observations using polarization microscope allowed to identify them as Cr1, Cr2, B_2 phase and isotropic phase. During the second heating run only one crystalline phase was

observed. The B_2 phase is enantiotropic one and shows up during heating in the short temperature range however during cooling it is the range of twenty degrees.

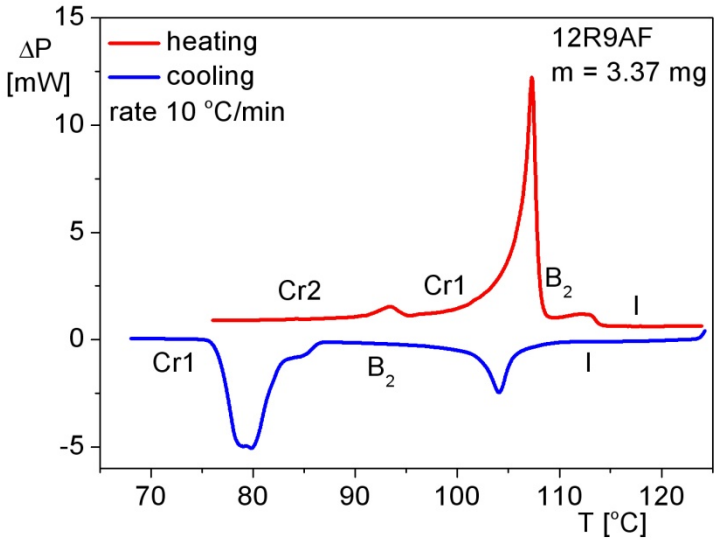

Fig. 4.5. DSC heating and cooling runs for 12R9AF

DSC results for 12R9AF mixture (Fig. 4.5.) shows also four phases during the heating run. Texture observations using polarization microscope allowed to identify them – Cr2, Cr1, B_2 phase and isotropic phase. Smectic B_2 phase of the mixture is enantiotropic one and its temperature range spans over twenty degrees just like for the pure 12OSOR compound but it is shifted to lower temperatures by about ten degrees.

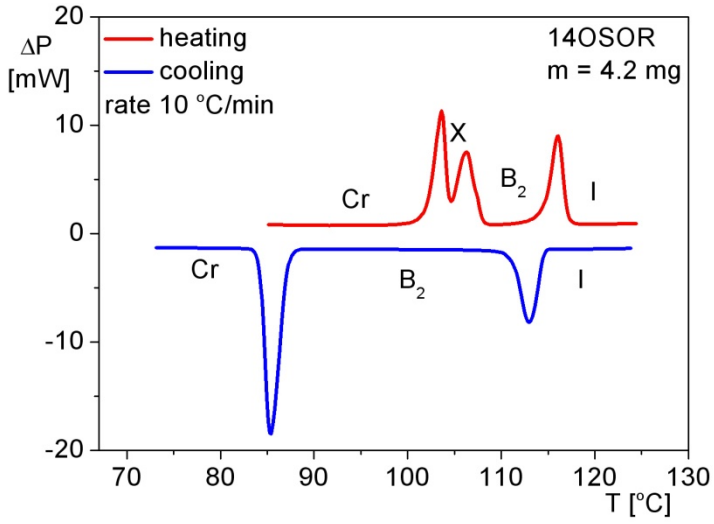

Fig. 4.6. DSC heating and cooling runs for 14OSOR

One more DSC curve is presented for 14OSOR compound (Fig. 4.6.) for which, during heating one observe four phases: crystal, phase which is not identified yet (X) and which do not shows up during cooling, B_2 phase and isotropic phase. The B_2 also for this compound is an enantiotropic one and during cooling shows up in the temperature range of twenty degrees.

DSC measurements allow also to obtain the transition temperatures, enthalpies and entropies of the transitions which are gathered in tables below for each material (Tab. 4.1., 4.2., 4.3., 4.4.). There are also presented phase diagrams (onset temperatures) for 9OSOR, 12OSOR, 12R9AF and 14OSOR.

9OSOR **M_{mol} = 747.94 g/mol**

Table 4.1. DSC results for 9OSOR

Rate [*°C/min*]		**Parameters**	**Glassy phase – Cr**	**Cr – X**	**X – B_1**	**B_1 – I**
10	ENDO	T_p [^oC]	74.5 ± 0.1	104.6 ± 0.1	114.0 ± 0.1	124.4 ± 0.1
		ΔH [*kJ/mol*]	- 23.1 ± 0.1	21.1 ± 0.1	13.6 ± 0.1	14.2 ± 0.1
		ΔS[*J/mol/K*]	- 66.4 ± 0.2	55.9 ± 0.2	35.0 ± 0.2	35.6 ± 0.2
	EXO	T_p [^oC]		81.0 ± 0.1		122.7 ± 0.1
		ΔH [*kJ/mol*]		- 13.9 ± 0.1		- 16.0 ± 0.1
		ΔS[*J/mol/K*]		- 39.1 ± 0.2		- 40.4 ± 0.2
				B_1 – Cr		**I – B_1**

Onset temperatures for phase transitions of 9OSOR compound:

Heating: Glassy phase 56.1 ^oC → Cr 103.4 ^oC → X 112.5 ^oC → B_1 123.0 ^oC → I

Cooling: I 123.4 ^oC → B_1 82.6 ^oC → Cr

12OSOR **M_{mol} = 790.03 g/mol**

Table 4.2. DSC results for 12OSOR

Rate [*°C/min*]		**Parameters**	**Cr2 – Cr1**	**Cr1 – B_2**	**B_2 – I**
10	ENDO	T_p [^oC]	90.0 ± 0.1	108.4 ± 0.1	114.3 ± 0.1
		ΔH [*kJ/mol*]	21.7 ± 0.1	39.7 ± 0.1	18.2 ± 0.1
		ΔS[*J/mol/K*]	59.7 ± 0.2	104.1 ± 0.2	46.9 ± 0.2
	EXO	T_p [^oC]		87.0 ± 0.1	111.7 ± 0.1
		ΔH [*kJ/mol*]		- 38.7 ± 0.1	- 18.5 ± 0.1
		ΔS[*J/mol/K*]		- 107.4 ± 0.2	- 48.1 ± 0.2
				B_2 – Cr1	**I – B_2**

Onset temperatures for phase transitions of 12OSOR compound:

Heating: Cr2 88.1 ^oC → Cr1 107.1 ^oC → B_2 113.4 ^oC → I

Cooling: I 112.6 ^oC → B_2 88.6 ^oC → Cr1

12R9AF **M_{mol} = 779.91 g/mol**

Table 4.3. DSC results for 12R9AF

Rate [*°C/min*]		**Parameters**	**Cr2 – Cr1**	**Cr1 – B_2**	**B_2 – I**
10	ENDO	T_p [^oC]	93.4 ± 0.1	107.3 ± 0.1	112.9 ± 0.1
		ΔH [*kJ/mol*]	1.5 ± 0.1	33.4 ± 0.1	1.3 ± 0.1
		ΔS[*J/mol/K*]	4.1 ± 0.2	87.9 ± 0.2	3.4 ± 0.2
	EXO	T_p [^oC]	79.9 ± 0.1		104.1 ± 0.1
		ΔH [*kJ/mol*]	- 32.3 ± 0.1		- 11.3 ± 0.1
		ΔS[*J/mol/K*]	- 91.5 ± 0.2		- 30.0 ± 0.2
			B_2 – Cr1		**I – B_2**

Onset temperatures for phase transitions of 12R9AF compound:

Heating: Cr2 91.0 °C → Cr1 106.1 °C → B_2 109.8 °C → I

Cooling: I 105.6 °C → B_2 82.5 °C → Cr1

14OSOR **M_{mol} = 818.09 g/mol**

Table 4.4. DSC results for 14OSOR

Rate [*°C/min*]		**Parameters**	**Cr – X**	**X – B_2**	**B_2 – I**
10	ENDO	T_p [^oC]	103.7 ± 0.1	106.4 ± 0.1	116.1 ± 0.1
		ΔH [*kJ/mol*]	11.1 ± 0.1	9.1 ± 0.1	16.8 ± 0.1
		ΔS[*J/mol/K*]	29.4 ± 0.2	24.1 ± 0.2	43.1 ± 0.2
	EXO	T_p [^oC]	85.2 ± 0.1		113.2 ± 0.1
		ΔH [*kJ/mol*]	- 57.6 ± 0.1		- 17.4 ± 0.1
		ΔS[*J/mol/K*]	- 160.8 ± 0.2		- 45.1 ± 0.2
			B_2 – Cr		**I – B_2**

Onset temperatures for phase transitions of 14OSOR compound:

Heating: Cr 102.4 °C → X 104.9 °C → B_2 114.7 °C → I

Cooling: I 114.6 °C → B_2 87.2 °C → Cr

For all phase transitions enthalpies and entropies are very large because these transitions are accompanied with large changes in the structure.

4.3. Texture Observations

Texture observations and pictures of them were made during heating and cooling for all materials. First investigated liquid crystals were put into the electrooptic cells. For 9OSOR, 12R9AF and 14OSOR the thickness of the electrooptic cell was 3.2 μm, for 12OSOR it was

1.7 µm. For all materials AWAT HG electrooptic cells (see section 3.1.2.) with ITO electrodes were used.

9OSOR

Heating

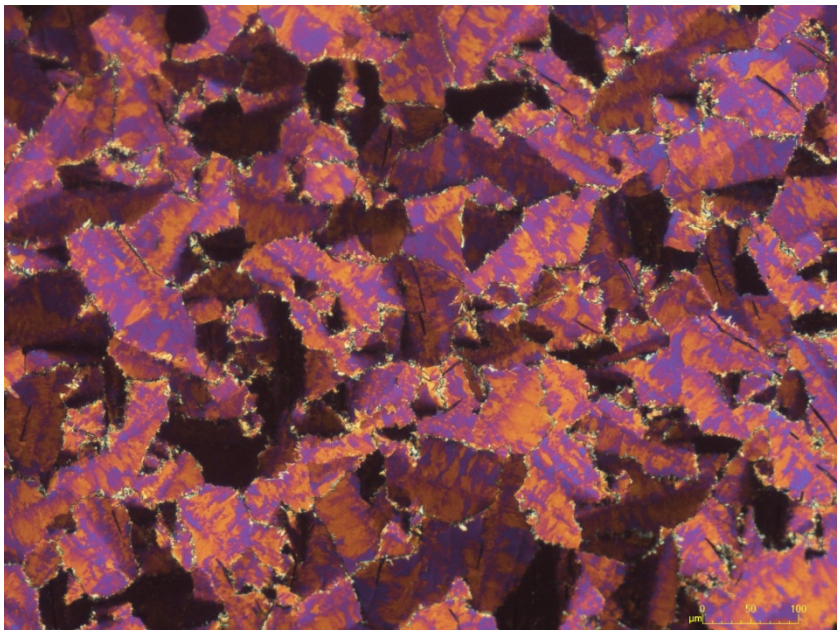

Photo 4.1. 9OSOR. Texture of glassy phase (T = 60.5 °C)

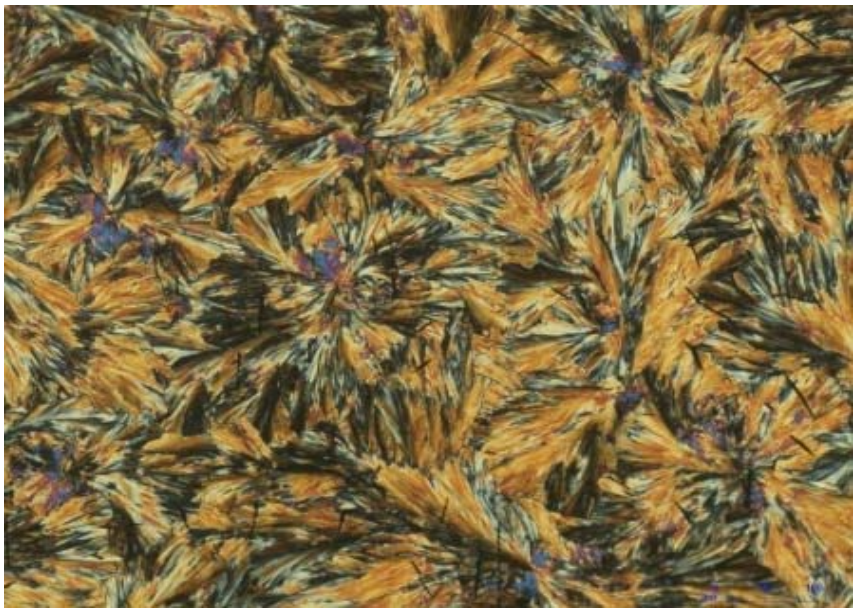

Photo 4.2. 9OSOR. Texture of crystal phase (T = 80.5 °C)

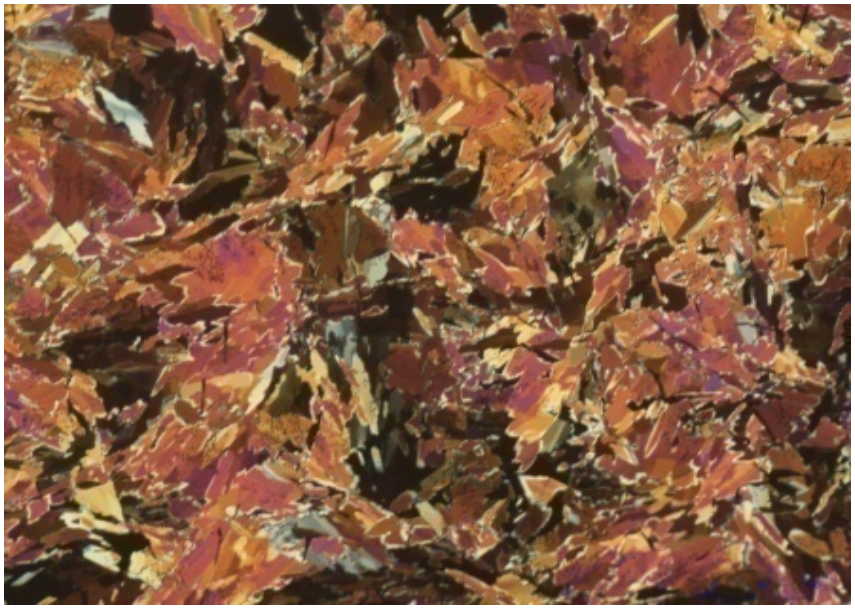

Photo 4.3. 9OSOR. Texture of the X phase (T = 105.3 ^{o}C)

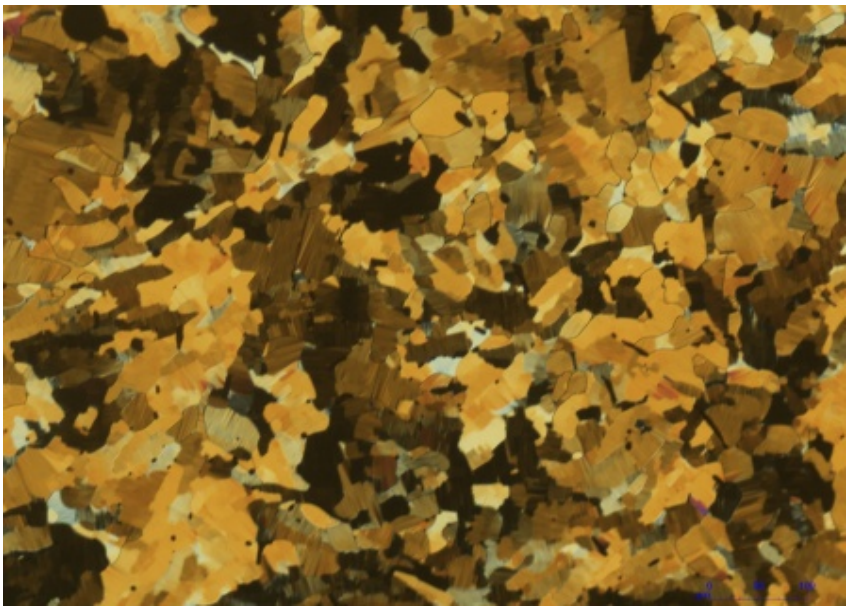

Photo 4.4. 9OSOR. Texture of the B_1 phase (T = 115.3 ^{o}C)

Cooling

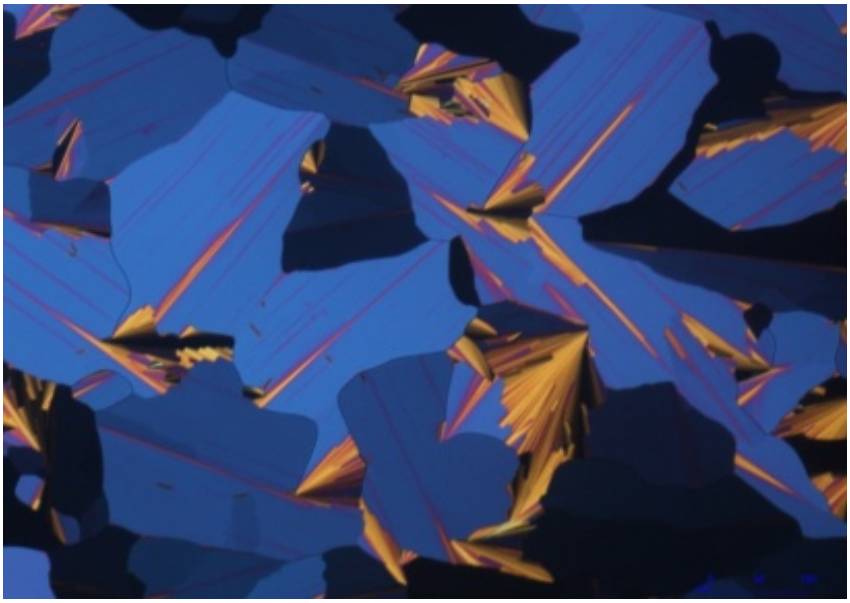

Photo 4.5. 9OSOR. Texture of the B_1 phase (T = 105 ^{o}C)

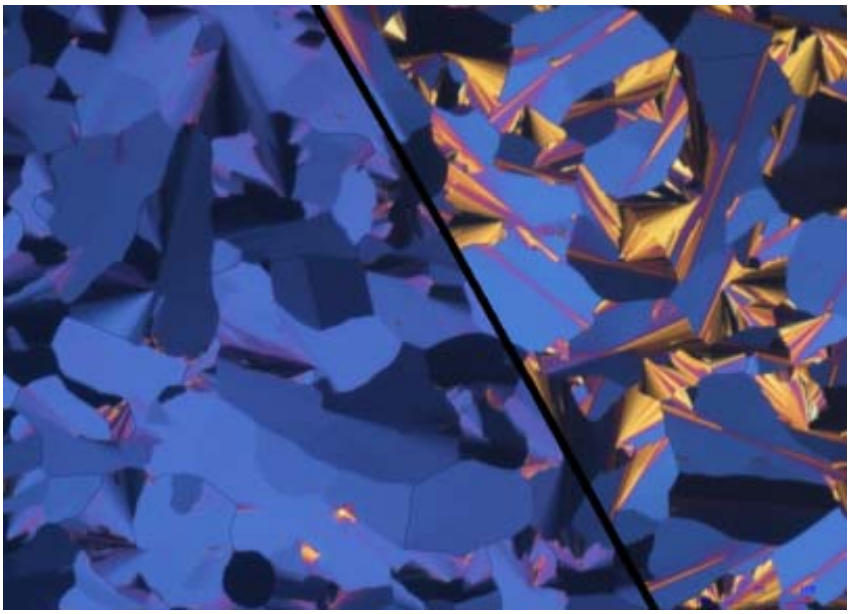

Photo 4.6. 9OSOR. Texture of the B_1 phase (T = 105 ^{o}C) with bias field of 25 $V_{p-p}/\mu m$

In Fig. 4.6. the black line indicates the border line of the electrodes. After applying electric field an electrooptic switching is not observed for this phase. Fig. 4.7. illustrates the structure of B_1 phase. Side chains of the molecule overlap the cores of molecules in neighboring layers and there is a compensation of macroscopic polarization.

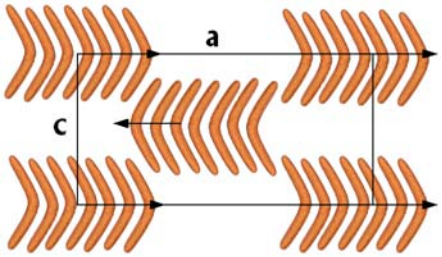

Fig. 4.7. Alignment of molecules in B_1 phase [6]

12OSOR

Heating

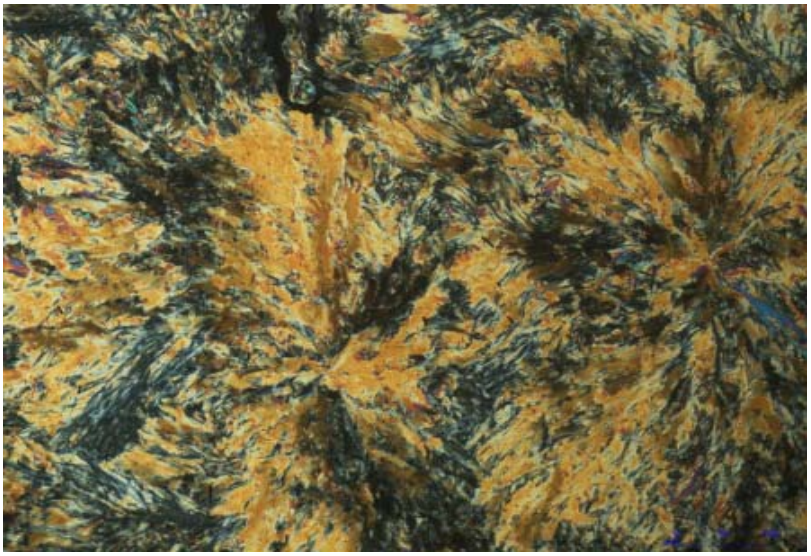

Photo 4.7. 12OSOR. Texture of the crystal (T = 90.3 °C)

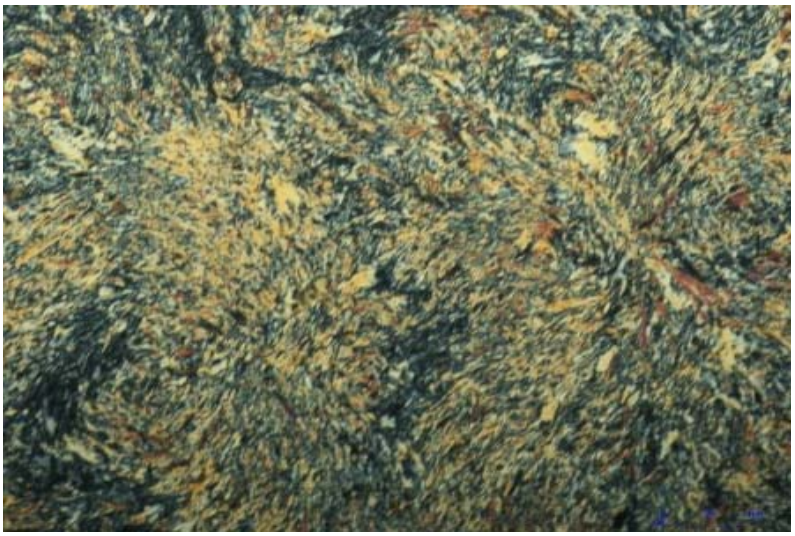

Photo 4.8. 12OSOR. Texture of the B_2 phase (T = 110 °C)

Cooling

Polarizing microscopy measurements allowed to observe on thin layers (1.7 μm) a quasi-planar inhomogeneous (Photo 4.9.) and quasi-homeotropic (Photo 4.10) texture of B_2 phase in 12OSOR. The quasi-homeotropic texture with the polar director perpendicular to the electrodes was observed after applying an electric bias field equal to 13 $V_{p\text{-}p}/\mu m$. This effect occurs to be reversible. Figs. 4.8. and 4.9. present a molecular arrangement of quasi-planar and quasi-homeotropic textures, respectively.

Photo 4.9. 12OSOR. Quasi-planar texture of the B_2 phase in thin 1.7 μm AWAT cell (X, Y plane is parallel to the electrodes) (T = 112 ^{o}C)

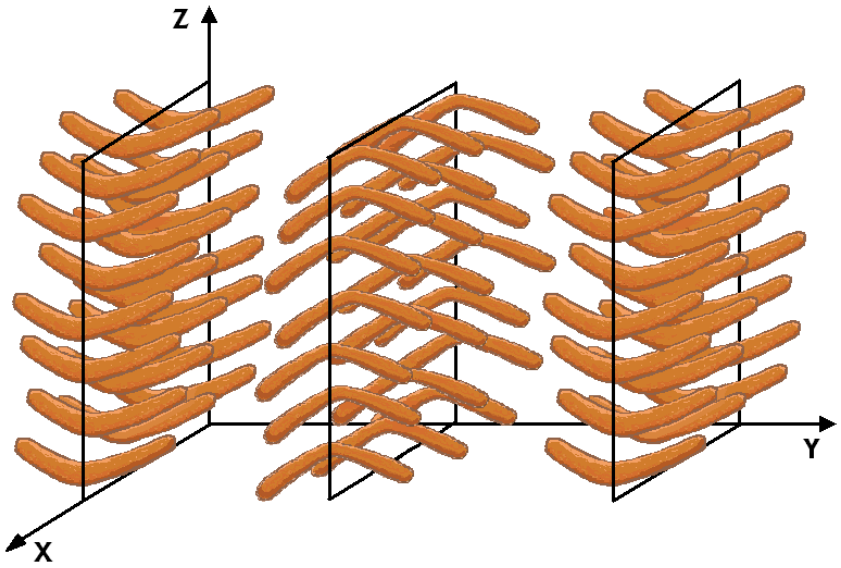

Fig. 4.8. Alignment of molecules in quasi-planar B_2 phase

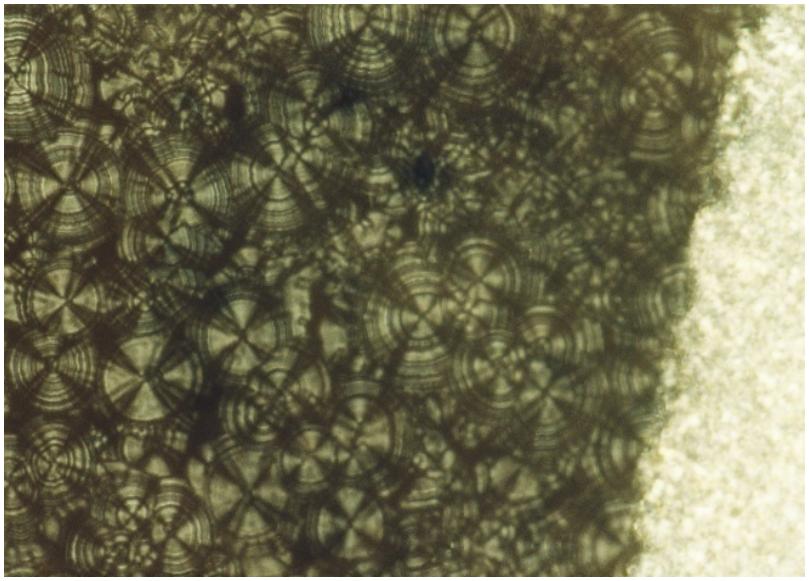

Photo 4.10. 12OSOR. Quasi-homeotropic texture of B_2 phase under electric field of 13 $V_{p\text{-}p}/\mu m$ parallel to z-axis (T = 112 °C)

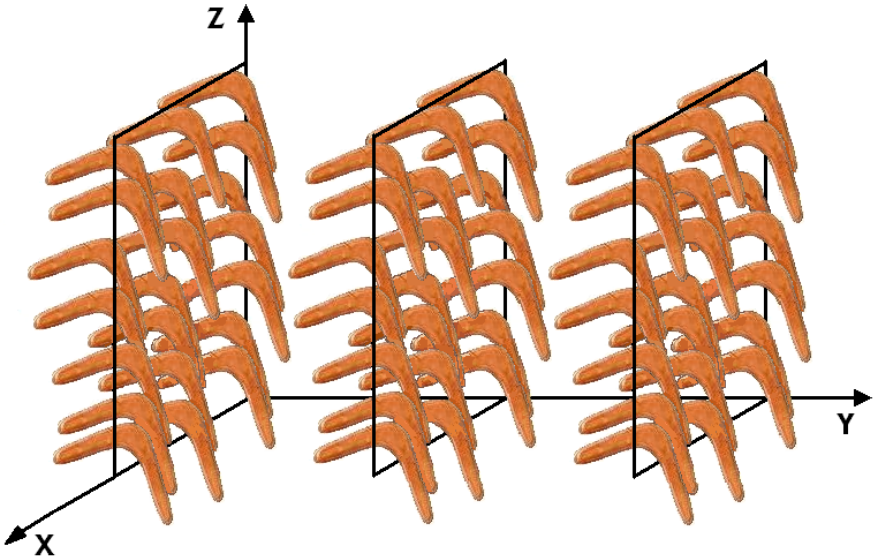

Fig. 4.9. Alignment of molecules in quasi-homeotropic B_2 phase

Textures of 12OSOR compound during cooling were made in Calais at LEMCEL using Olympus Polarizing Microscope BX60 and LINCAM temperature controller.

12R9AF

Heating

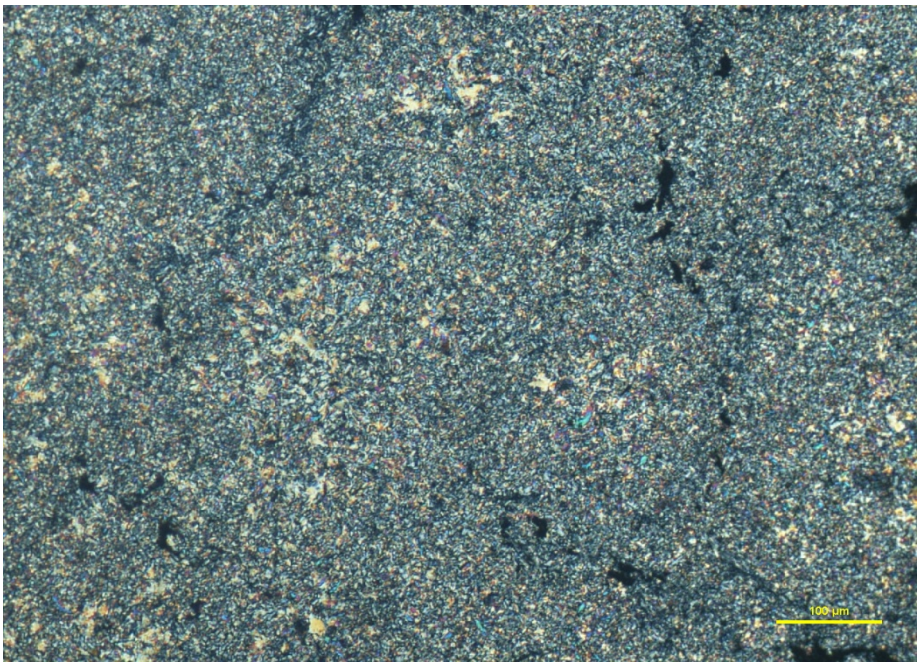

Photo 4.11. 12R9AF. Texture of the crystal 2 (T = 70 °C). Yellow bar scale – 100 µm

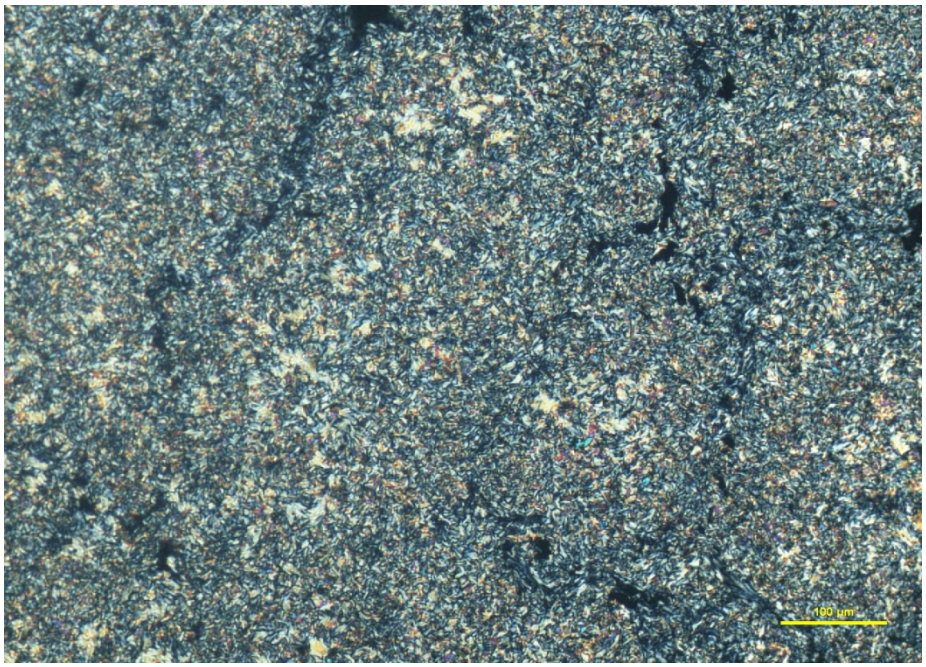

Photo 4.12. 12R9AF. Texture of the crystal 1 (T = 100 °C). Yellow bar scale – 100 µm

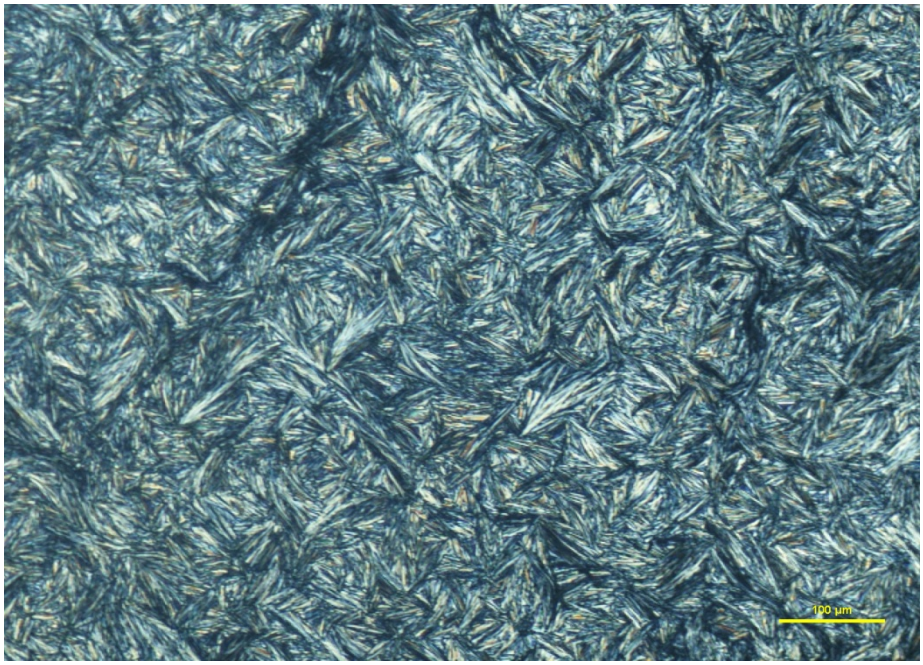

Photo 4.13. 12R9AF. Texture of the B_2 phase (T = 107 °C). Yellow bar scale – 100 µm

Cooling

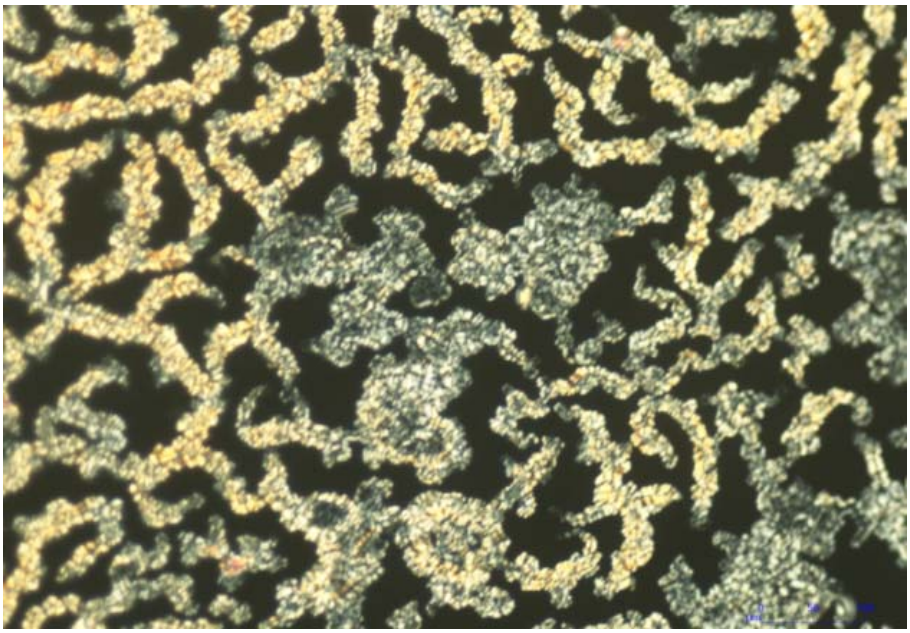

Photo 4.11. 12R9AF. Texture of the B_2 phase (T = 104 °C)

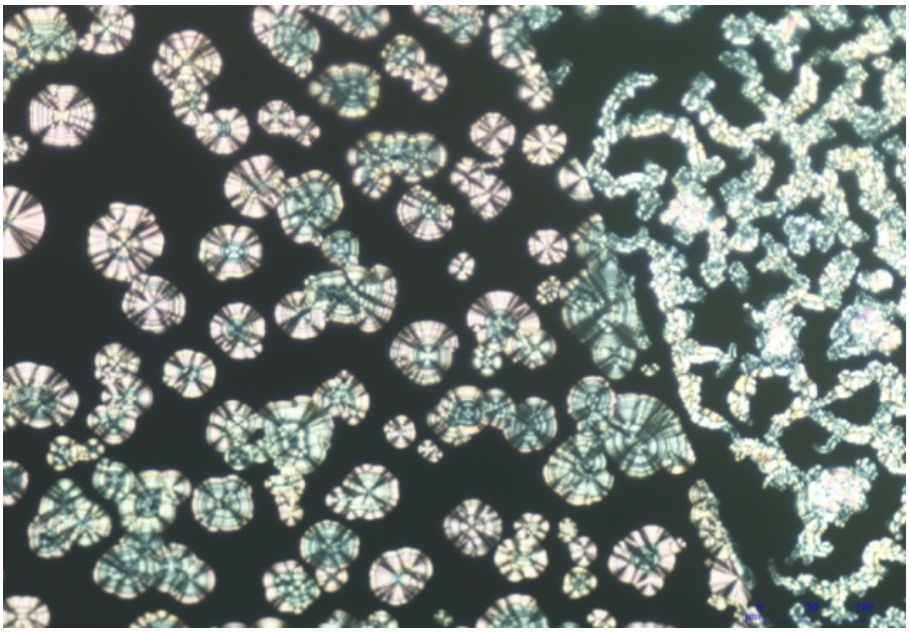

Photo 4.12. 12R9AF. Texture of the B_2 phase (T = 104 ^{o}C) with bias field of 25 $V_{p-p}/\mu m$

There is a line indicating the border of the electrodes. On the left-hand side one can see the texture between the electrodes.

14OSOR

Heating

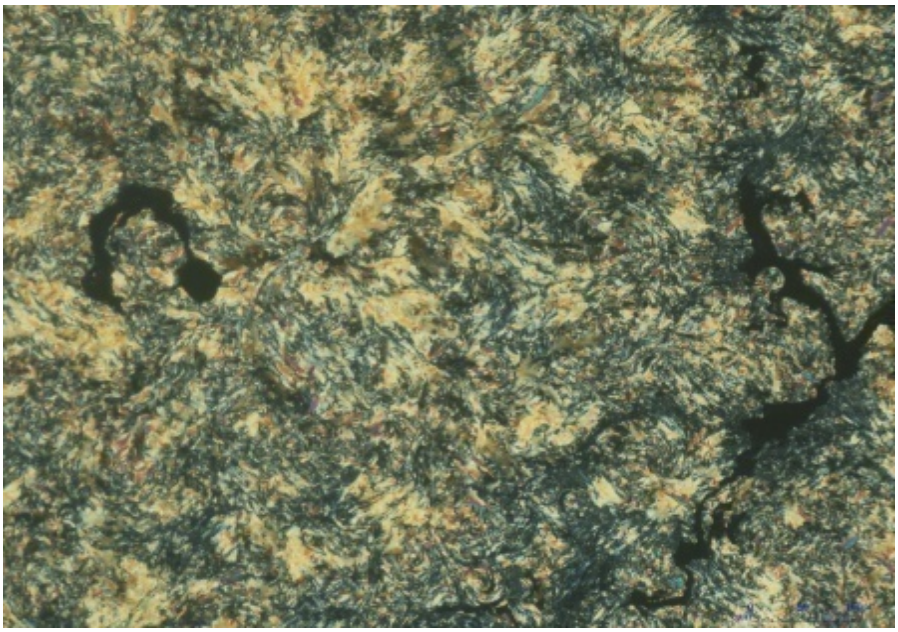

Photo 4.13. 14OSOR. Texture of the crystal (T = 87.5 ^{o}C)

Photo 4.14. 14OSOR. Texture of the X phase (T = 105.5 ^{o}C)

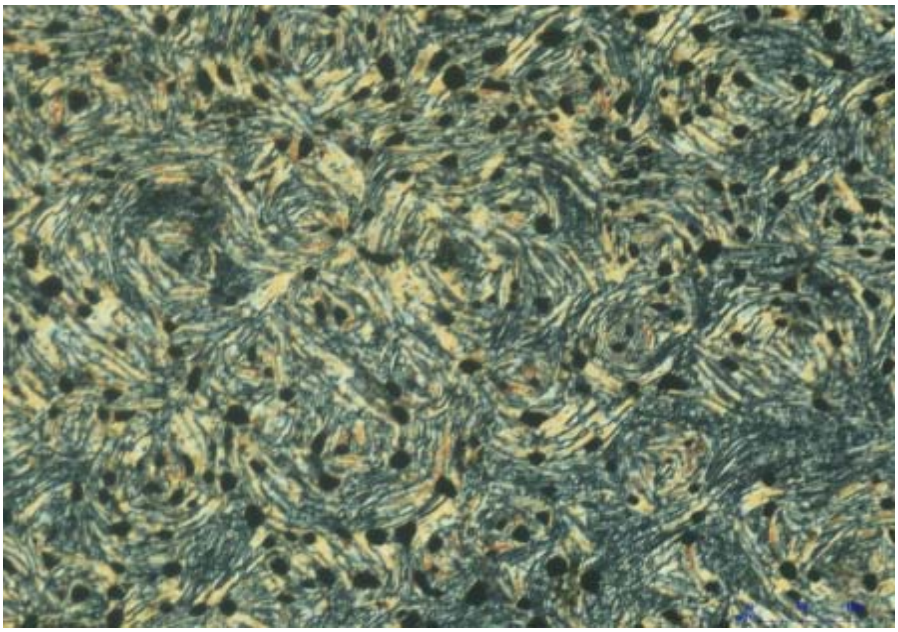

Photo 4.14. 14OSOR. Texture of the B_2 phase (T = 112.2 ^{o}C)

Cooling

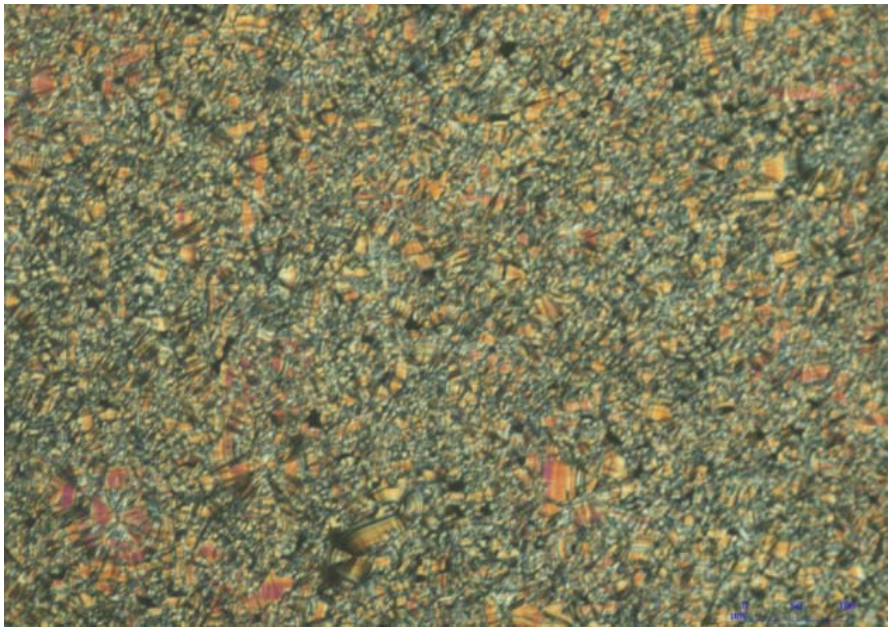

Photo 4.15. 14OSOR. Texture of the B_2 phase (T = 110 °C)

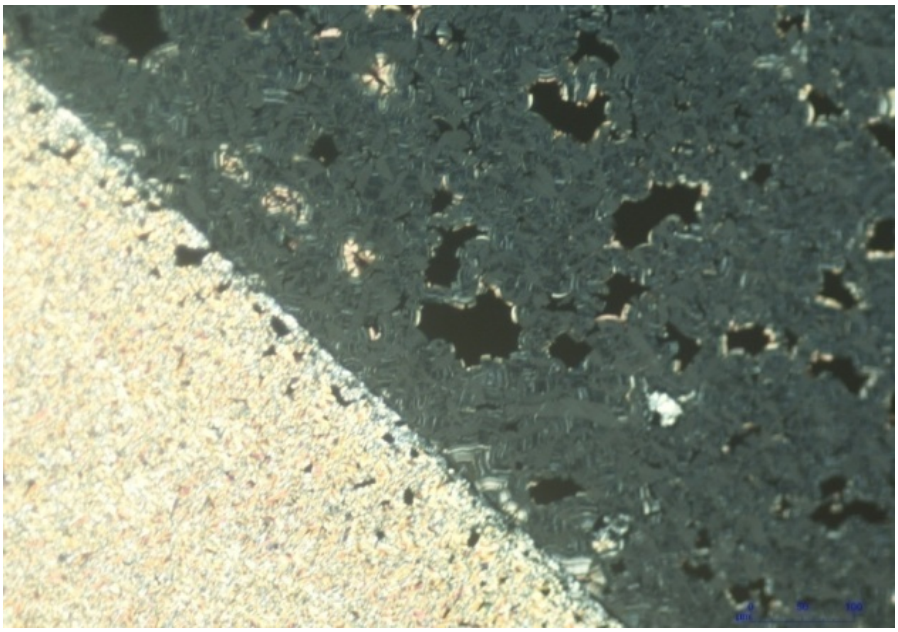

Photo 4.16. 14OSOR. Quasi-homeotropic texture of the B_2 phase (T = 110 °C) with bias field of 25 $V_{p\text{-}p}/\mu m$

One can see the border line of the electrodes. On the right-hand side one can see a quasi-homeotropic texture between the electrodes.

4.4. Spontaneous Polarization Measurements

Spontaneous polarization measurements have been performed by reversal current method during cooling using for 9OSOR and 12OSOR 1.7 μm and for 12OSOR, 12R9AF and 14OSOR 3.2 μm AWAT ITO electrooptic cells. For 12OSOR, 14OSOR compounds and 12R9AF mixture measurements have been done on partially aligned (planar inhomogeneous) B_2 phase.

The current response to applied field showed the B_1 phase of 9OSOR to be a ferroelectric one – a broad peak was observed (Fig. 4.17.). Usually B_1 phases do not show spontaneous polarization, although for this compound an apparent polarization is observed. This polarization is rather small and it's temperature dependence is unusual as for ferroelectric liquid crystals – it increases with temperature (Fig. 4.18.) [26]. Mechanism of it is not quite clear. It may originate either from space charge polarization or from non-compensated part of polarization which decreases with temperature lowering due to negative correlations. Measurements were done using triangular electric field having frequency of 5 Hz and amplitude equal to 47.1 $V_{p-p}/\mu m$ for which polarization is saturated (see Fig.4.19.).

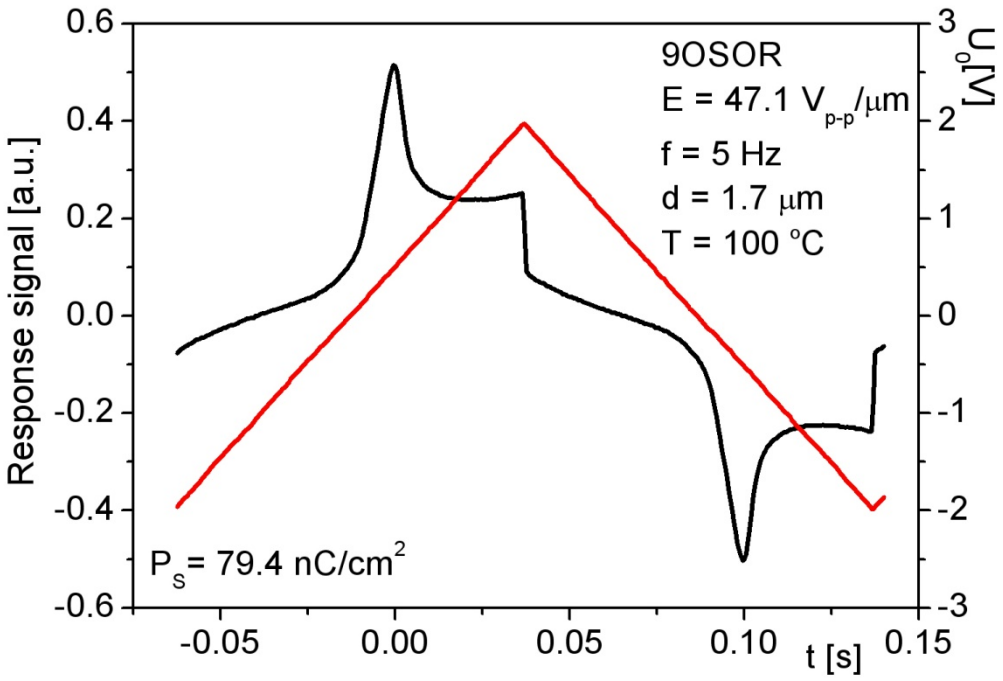

Fig. 4.17. Triangular driving voltage (right-hand side scale) applied vs. time and reversal current spectrum (left-hand side scale) of 9OSOR B_1 phase for E = 47.1 $V_{p-p}/\mu m$, f = 5 Hz, d = 1.7 μm and T = 100 °C

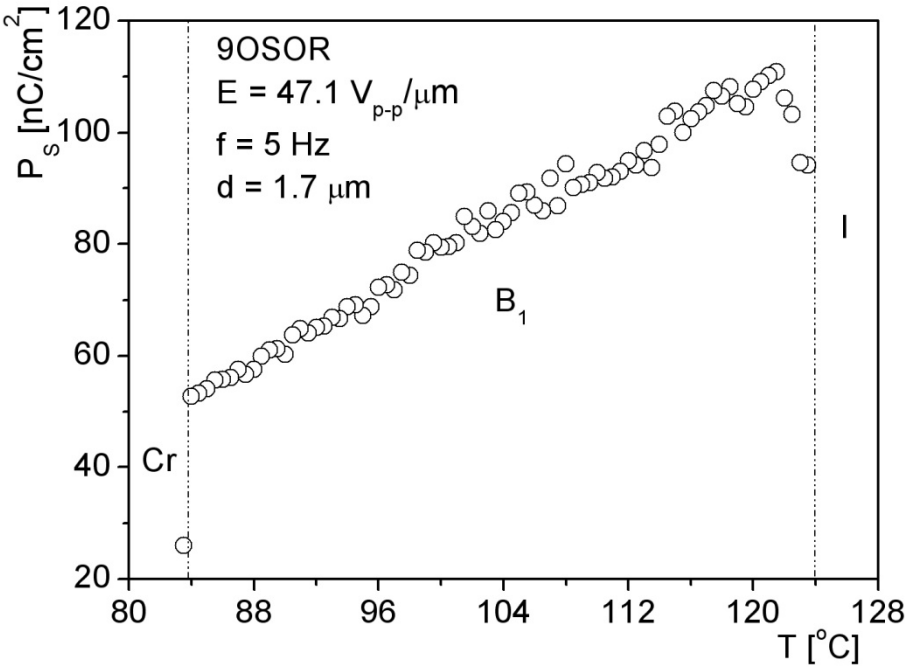

Fig. 4.18. Spontaneous polarization of 9OSOR ferroelectric B_1 phase vs. temperature measured for E = 42.4 V_{p-p}/μm, f = 5 Hz, d = 1.7 μm

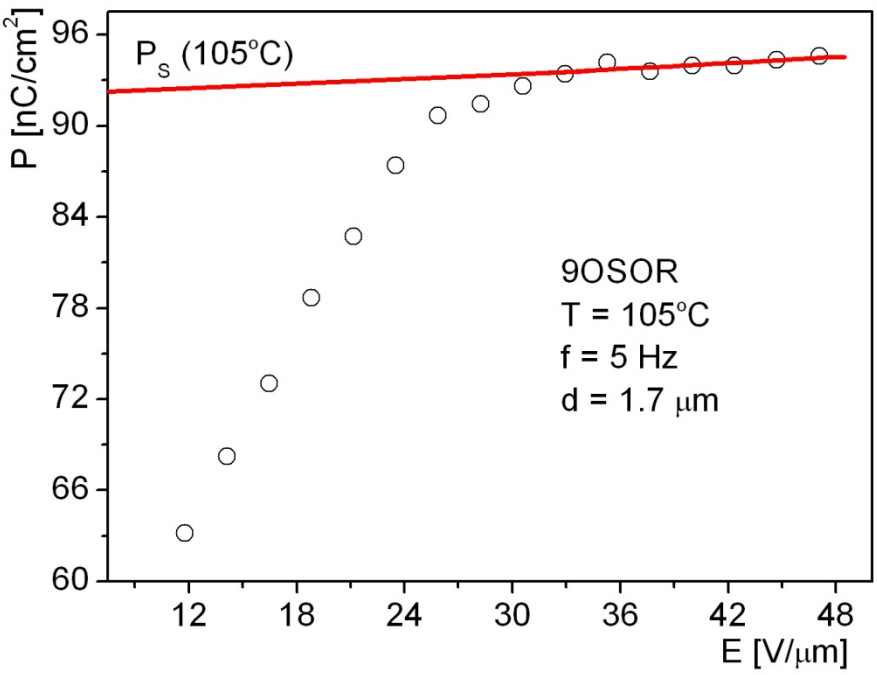

Fig. 4.19. Polarization vs. electric field for 9OSOR B_1 phase (T = 100 °C)

The B_2 phase of 12OSOR compound seems to be antyclinic – antiferroelectric (SmC_AP_A), after applying to the electrodes triangular electric wave two well separated peaks were observed as a response current (Fig. 4.20.) for the sample.

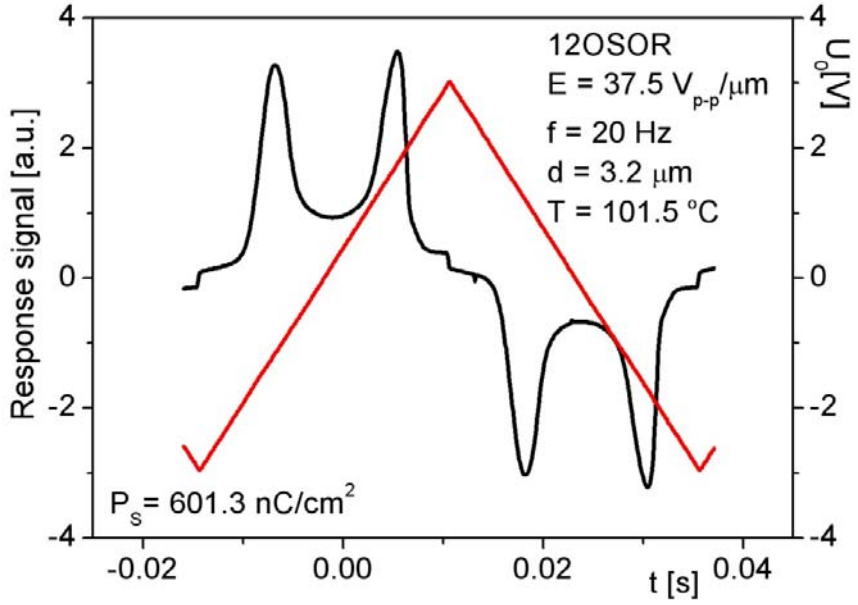

Fig. 4.20. Triangular driving voltage (right-hand side scale) applied vs. time and reversal current spectrum (left-hand side scale) of 12OSOR B_2 phase for E = 37.5 $V_{p-p}/\mu m$, f = 20 Hz, d = 3.2 μm and T = 101.5 °C

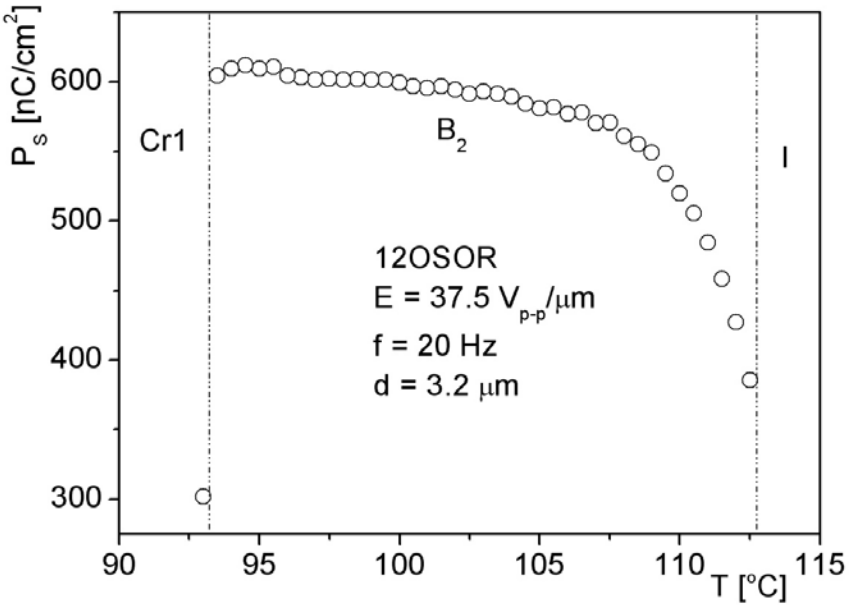

Fig. 4.21. Spontaneous polarization of 12OSOR B_2 phase vs. temperature acquired for E = 37.5 $V_{p-p}/\mu m$, f = 20 Hz, d = 3.2 μm

Measurements were carried out using driving electric field of 37.5 $V_{p-p}/\mu m$, high enough for polarization to be saturated (see Fig. 4.22.), and signal frequency of 20 Hz in temperature of 101.5 °C that is, according to DSC measurements, more less in the middle of B_2 phase. Fig. 4.20. shows spontaneous polarization dependence on temperature for electric field of 37.5 $V_{p-p}/\mu m$ and signal frequency of 20 Hz. For B_2 phase of 12OSOR the spontaneous polarization is very high, it is close to 600 nC/cm^2 [9]. Non-linear dependence of polarization vs. electric field applied is demonstrated in Figs. 4.22. (110 °C), 4.23. (105 °C) and 4.25. (100 °C). One can see that the saturation electric field is rather high – about 30 $V_{p-p}/\mu m$ for entire temperature range of B_2 phase. Very large critical electric field can indicate to anticlinicity of B_2 phase in this compound.

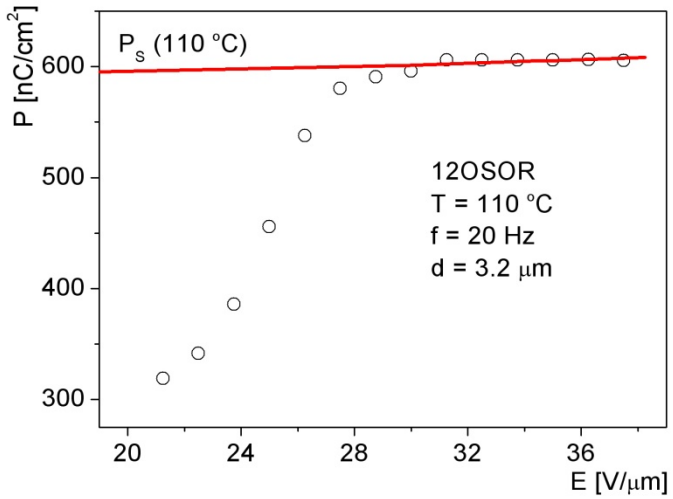

Fig. 4.22. Polarization vs. electric field for 12OSOR B_2 phase (T = 110 °C)

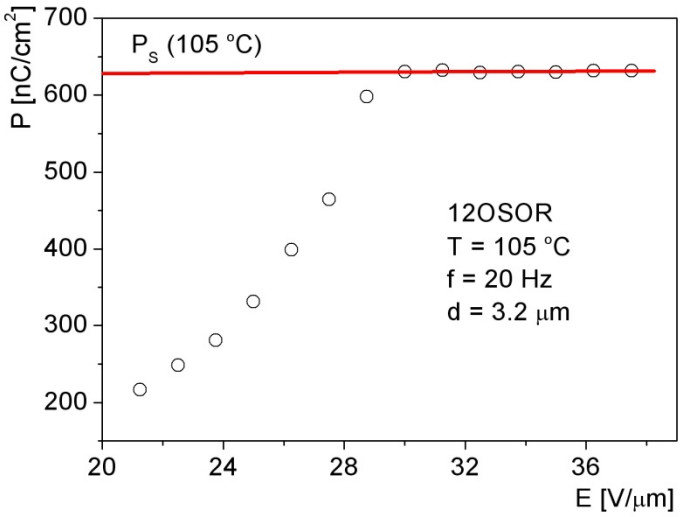

Fig. 4.23. Polarization vs. electric field for 12OSOR B_2 phase (T = 105 °C)

Fig. 4.24. shows two peaks of antiferroelectric B_2 phase for four different electric fields (21.25 $V_{p-p}/\mu m$, 25 $V_{p-p}/\mu m$, 28.75 $V_{p-p}/\mu m$ and 35 $V_{p-p}/\mu m$) in the temperature of 105 ^oC. As one can see, peaks are growing when the value of the electric field is rising. Along with the increase of the electric field – the spontaneous polarization increases.

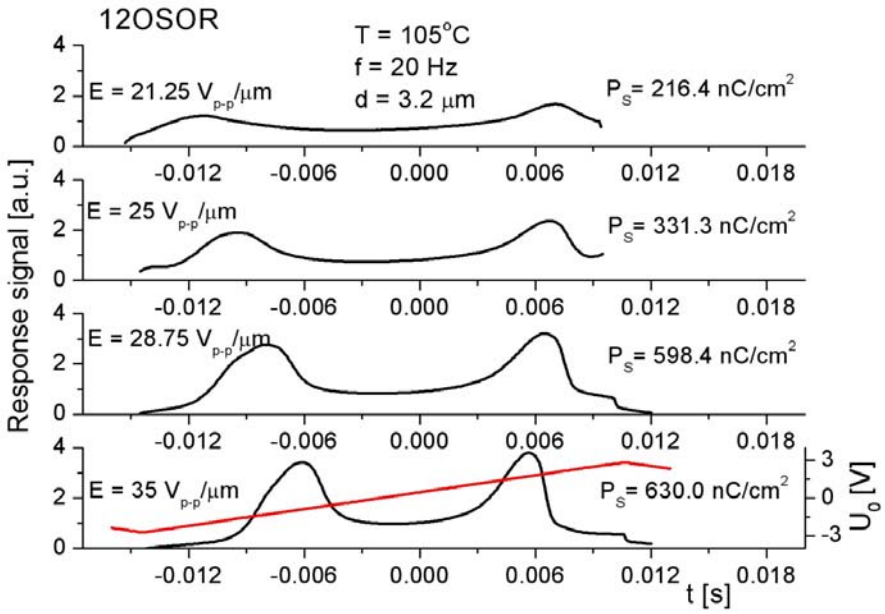

Fig. 4.24. The reversal current peaks vs. time for B_2 phase of 12OSOR for different values of the electric field (f = 20 Hz, d = 3.2 μm and T = 101.5 ^oC)

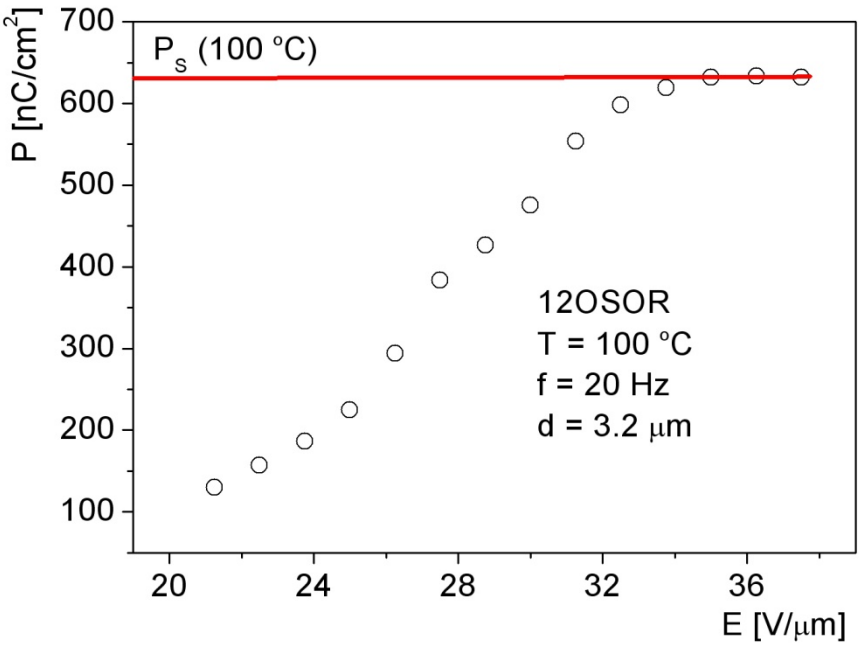

Fig. 4.25. Polarization vs. electric field for 12OSOR B_2 phase (T = 100 ^oC)

Spontaneous polarization vs. temperature measurements of B_2 phase of 12OSOR for different frequencies of the signal were also performed. In Fig. 4.26. one can see reversal current peaks for 37.5 $V_{p-p}/\mu m$ in 100 ^oC for three values of frequency – 15 Hz, 25 Hz and 35 Hz. Reversal current peaks grows higher and become narrower with increase of frequency of the signal. Spontaneous polarization also increases along with increase of frequency.

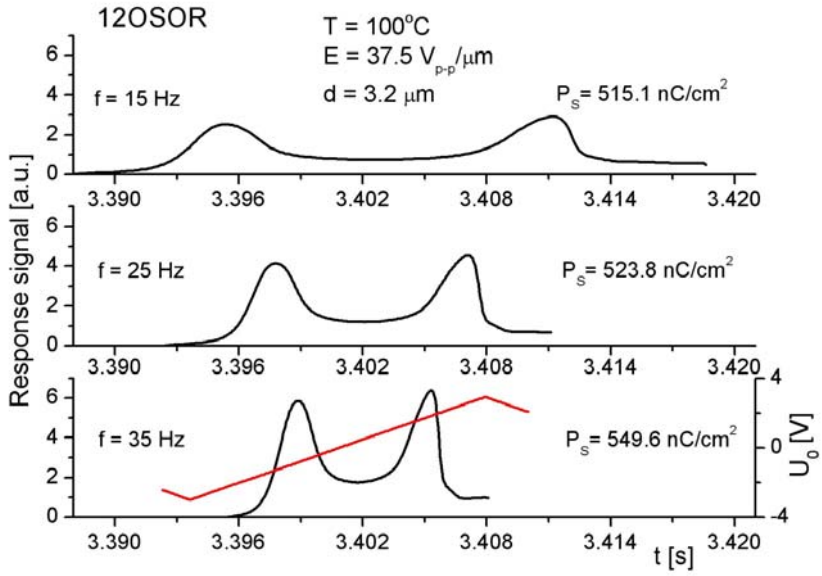

Fig. 4.26. The reversal current peaks vs. time for B_2 phase of 12OSOR for different values of frequency of the signal (E = 37.5 $V_{p-p}/\mu m$, d = 3.2 μm and T = 100 ^oC)

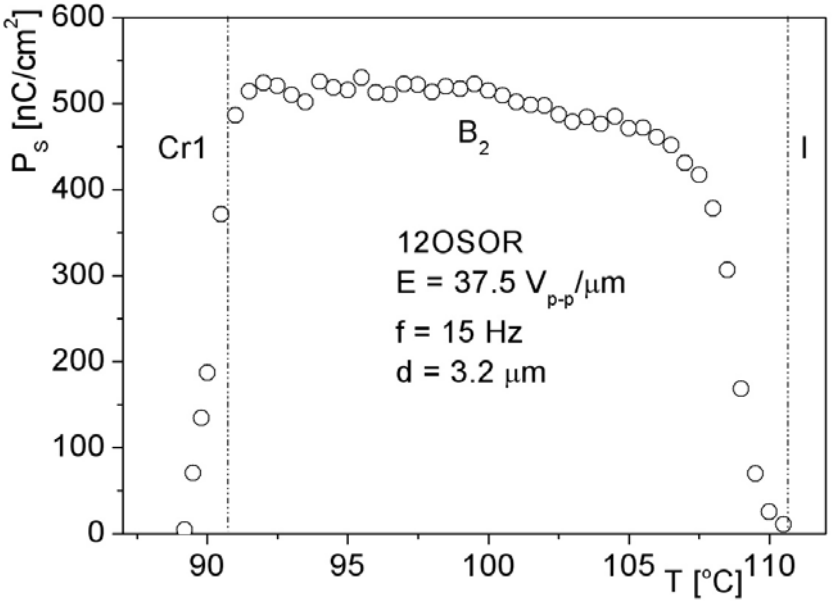

Fig. 4.27. Spontaneous polarization of 12OSOR B_2 phase vs. temperature obtained for E = 37.5 $V_{p-p}/\mu m$, f = 15 Hz, d = 3.2 μm

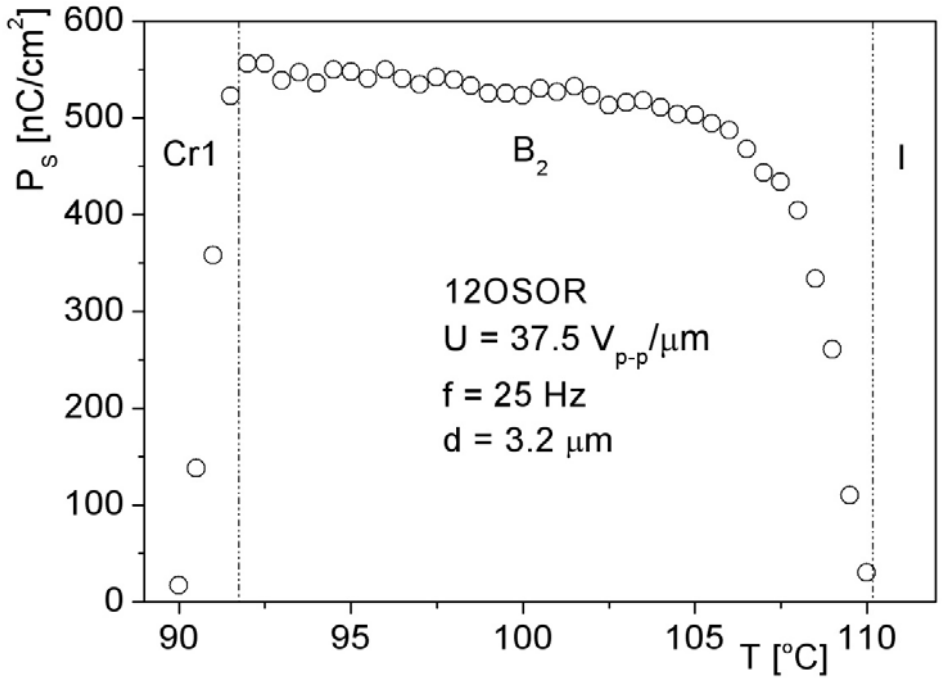

Fig. 4.28. Spontaneous polarization of 12OSOR B_2 phase vs. temperature acquired for E = 37.5 $V_{p-p}/\mu m$, f = 25 Hz, d = 3.2 μm

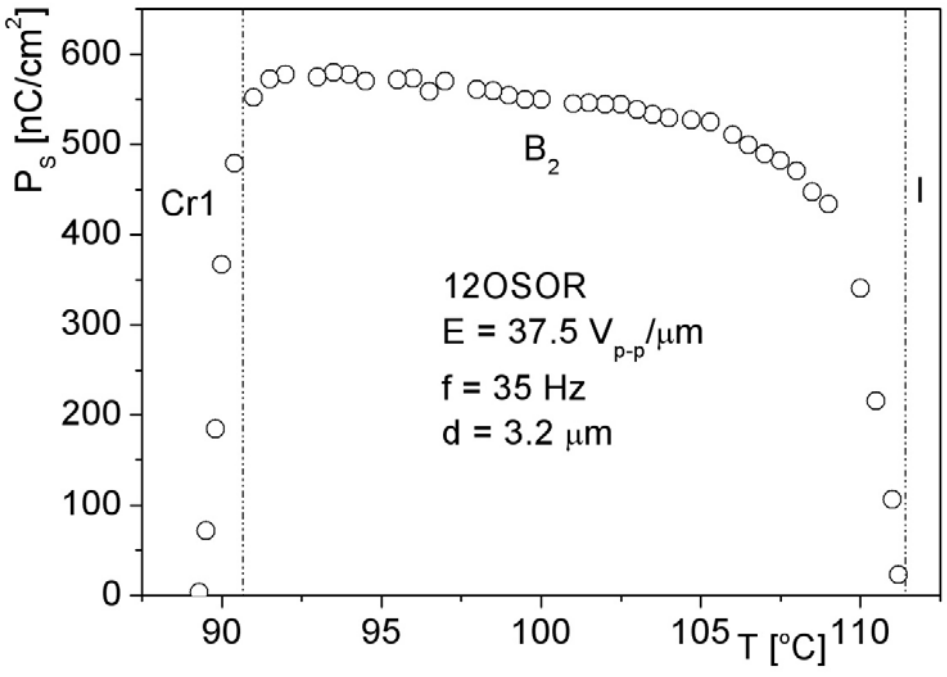

Fig. 4.29. Spontaneous polarization of 12OSOR B_2 phase vs. temperature measured for E = 37.5 $V_{p-p}/\mu m$, f = 35 Hz, d = 3.2 μm

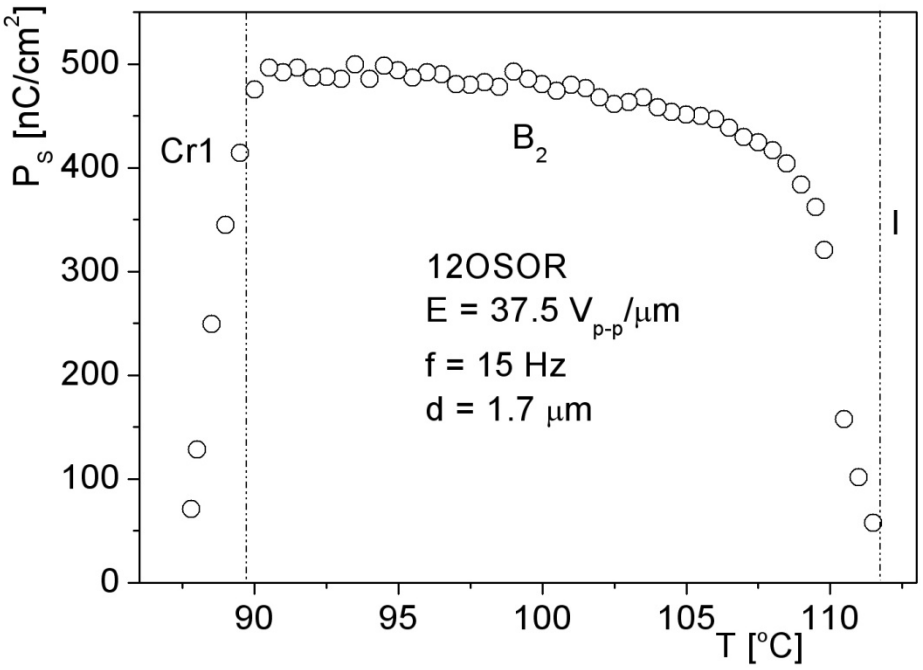

Fig. 4.30. Spontaneous polarization of 12OSOR B_2 phase vs. temperature obtained for E = 37.5 $V_{p-p}/\mu m$, f = 15 Hz, d = 1.7 μm

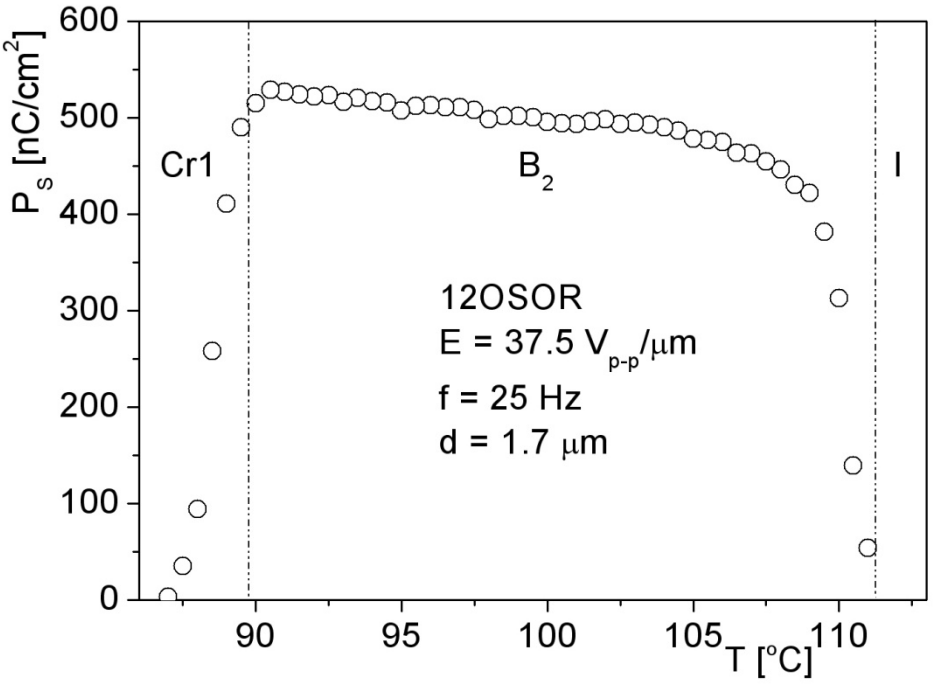

Fig. 4.31. Spontaneous polarization of 12OSOR B_2 phase vs. temperature obtained for E = 37.5 $V_{p-p}/\mu m$, f = 25 Hz, d = 1.7 μm

Figs. 4.27., 4.28. and 4.29. show spontaneous polarization vs. temperature dependence for driving electric field of 37.5 $V_{p-p}/\mu m$ and frequency of the signal of 15 Hz, 25 Hz and 35 Hz respectively for the electrooptic cell thickness equal to 3.2 μm. The following figures (4.30., 4.31. and 4.32.) show also spontaneous polarization vs. temperature dependence for the electric field of 37.5 $V_{p-p}/\mu m$ and frequency of the signal of 15 Hz, 25 Hz and 35 Hz respectively, but for the electrooptic cell thickness equal to 1.7 μm.

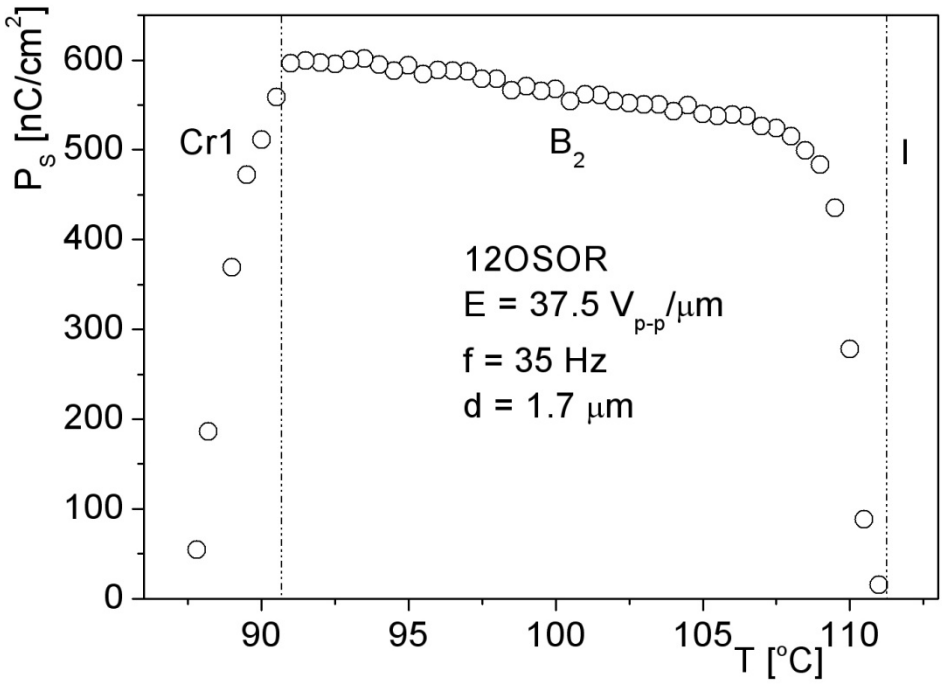

Fig. 4.32. Spontaneous polarization of 12OSOR B_2 phase vs. temperature acquired for E = 37.5 $V_{p-p}/\mu m$, f = 35 Hz, d = 1.7 μm

The B_2 phase of 12R9AF mixture is also antiferroelectric one – after applying to the electrodes triangular electric voltage, two well separated current peaks were also observed as a response current (Fig. 4.33.). Fig. 4.34. shows polarization dependence on electric field applied to the sample in temperature of 102 °C and frequency of the signal of 20 Hz. As seen for B_2 phase of the mixture electric field of 25 $V_{p-p}/\mu m$ is high enough for polarization to be saturated while for the B_2 phase of 12OSOR it has to be higher – up to about 30 $V_{p-p}/\mu m$.

In Fig. 4.35. spontaneous polarization for B_2 phase of 12R9AF mixture is shown. It is about 500 nC/cm^2, by 20% smaller in comparison to pure compound and it is shifted to lower temperatures by about 10 °C. At low temperatures in the vicinity of isotropic – B_2 phase

transition there is some kind of electroclinic effect in isotropic phase (see Fig. 4.35.). Measurements were done for field of 25 $V_{p-p}/\mu m$ and signal frequency of 30 Hz.

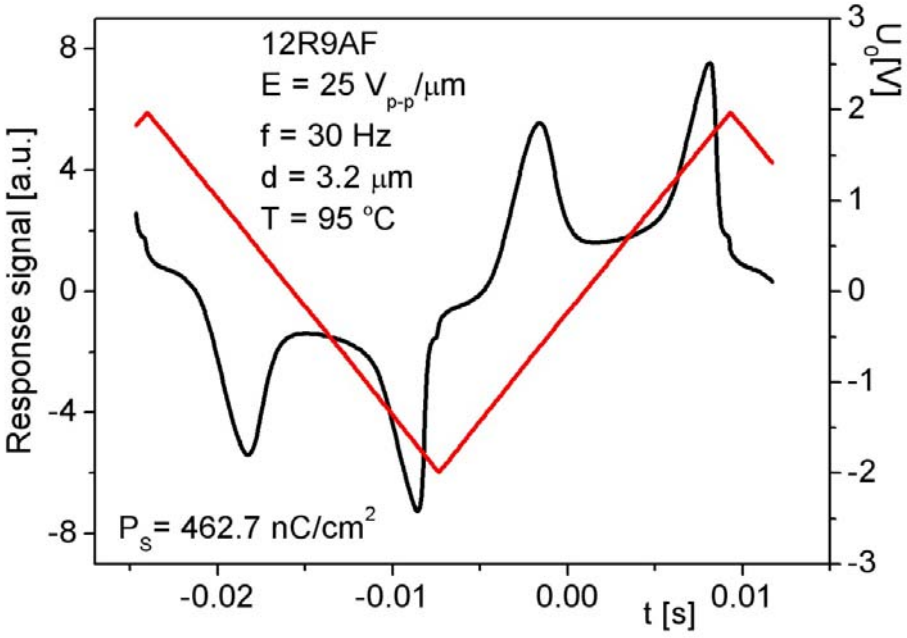

Fig. 4.33. Triangular driving voltage (right-hand side scale) applied vs. time and reversal current spectrum (left-hand side scale) of 12R9AF B_2 phase for E = 25 $V_{p-p}/\mu m$, f = 30 Hz, d = 3.2 μm and T = 95 °C

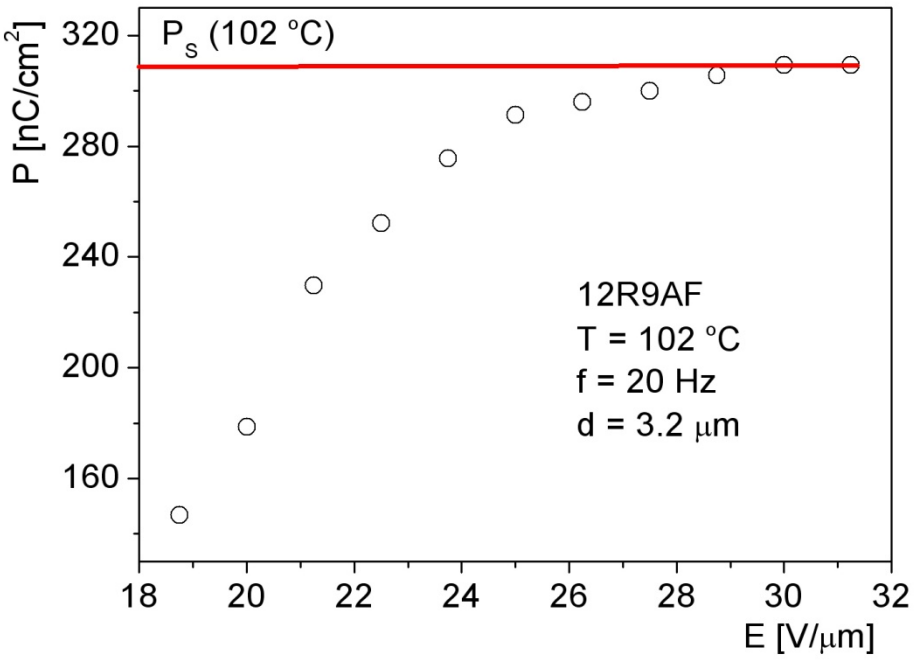

Fig. 4.34. Polarization vs. electric field for 12R9AF B_2 phase (T = 102 °C)

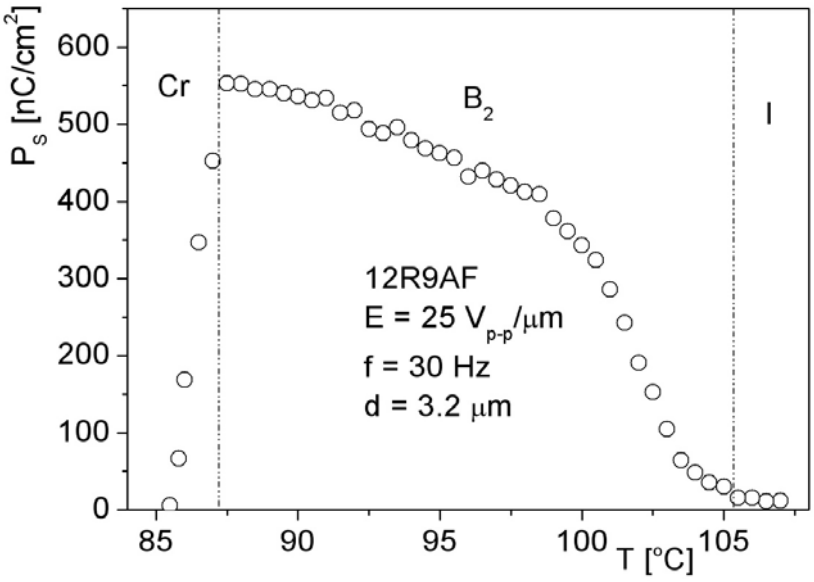

Fig. 4.35. Spontaneous polarization of 12R9AF B_2 phase vs. temperature obtained for E = 25 $V_{p-p}/\mu m$, f = 30 Hz, d = 3.2 μm

The B_2 phase of 14OSOR is antiferroelectric one as for 12OSOR and 12R9AF mixture (Fig. 4.36.).

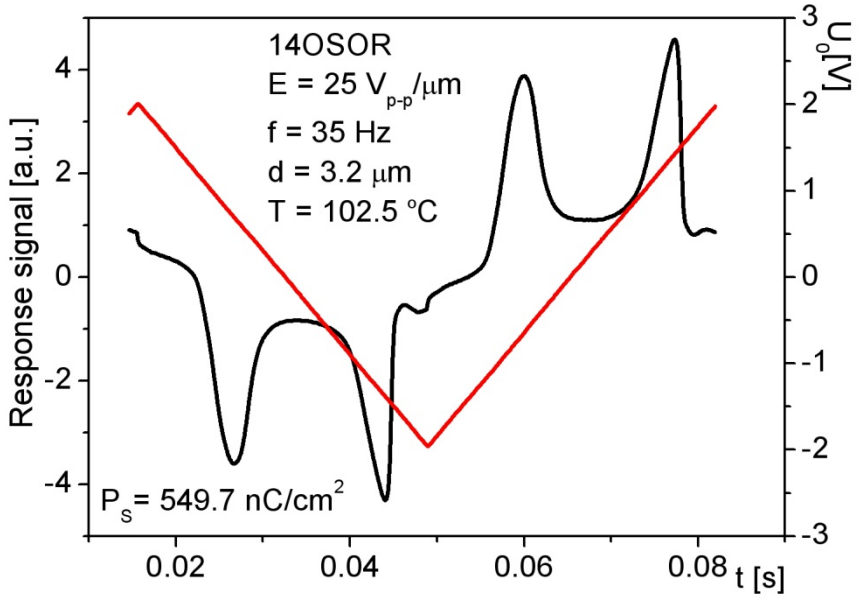

Fig. 4.36. Triangular driving voltage (right-hand side scale) applied vs. time and reversal current spectrum (left-hand side scale) of 14OSOR B_2 phase for E = 25 $V_{p-p}/\mu m$, f = 35 Hz, d = 3.2 μm and T = 102.5 °C

Measurements of polarization dependence on electric field applied to the sample were done in the temperature of 97 °C and 107 °C and frequency of the signal of 15 Hz. The electric field needed for polarization to be saturated, in both cases, is about 25 $V_{p\text{-}p}/\mu m$ as for 12R9AF mixture (Fig. 4.37. and 4.38.).

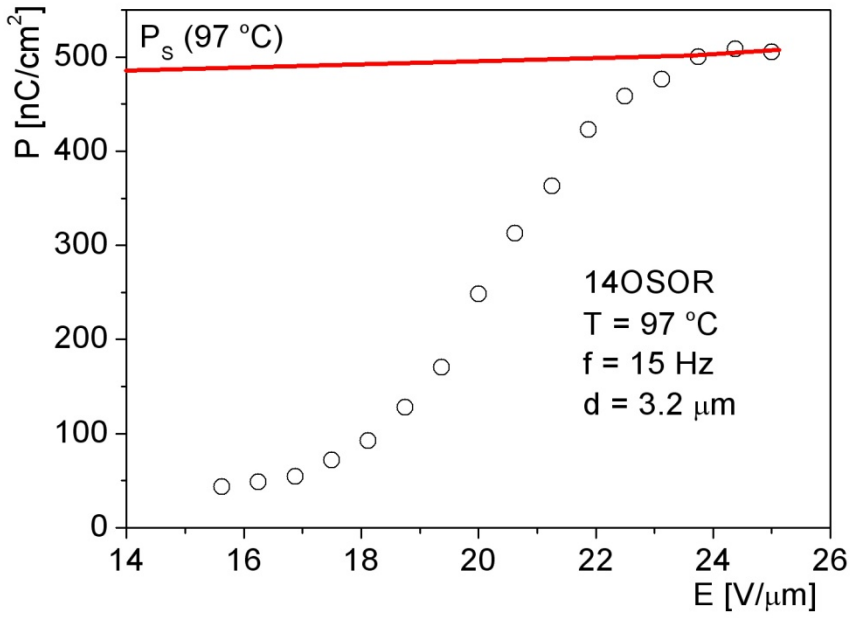

Fig. 4.37. Polarization vs. electric field for 14OSOR B_2 phase (T = 97 °C)

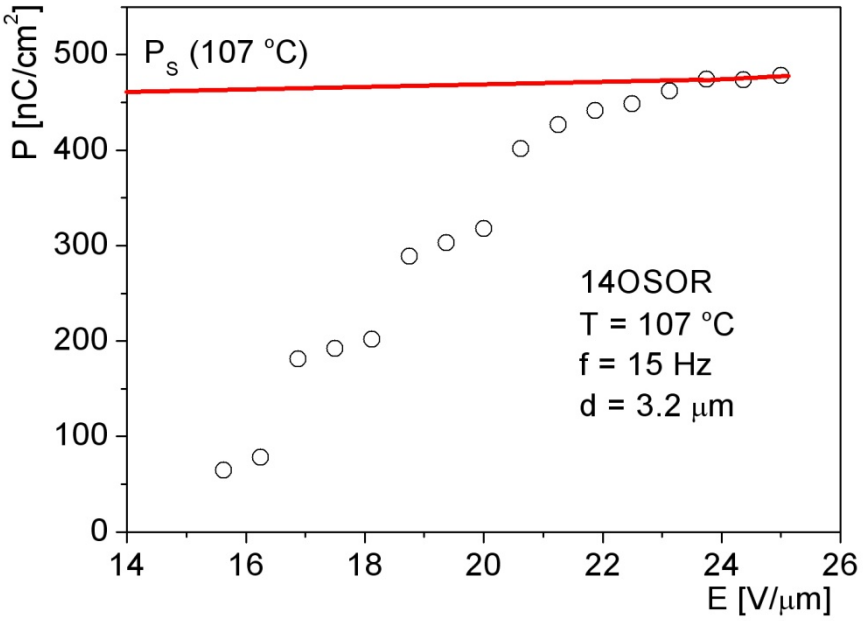

Fig. 4.38. Polarization vs. electric field for 14OSOR B_2 phase (T = 107 °C)

Spontaneous polarization of B_2 phase of 14OSOR is about 550 nC/cm^2, it is higher than for 12R9AF mixture (500 nC/cm^2) and lower than for 12OSOR compound (600 nC/cm^2). Measurements were performed for the electric field of 25 $V_{p\text{-}p}$/μm (when the polarization is saturated) and for signal frequency of 15 Hz (Fig. 4.39.).

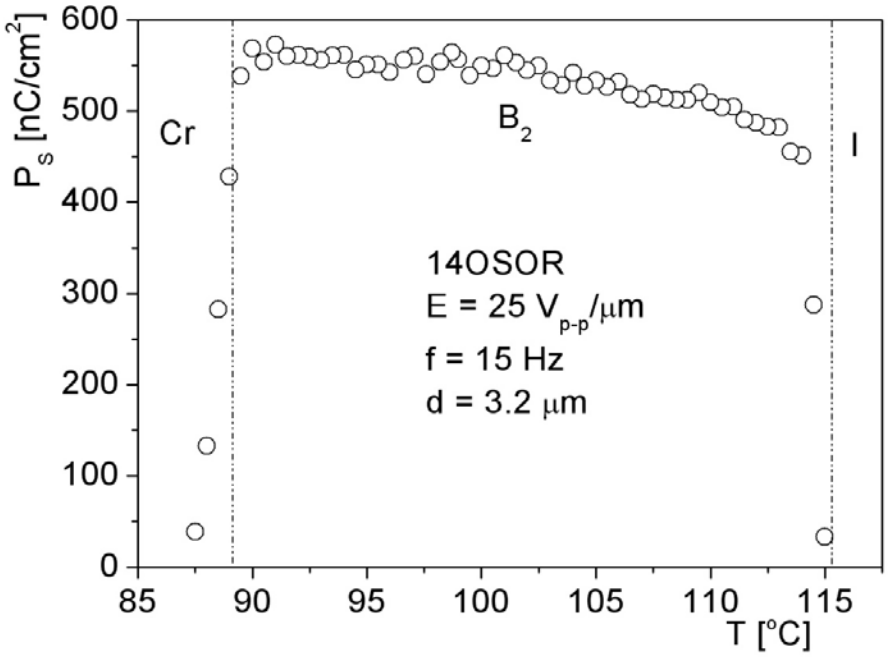

Fig. 4.39. Spontaneous polarization of 14OSOR B_2 phase vs. temperature measured for E = 25 $V_{p\text{-}p}$/μm, f = 15 Hz, d = 3.2 μm

4.5. Dielectric Measurements

4.5.1. Dielectric relaxation processes

As it was mentioned before, (see section 3.4.) using frequency domain dielectric spectroscopy (FDDS) it was possible to measure two principal components – $\varepsilon^*_{\perp 1}(\nu)$ and $\varepsilon^*_{\perp 2}(\nu)$ of the dielectric permittivity. There were some difficulties with choosing the right fitting function for the low frequency part of the spectrum, where conductivity contribution to the dielectric loss plays an important role. At low frequencies the dispersion behaves rather unusual – it is linear on the logarithmic scale for all investigated materials. The best fitting function occurred to be a function with extra parameters (Eq. 2.6).

Dielectric measurements were carried out using AWAT HG electrooptic cells with gold electrodes and thickness of 5 μm for all materials. Figs. 4.40. – 4.47. show 3D graphs of dielectric permittivity (a) and dielectric loss (b) vs. frequency for 9OSOR, 12OSOR, 12R9AF and 14OSOR, respectively.

9OSOR

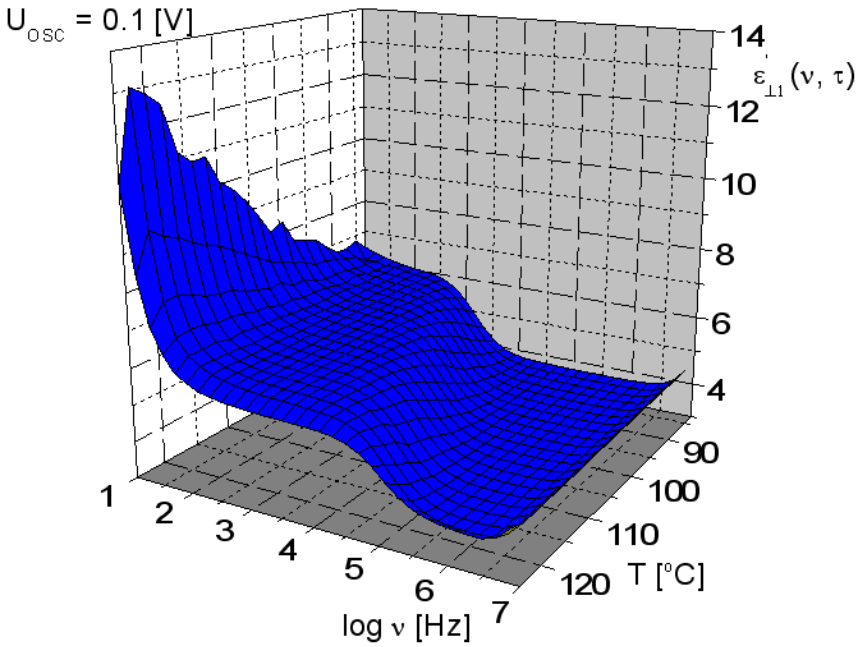

Fig. 4.40. (a) Dielectric permittivity vs. frequency for 9OSOR

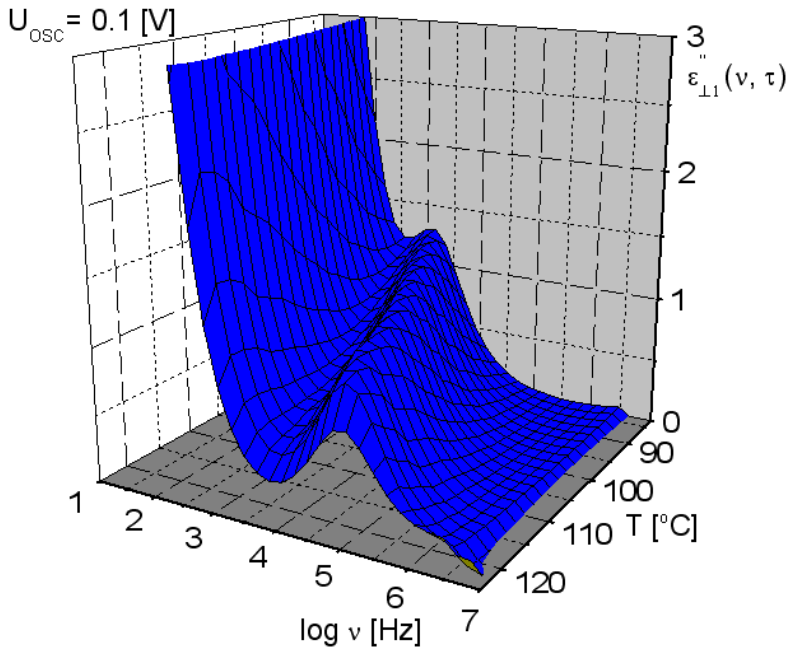

Fig. 4.40. (b) Dielectric loss vs. frequency for 9OSOR

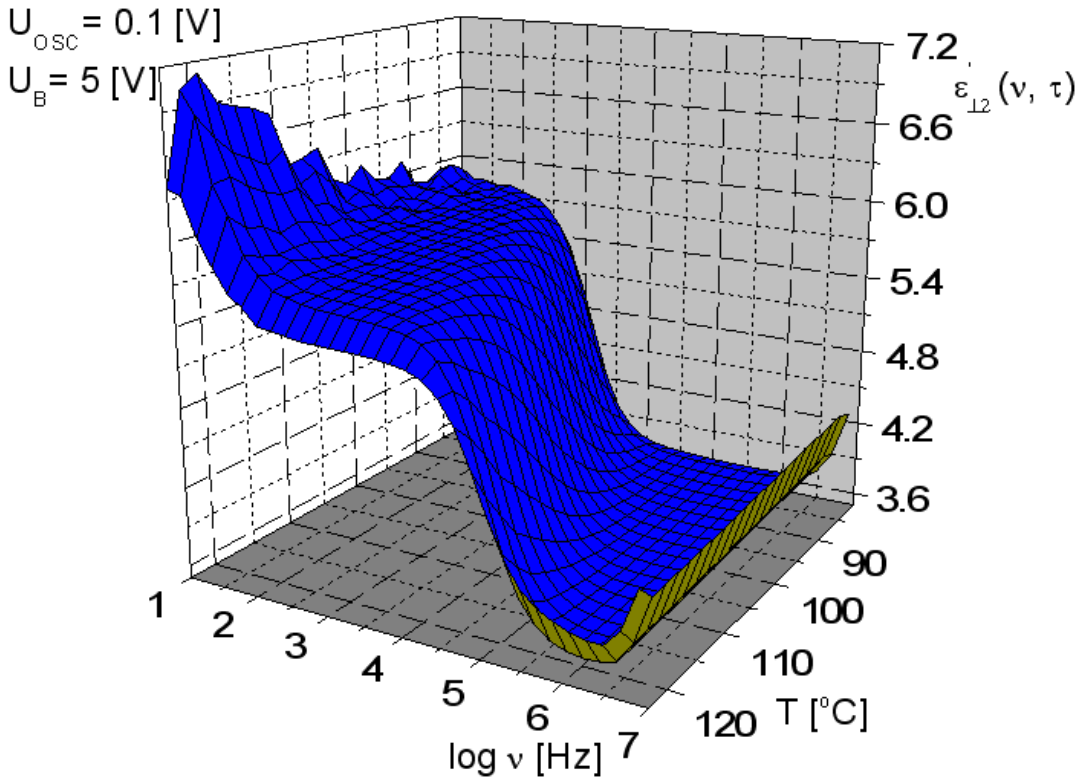

Fig. 4.41. (a) Dielectric permittivity vs. frequency measured under the bias voltage of $U_B = 5$ V for 9OSOR

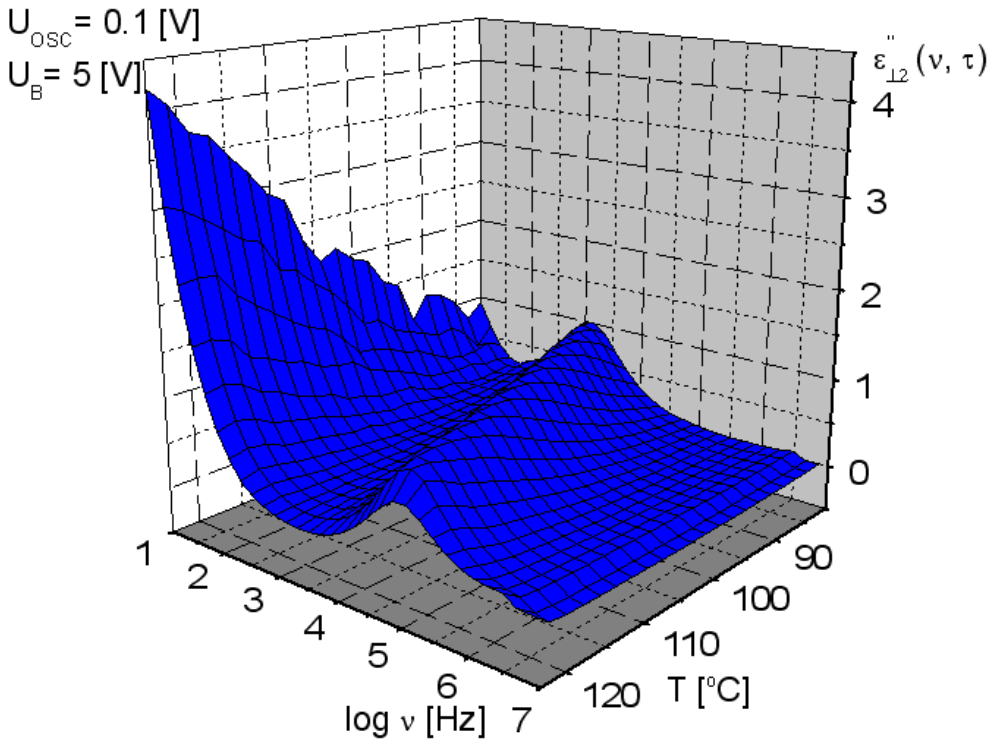

Fig. 4.41. (b) Dielectric loss vs. frequency obtained under the bias voltage of $U_B = 5$ V for 9OSOR

12OSOR

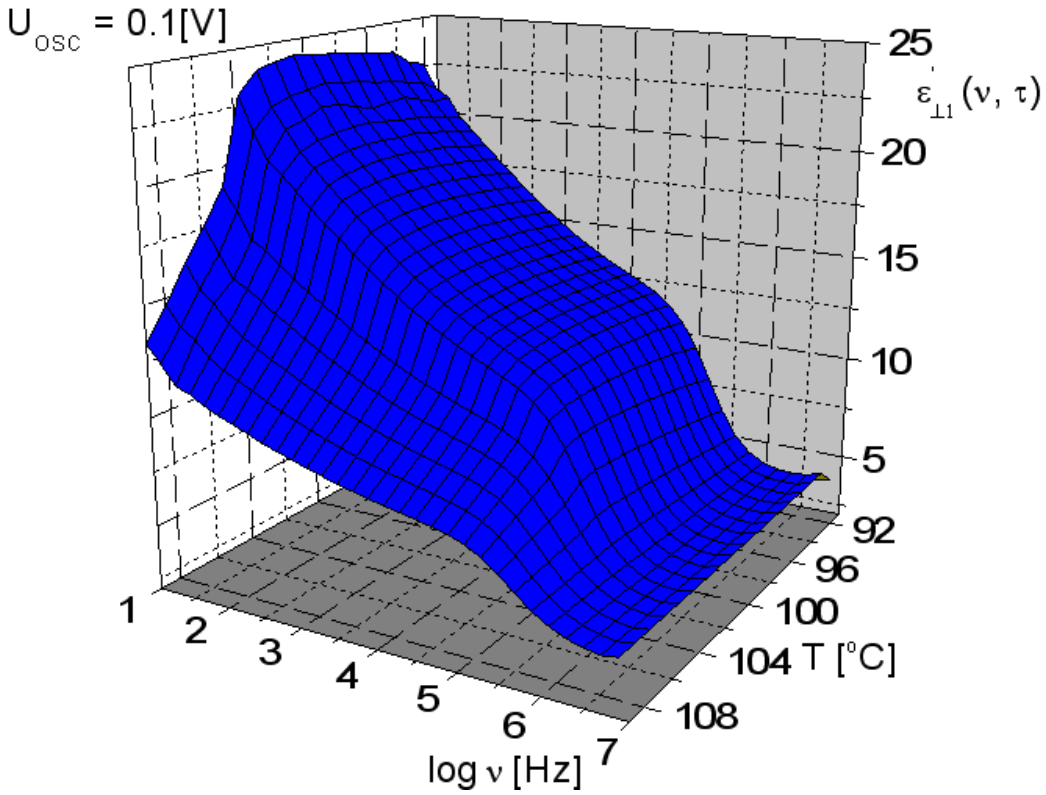

Fig. 4.42. (a) Dielectric permittivity vs. frequency for 12OSOR

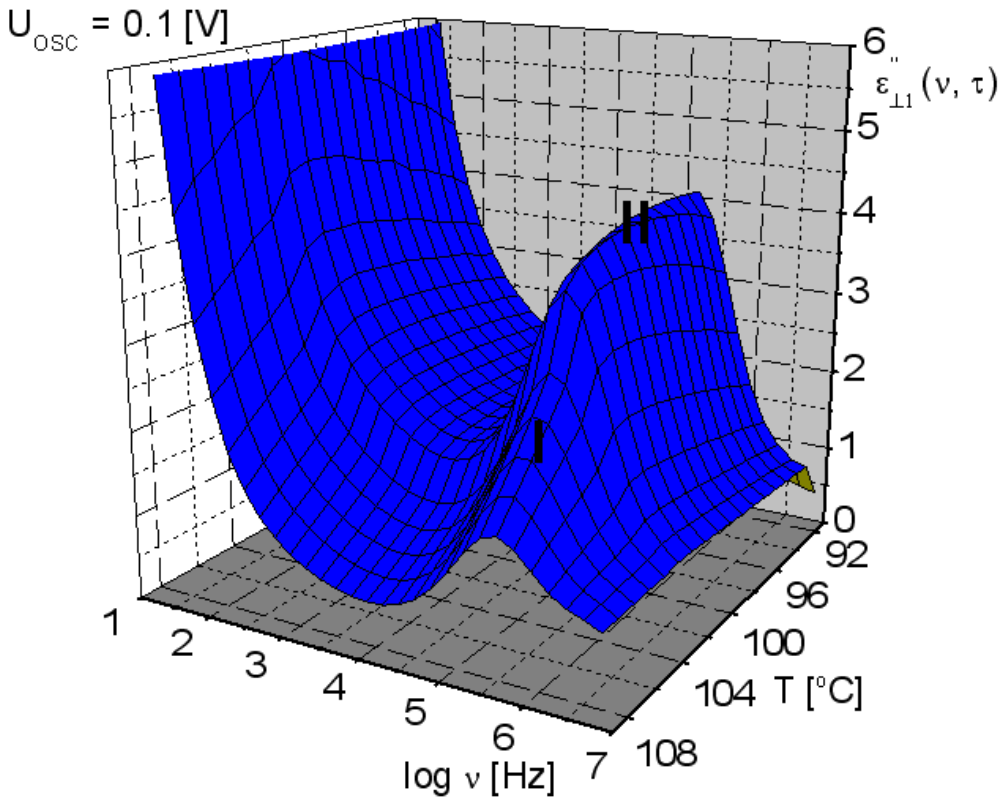

Fig. 4.42. (b) Dielectric loss vs. frequency for 12OSOR

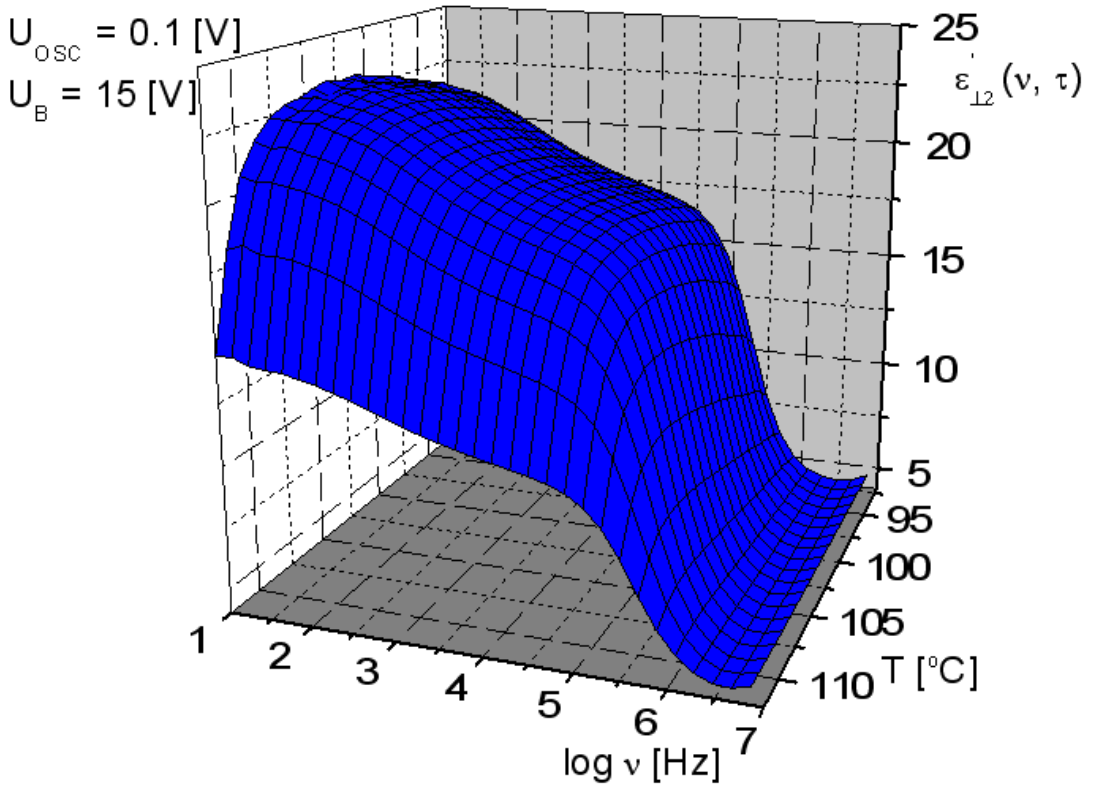

Fig. 4.43. (a) Dielectric permittivity vs. frequency acquired under the bias voltage of $U_B = 15$ V for 12OSOR

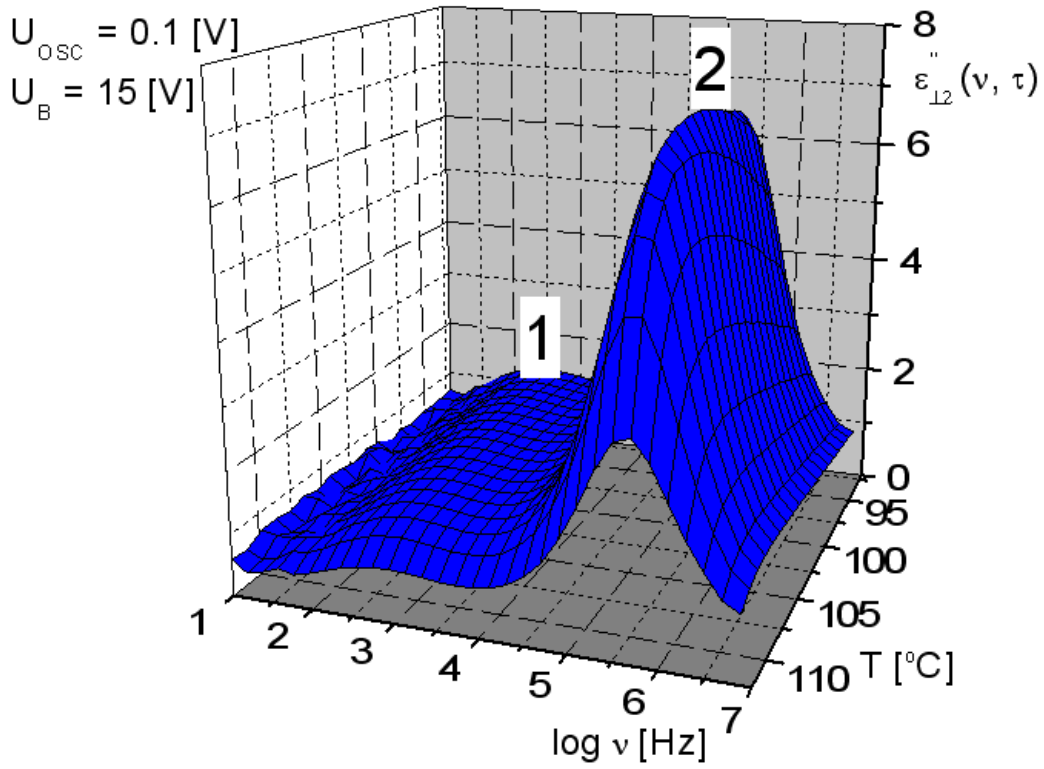

Fig. 4.43. (b) Dielectric loss vs. frequency measured under the bias voltage of $U_B = 15$ V for 12OSOR

12R9AF

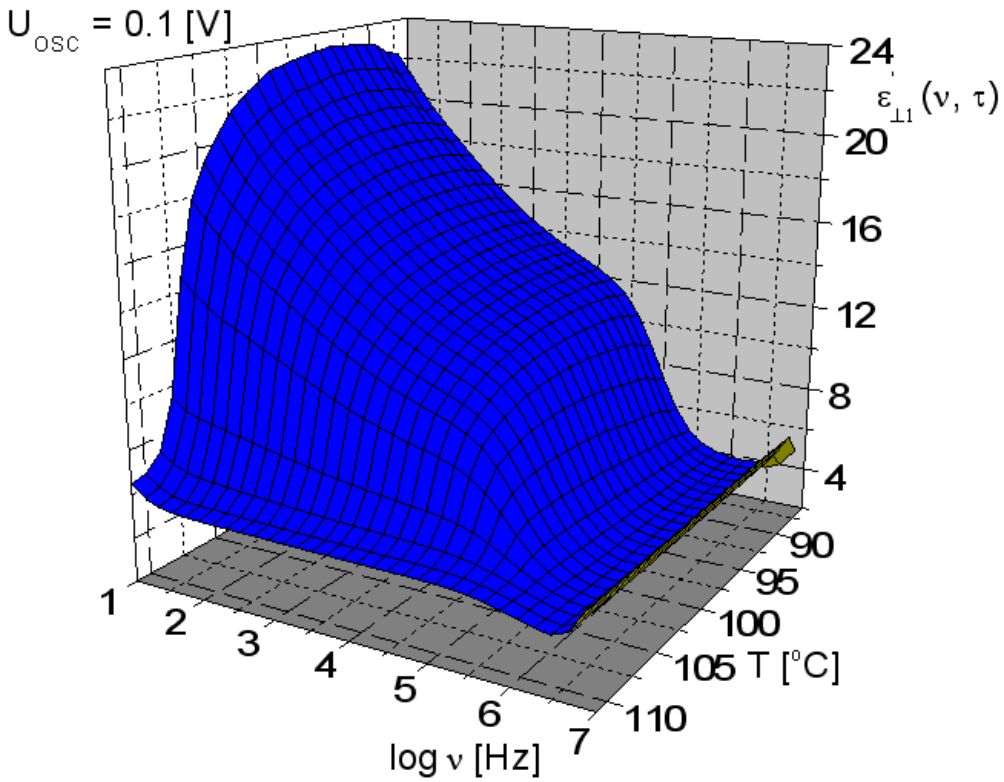

Fig. 4.44. (a) Dielectric permittivity vs. frequency for 12R9AF

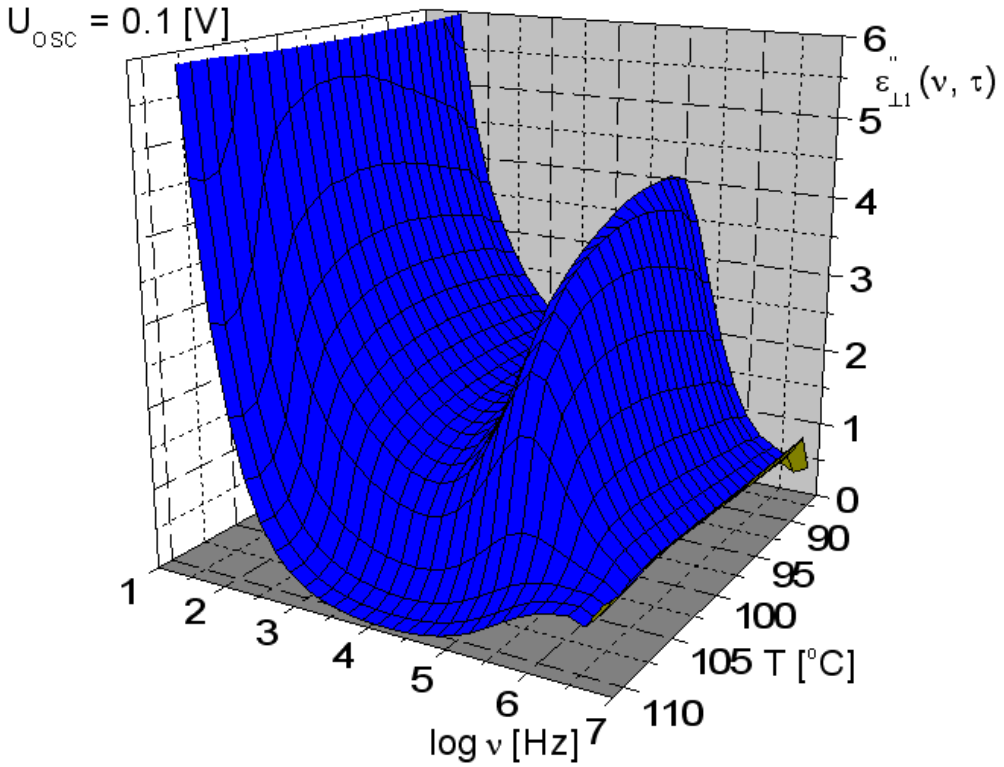

Fig. 4.44. (b) Dielectric loss vs. frequency for 12R9AF

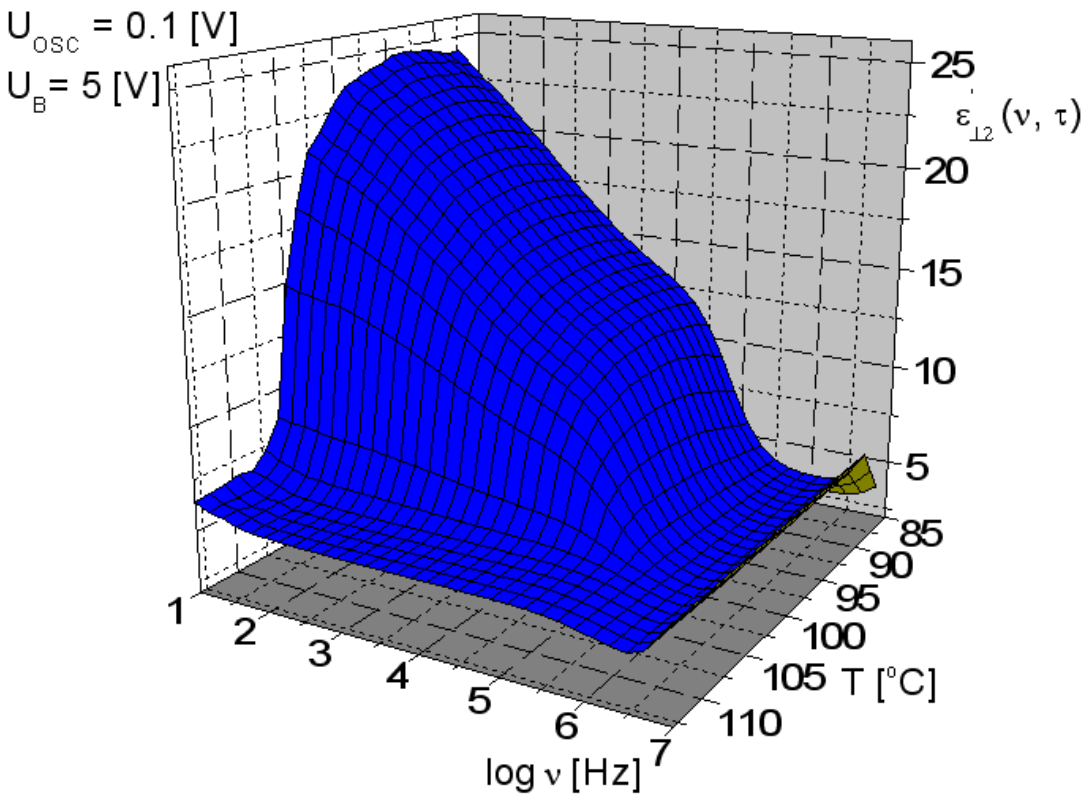

Fig. 4.45. (a) Dielectric permittivity vs. frequency obtained under the bias voltage of $U_B = 5$ V for 12R9AF

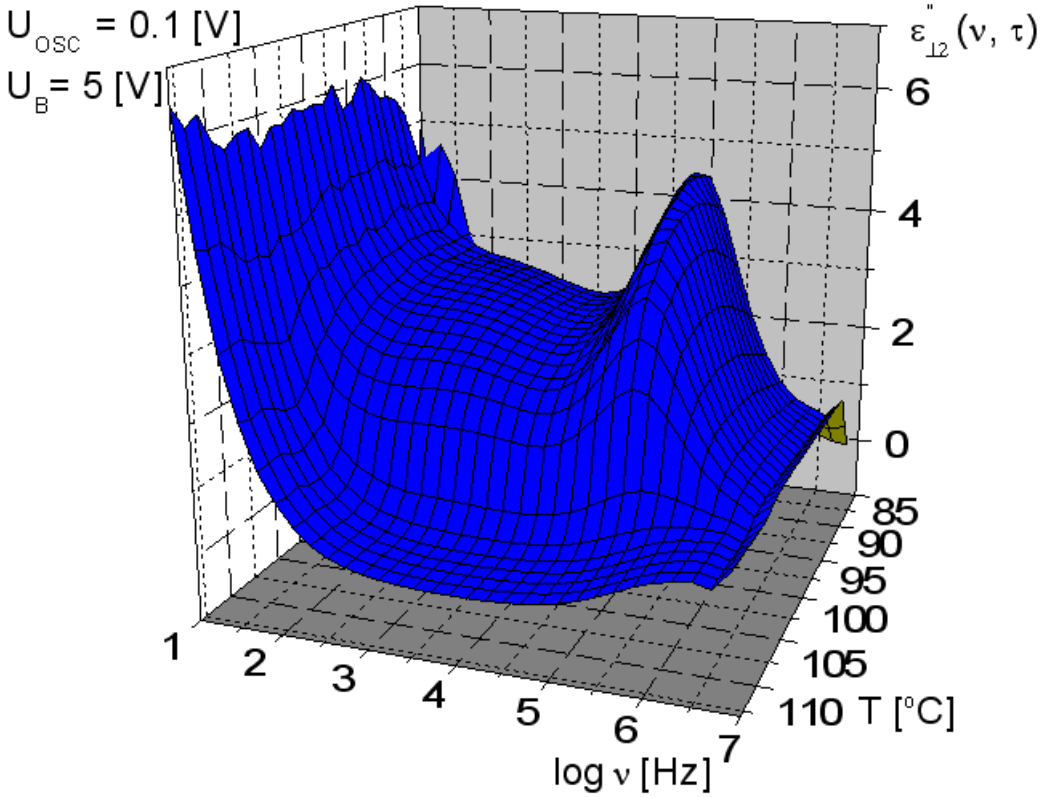

Fig. 4.45. (b) Dielectric loss vs. frequency acquired under the bias voltage of $U_B = 5$ V for 12R9AF

14OSOR

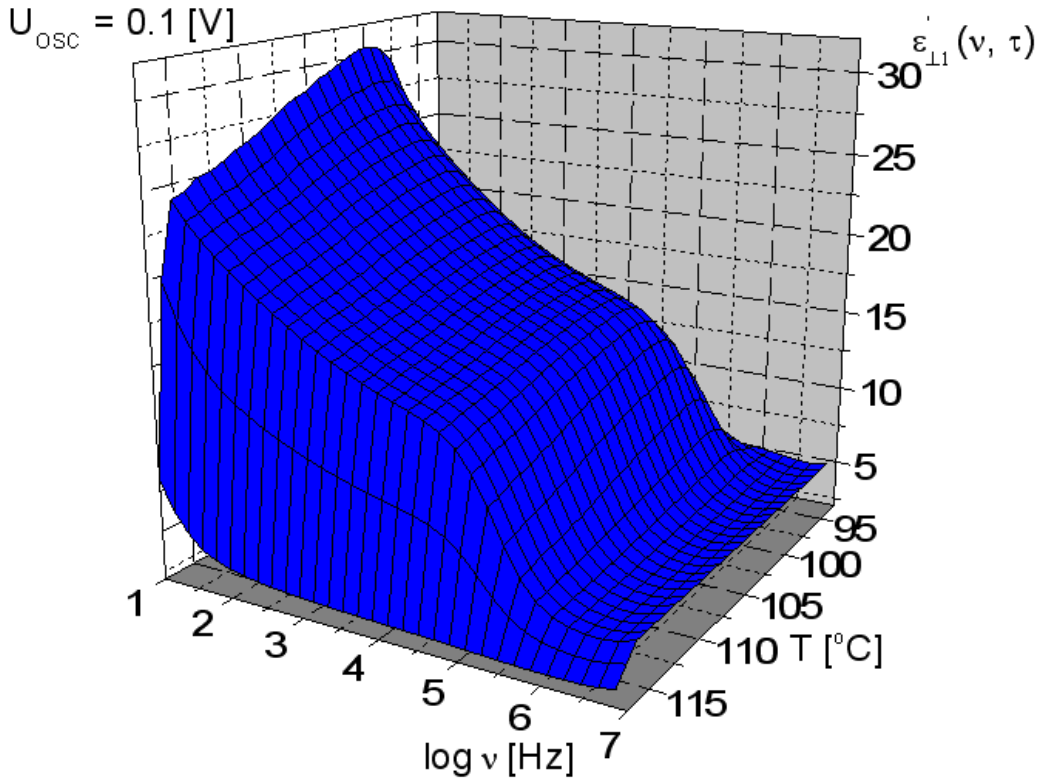

Fig. 4.46. (a) Dielectric permittivity vs. frequency for 14OSOR

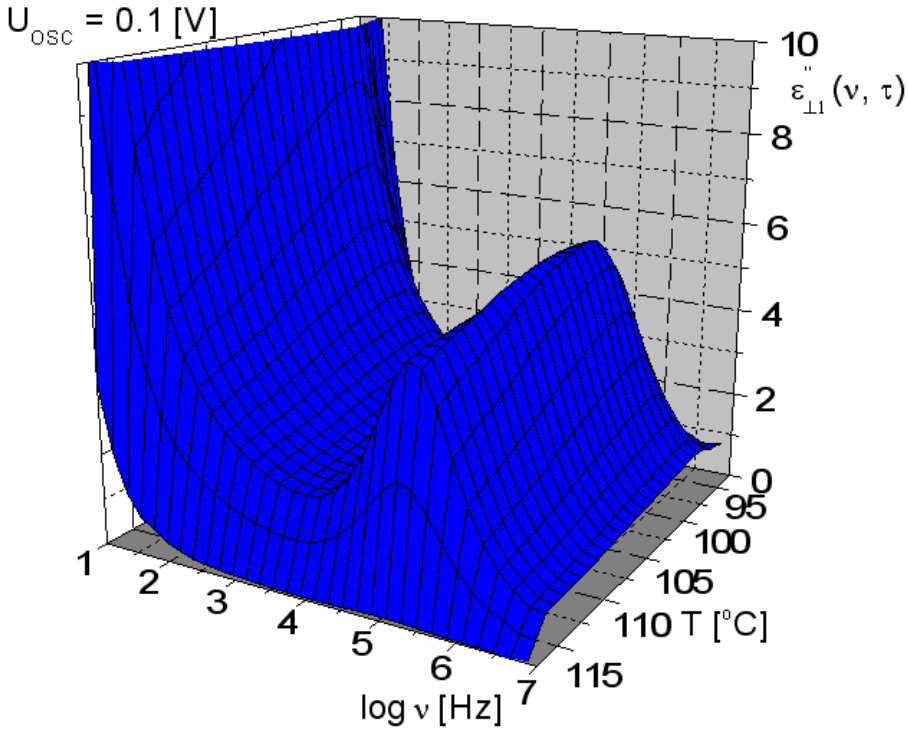

Fig. 4.46. (b) Dielectric loss vs. frequency for 14OSOR

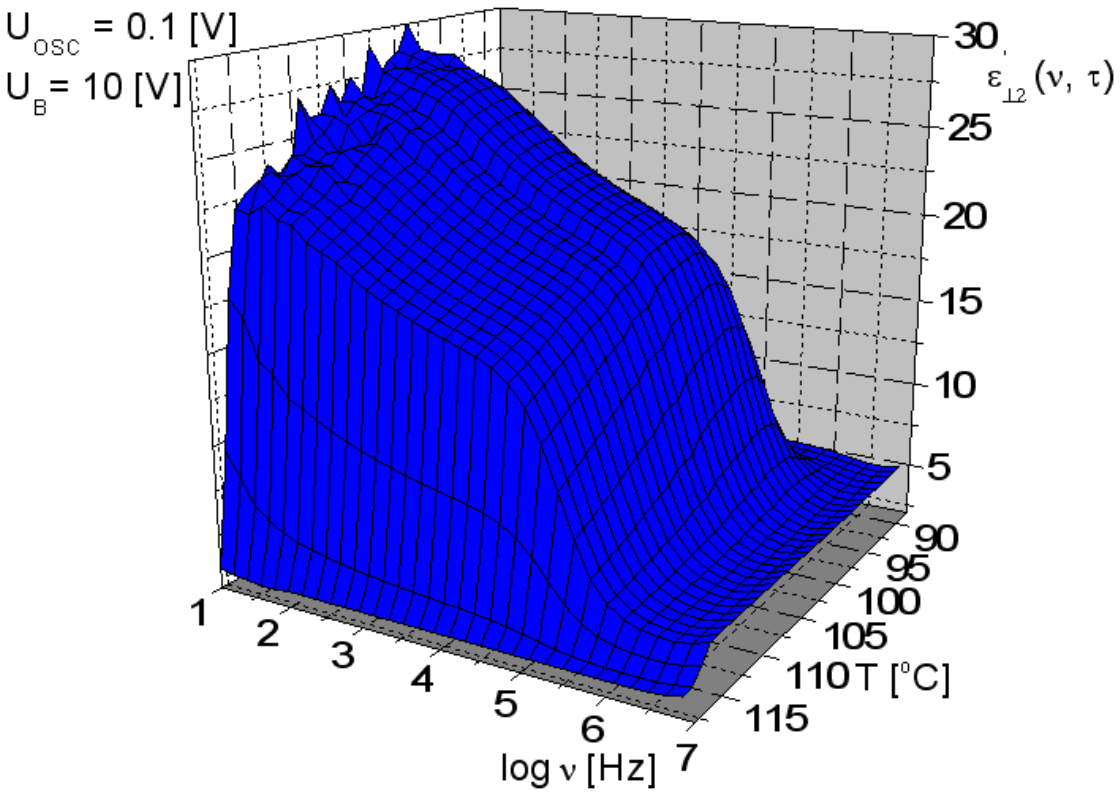

Fig. 4.47. (a) Dielectric permittivity vs. frequency measured under the bias voltage of $U_B = 10$ V for 14OSOR

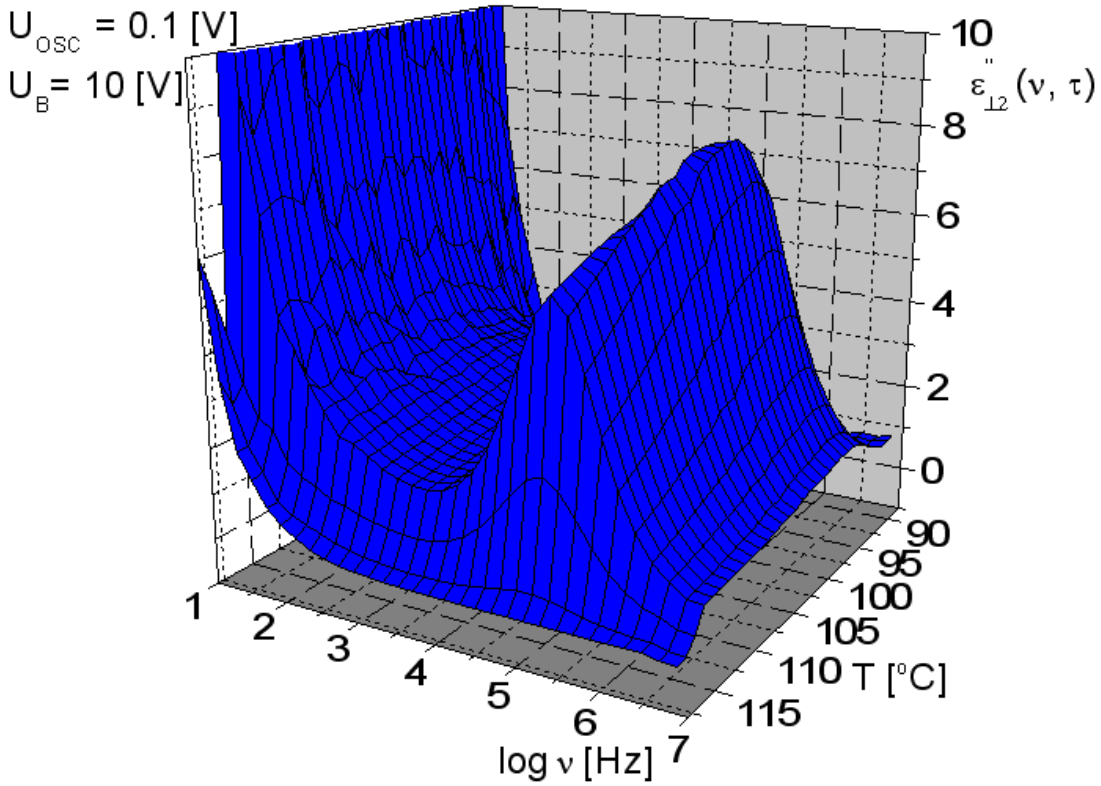

Fig. 4.47. (b) Dielectric loss vs. frequency obtained under the bias voltage of $U_B = 10$ V for 14OSOR

Dielectric spectra measured for B_1 phase of 9OSOR without and with bias voltage shows, that this phase in both cases exhibits only one Debye-type dielectric relaxation process connected with molecule reorientation around the short axes.

As for B_2 phase of 12OSOR, 12R9AF and 14OSOR dielectric spectra measured with bias voltage shows two well separated relaxation processes. In the low frequency range the relaxation process is connected with fluctuations of ferroelectric domains revealing in homeotropic structure of B_2 phase. The relaxation process in the high frequency range appearing also without bias field for B_2 phase of 12R9AF and 14OSOR is connected with molecular reorientation around the long axis. For 12OSOR this process is complex: in the high temperature range of B_2 phase it is connected with reorientation of molecules around the short axis (process **I** in Fig. 4.42. (b)), whereas in the low temperature range – around the long axis (process **II** in Fig. 4.42. (b)) [27]. Dielectric measurements showed that at low frequencies there is electrode polarization contribution to the dielectric permittivity and the electrical ionic conductivity contribution to the dielectric loss for all materials studied.

In Figs. 4.48. – 4.51. (a) and (b) one can see an exemplary dielectric spectra and Cole – Cole plots for 9OSOR, 12OSOR and 12R9AF, respectively, with and without bias voltage. Tables I – IV show fitting parameters for relaxation processes observed in investigated phases with and without bias field.

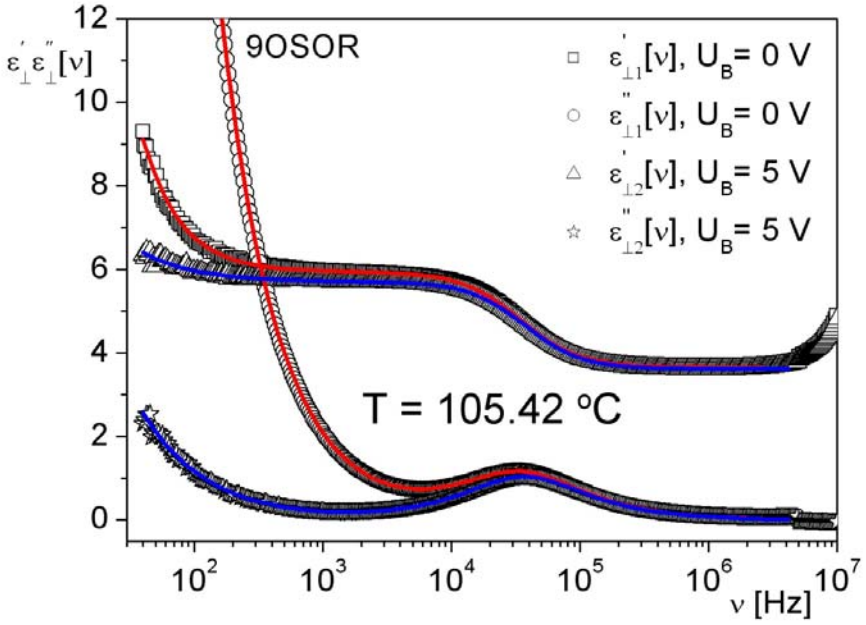

Fig. 4.48. (a) Exemplary dielectric spectrum of 9OSOR B_1 phase measured with and without bias voltage in the temperature of 105.42 ^oC

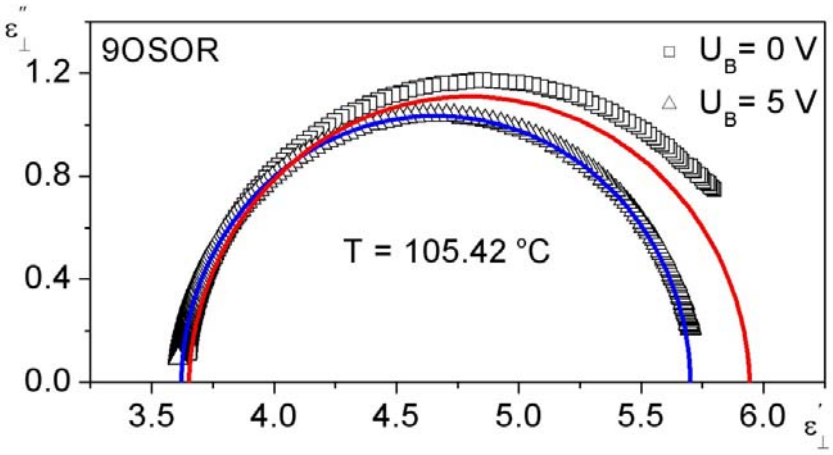

Fig. 4.48. (b) Cole – Cole plot of the dielectric spectrum for 9OSOR B_1 phase obtained with and without bias voltage in the temperature of 105.42 °C

9OSOR		T = 105.42 °C					
U_B [V]	Process	ε(0)	τ [s]	α	ε(∞)	σ [S/m]	M
U_B = 5	---------	5.7	4.3 E-6	0.003	3.6	2.9 E-9	0.9
U_B = 0	---------	5.9	4.7 E-6	0.021	3.7	9.8 E-8	0.98

Table I. Fitting parameters for two relaxation processes shown in Fig. 4.47. (a) and (b) for B_1 phase of 9OSOR

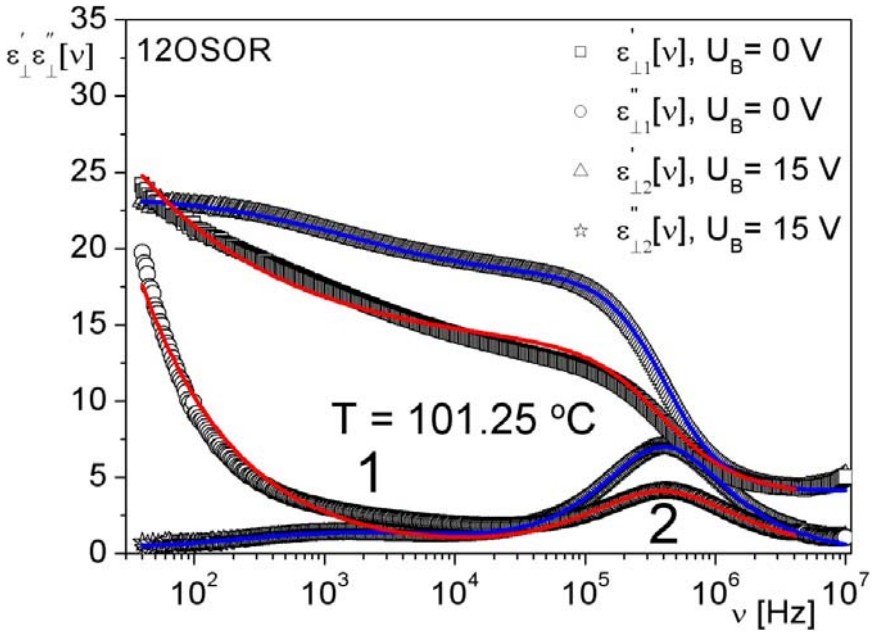

Fig. 4.49. (a) Exemplary dielectric spectrum of 12OSOR B_2 phase studied with and without bias voltage in the temperature of 101.25 °C

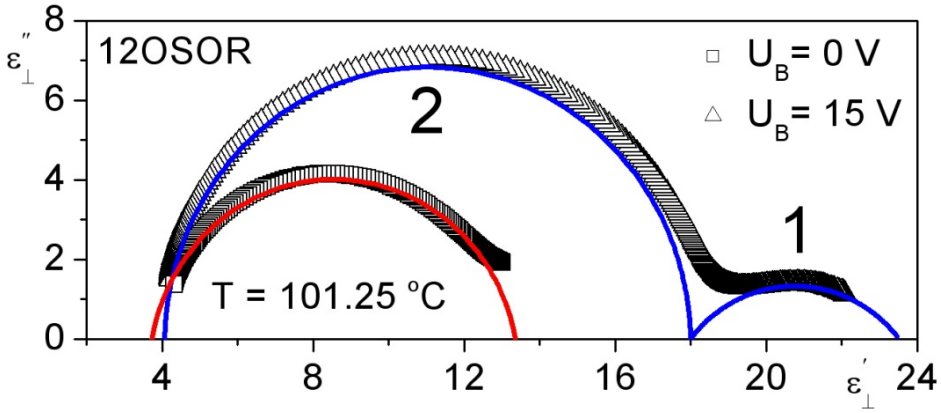

Fig. 4.49. (b) Cole – Cole plot of the dielectric spectrum for 12OSOR B_2 phase obtained with and without bias voltage in the temperature of 101.25 °C

12OSOR		T = 101.25 °C					
U_B [V]	Proces	ε(0)	τ [s]	α	ε(∞)	σ [S/m]	M
U_B = 15	------- 1	23.5	1 E-4	0.42	18	0	1
	------- 2	18	4 E-7	0.01	4.1	6 E-11	1
U_B = 0	----------	13.4	4 E-7	0.12	3.7	3.9 E-9	0.6

Table II. Fitting parameters for three relaxation processes shown in Fig. 4.48. (a) and (b) for B_2 phase of 12OSOR

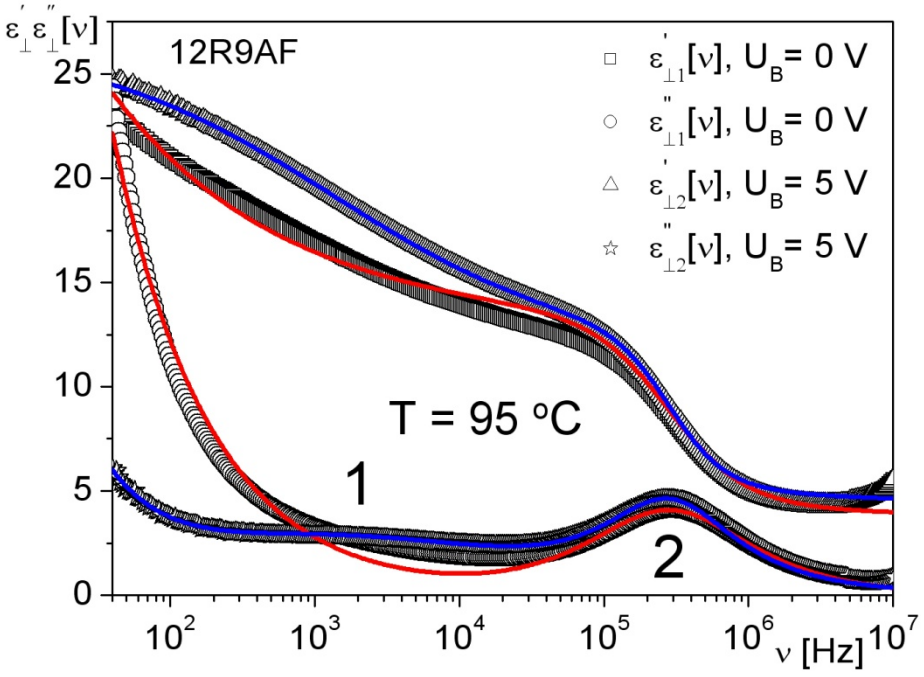

Fig. 4.50. (a) Exemplary dielectric spectrum of B_2 phase of 12R9AF with and without bias voltage in the temperature of 95 °C

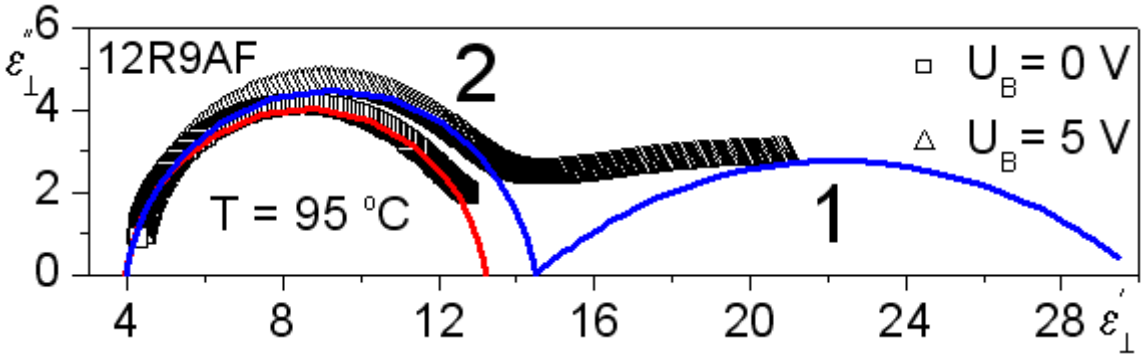

Fig. 4.50. (b) Cole – Cole plot of the dielectric spectrum for 12R9AF B_2 phase measured with and without bias voltage in the temperature of 95 °C

12R9AF		T = 95 °C					
U_B [V]	Proces	ε(0)	τ [s]	α	ε(∞)	σ [S/m]	M
U_B = 15	------- 1	30	1.2 E-4	0.5	14.5	0	1
	------- 2	14.5	5.6 E-7	0.1	4	6.3 E-10	1
U_B = 0	----------	13	5.6 E-7	0.09	3.8	7.8 E-9	0.7

Table III. Fitting parameters for three relaxation processes shown in Fig. 4.49. (a) and (b) for B_2 phase of 12R9AF

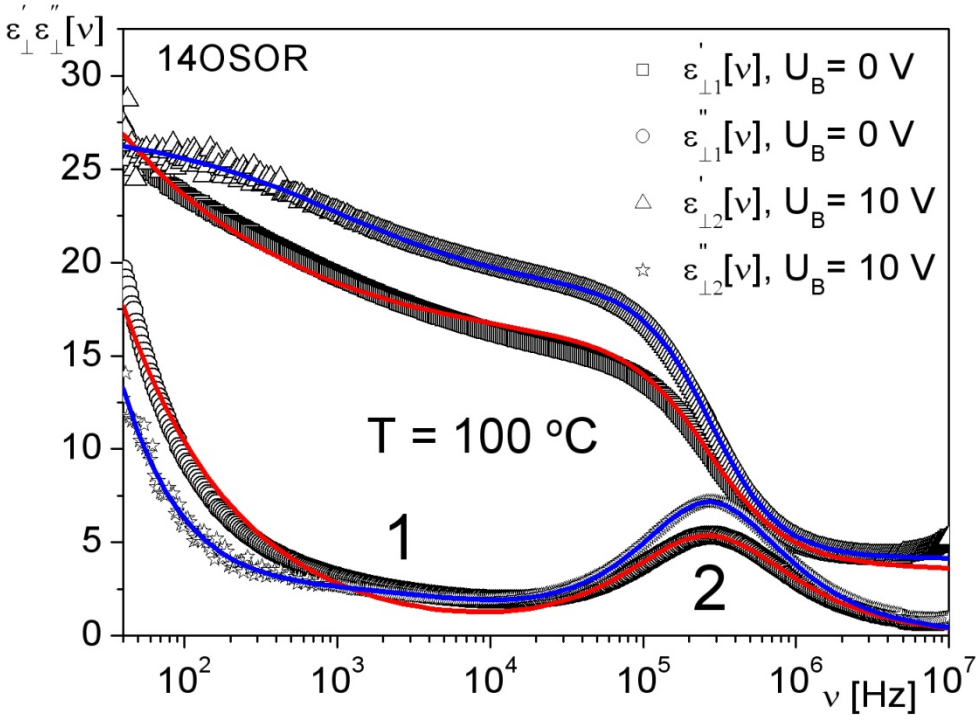

Fig. 4.51. (a) Exemplary dielectric spectrum of 14OSOR B_2 phase obtained with and without bias voltage in the temperature of 100 °C

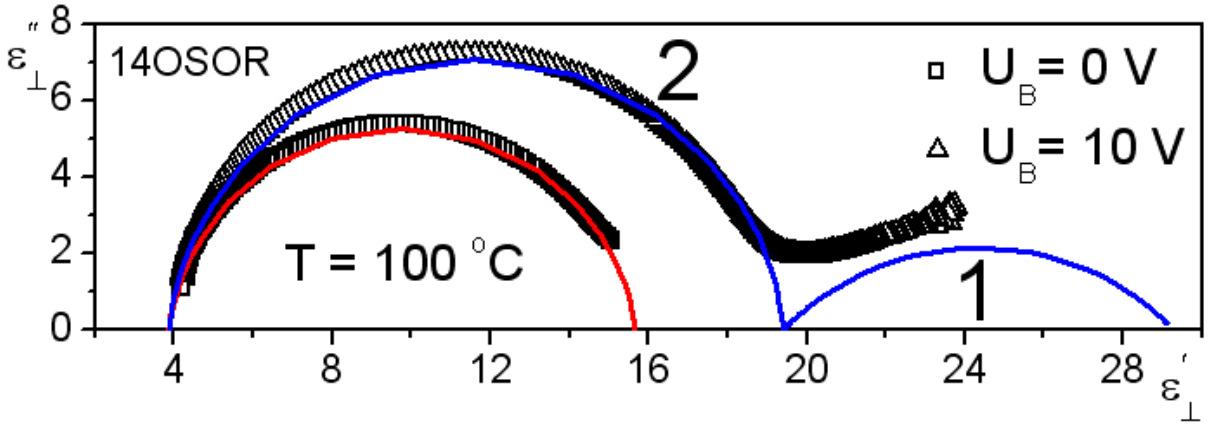

Fig. 4.51. (b) Cole – Cole plot of the dielectric spectrum for 14OSOR B_2 phase acquired with and without bias voltage in the temperature of 100 °C

14OSOR		T = 100 °C					
U_B [V]	Proces	ε(0)	τ [s]	α	ε(∞)	σ [S/m]	M
U_B = 10	------- 1	29.3	1.3 E-4	0.48	19.4	0	1
	------- 2	19.4	6 E-7	0.06	3.9	3 E-8	1
U_B = 0	---------	15.7	5.9 E-7	0.07	3.9	3.8 E-9	0.6

Table III. Fitting parameters for three relaxation processes shown in Fig. 4.50. (a) and (b) for B_2 phase of 14OSOR

As seen M parameters obtained for all materials without bias field are smaller than 1. One should notice that for calamitic LCs M = 1 as well as for the systems studied in this work under bias voltage. For all materials $\varepsilon(\infty)$ with and without bias field is distinctly greater than n^2, so one can assume that there is another molecular process in gigahertz range, maybe connected with intramolecular reorientations of polar groups and reorientation of mesogenic units.

Figs. 4.52. (a) and (b) show Arrhenius plots for B_1 phase of 9OSOR with (a) and without bias voltage (b). Like it was mentioned before, with as well as without bias voltage the process is connected with reorientation of molecules around the short axes and its activation energy in both cases is equal to 112 kJ/mol.

For B_2 phase of 12OSOR activation energy of the process connected with fluctuations of domains is equal to 62 kJ/mol with bias voltage (Fig. 4.53. (a)), whereas for the process connected with reorientation around the long molecular axis it is of about 45 kJ/mol with and without bias voltage (Figs. 4.53. (a) and (b)). Activation energy for reorientation around the short axis process – observed in the pretransition region – is equal to 102 kJ/mol (Fig. 4.53.

(b)). One should explain, that low frequency relaxation process (fluctuations of domains) exhibits a distribution of the relaxation times ($\alpha = 0.48$), so the adequate activation energy has not a simple interpretation.

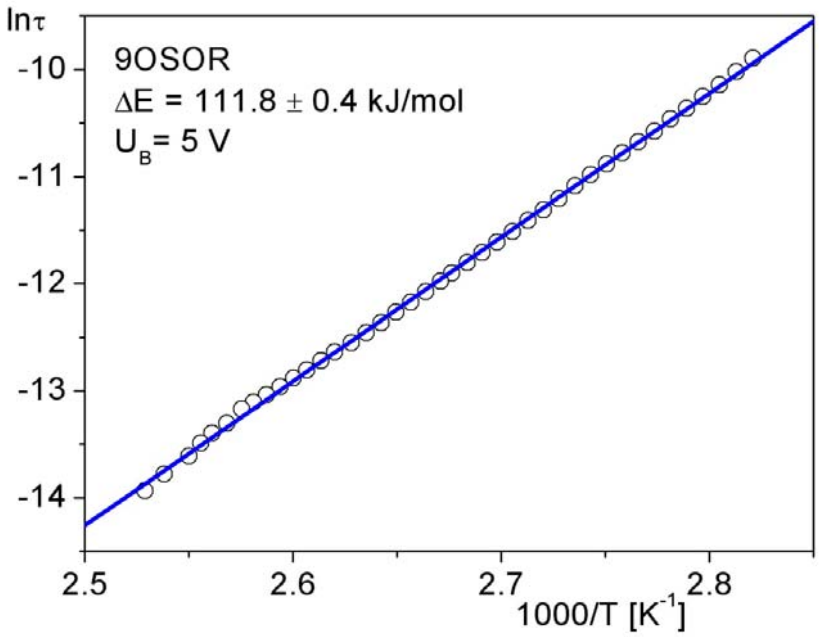

Fig. 4.52. (a) Arrhenius plot for the dielectric relaxation process for 9OSOR B_1 phase observed with bias voltage equal to 5 V

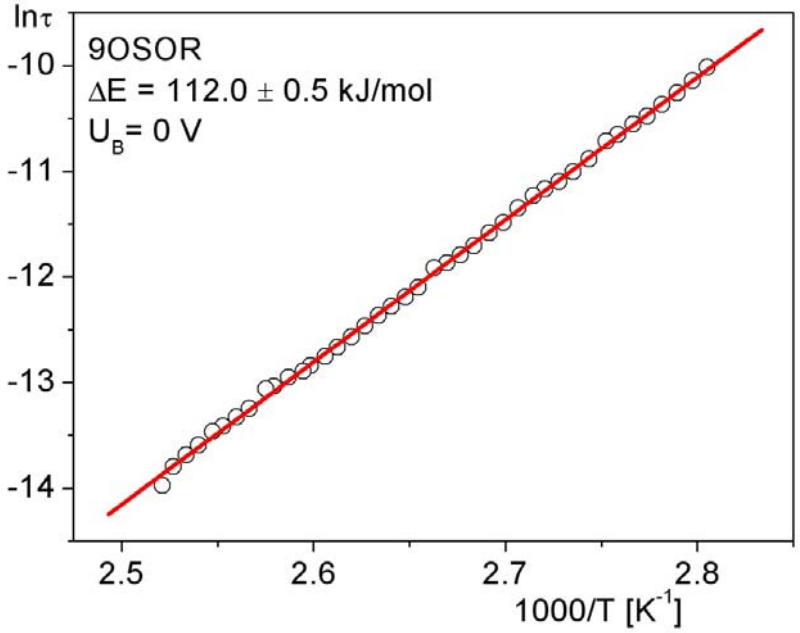

Fig. 4.52. (b) Arrhenius plot for the dielectric relaxation process for 9OSOR B_1 phase observed without bias voltage

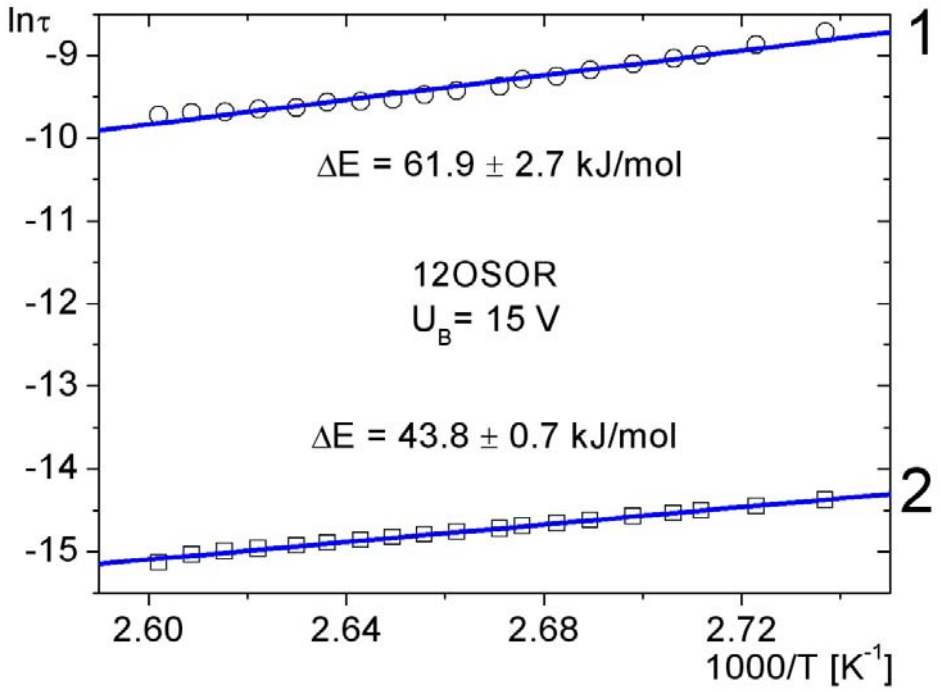

Fig. 4.53. (a) Arrhenius plot for the dielectric relaxation process for 12OSOR B_2 phase observed with bias voltage equal to 15 V

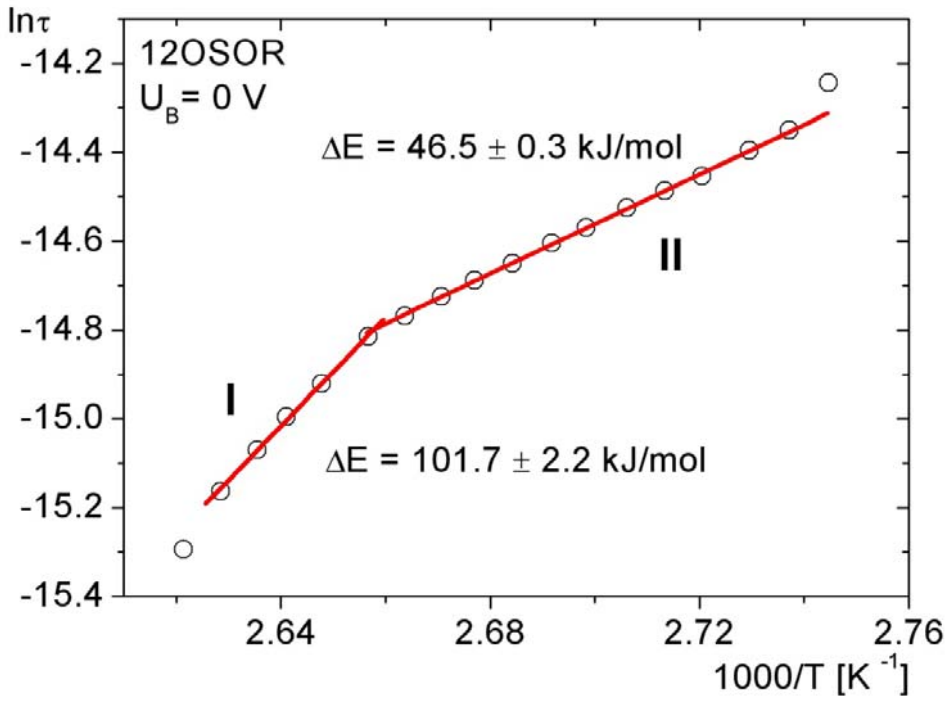

Fig. 4.53. (b) Arrhenius plot for the dielectric relaxation process for 12OSOR B_2 phase observed without bias voltage

For B_2 phase of the mixture, the activation energy for the process connected with fluctuations of domains is equal 61 kJ/mol (Fig. 4.54. (a)) just like for pure compound.

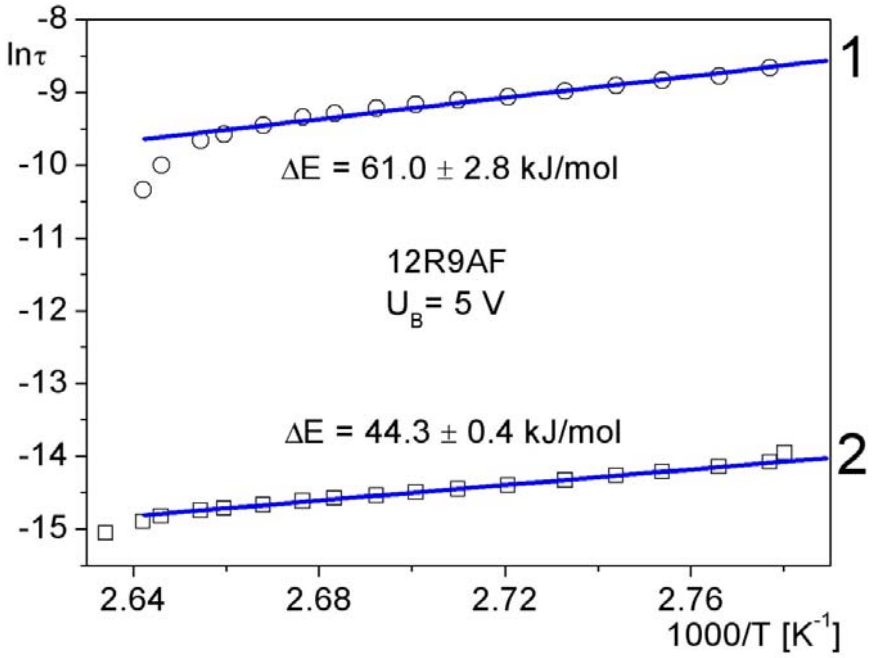

Fig. 4.54. (a) Arrhenius plot for the dielectric relaxation process for 12R9AF B_2 phase observed with bias voltage equal to 5 V

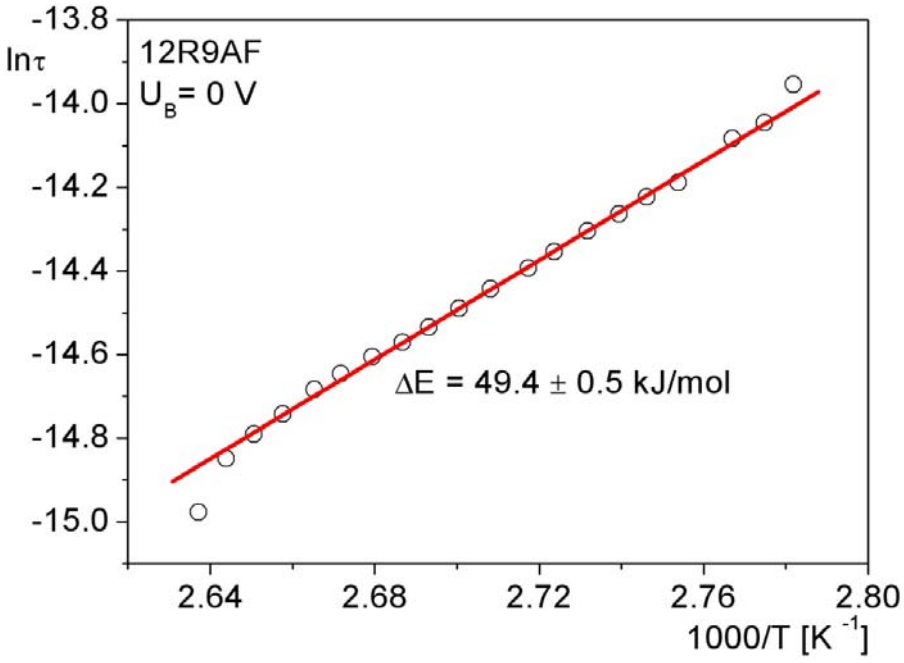

Fig. 4.54. (b) Arrhenius plot for the dielectric relaxation process for 12R9AF B_2 phase observed without bias voltage

For process connected with the reorientation around the long axis it is about 48 kJ/mol with and without bias field (Figs. 4.54. (a) and (b)).

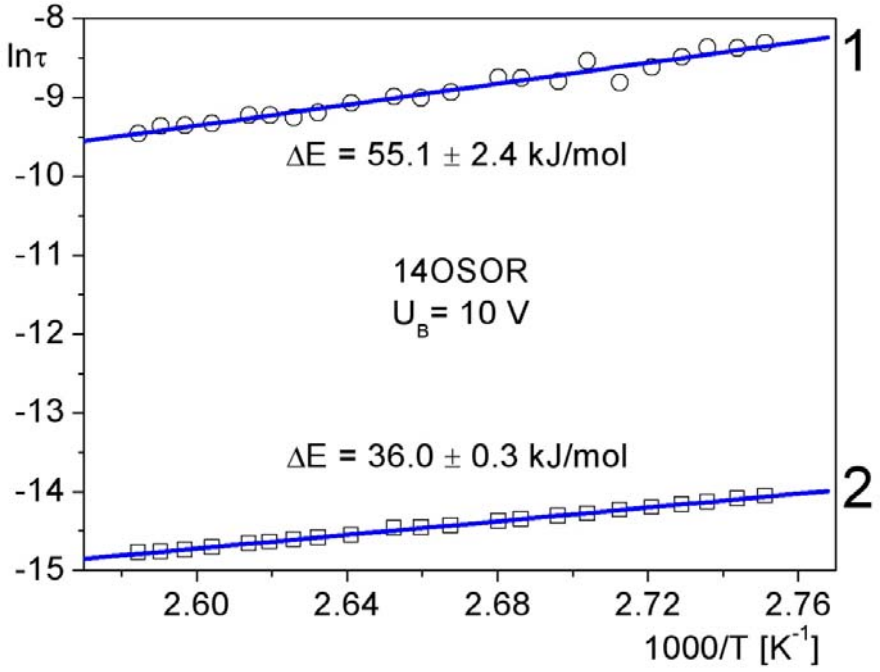

Fig. 4.55. (a) Arrhenius plot for the dielectric relaxation process for 14OSOR B_2 phase observed with bias voltage equal to 10 V

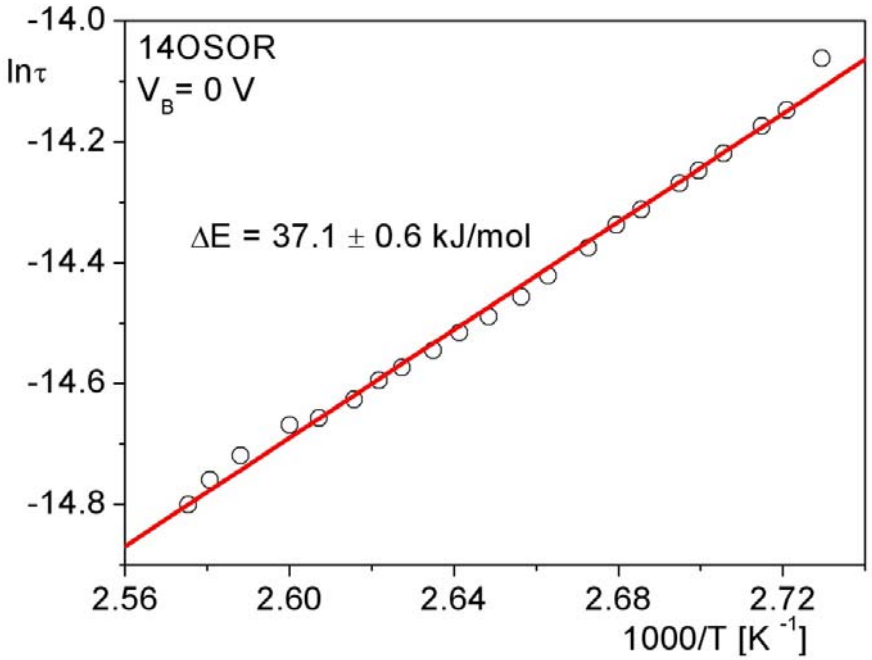

Fig. 4.55. (b) Arrhenius plot for the dielectric relaxation process for 14OSOR B_2 phase observed without bias voltage

Activation energy of the process connected with fluctuations of domains for B_2 phase of 14OSOR is equal to 55 kJ/mol with bias voltage (Fig. 4.55. (a)), whereas for the process connected with reorientation around the long molecular axis it is of about 36.5 kJ/mol with and without bias voltage (Figs. 4.55. (a) and (b)).

Dispersion and absorption dependence on bias voltage measurements were done for B_2 phase of 12OSOR (in 100 ^oC), 12R9AF (in 95 ^oC) and 14OSOR (in 111.4 ^oC). Figs. 4.56. (a) and (b) show 3D graphs of dispersion and absorption vs. bias field for B_2 phase of 12OSOR. Figs. 4.57. present absorption spectrum for positive values of bias electric voltage: 10 and 20 V (a) and for negative values: -10 and -20 V ((b)). For positive as well as for negative voltages maximum of absorption for both processes rises. In the first case maximum of absorption for process connected with fluctuations of domains rises more than for reorientation around the long axes process. In the second case it is other way round.

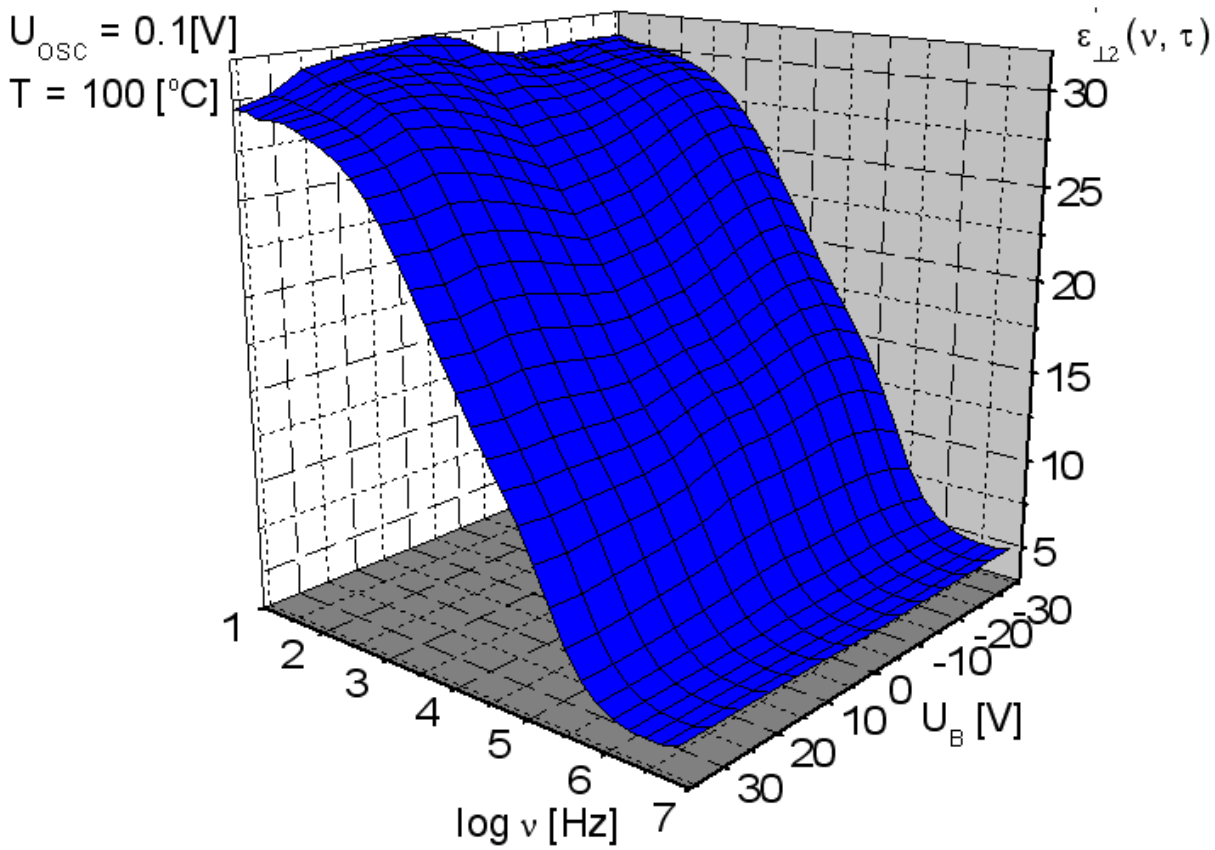

Fig. 4.56. (a) Influence of bias field on dispersion for B_2 phase of 12OSOR in the temperature of 100 ^oC

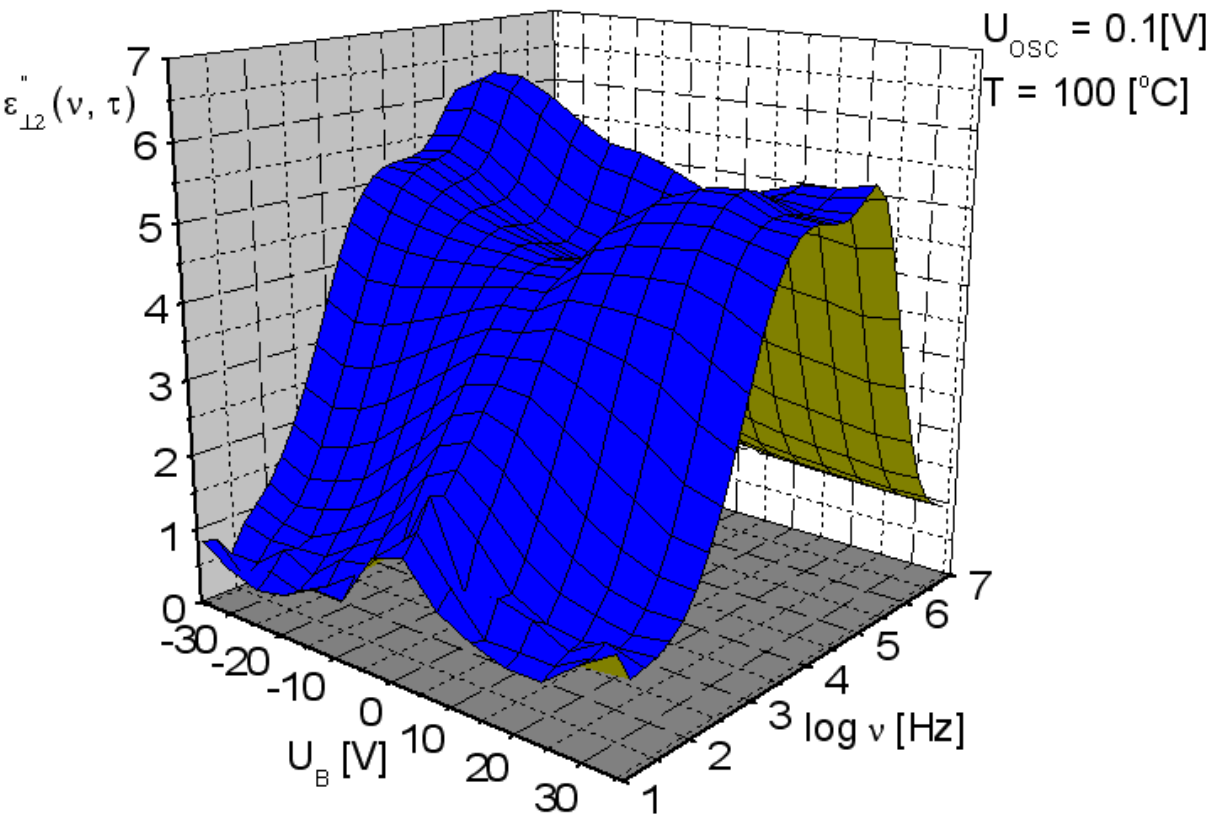

Fig. 4.56. (b) Influence of bias field on absorption for B_2 phase of 12OSOR in the temperature of 100 °C

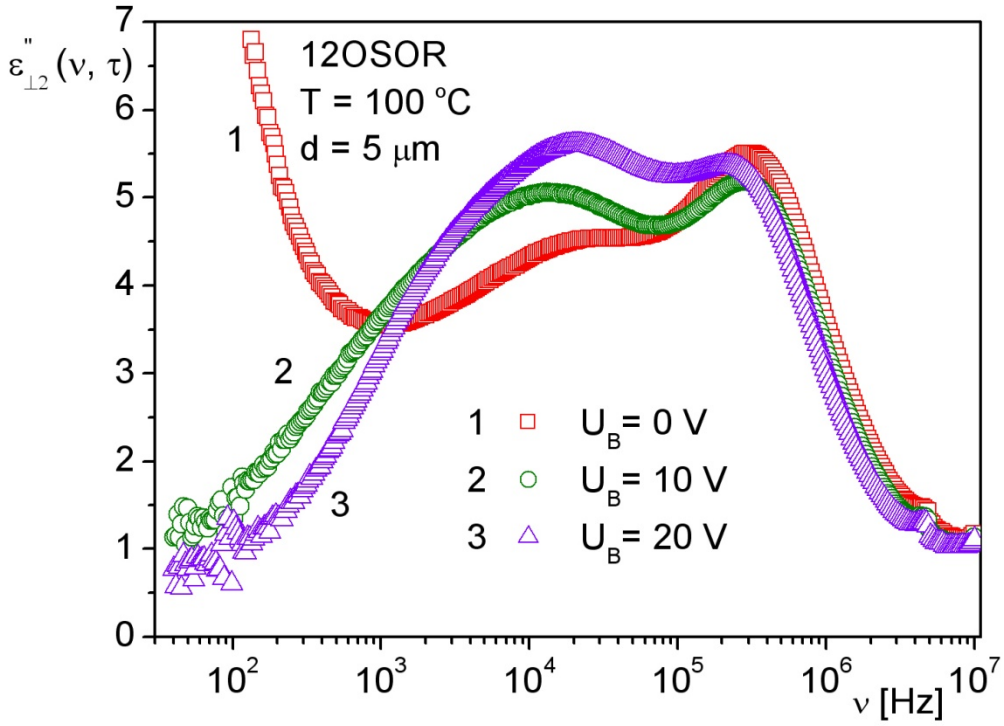

Fig. 4.57. (a) Bias field dependences of absorption spectrum measured for B_2 phase of 12OSOR for positive voltages in the temperature of 100 °C

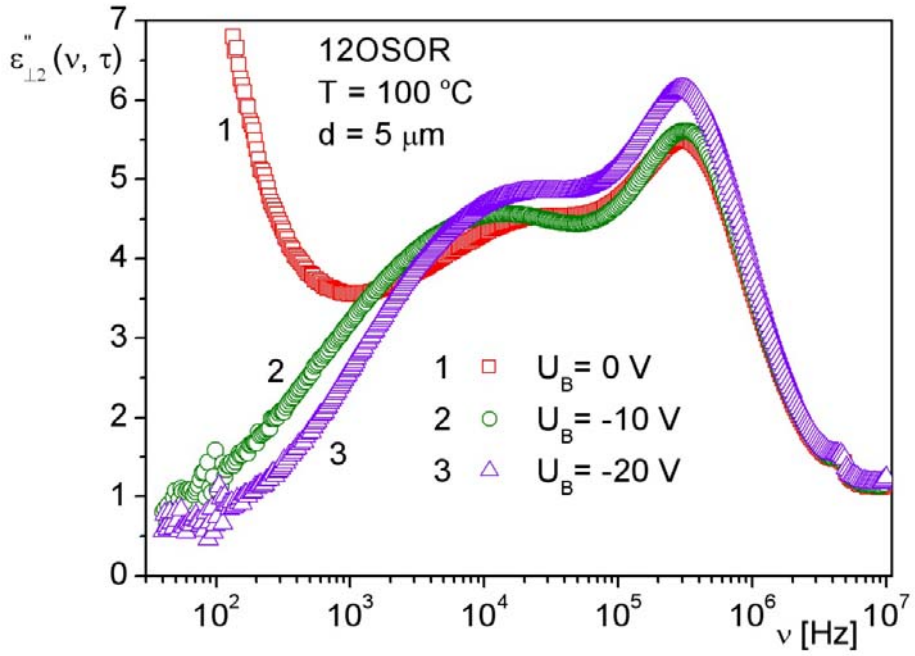

Fig. 4.57. (b) Bias field dependences of absorption spectrum measured for B_2 phase of 12OSOR for negative voltages in the temperature of 100 °C

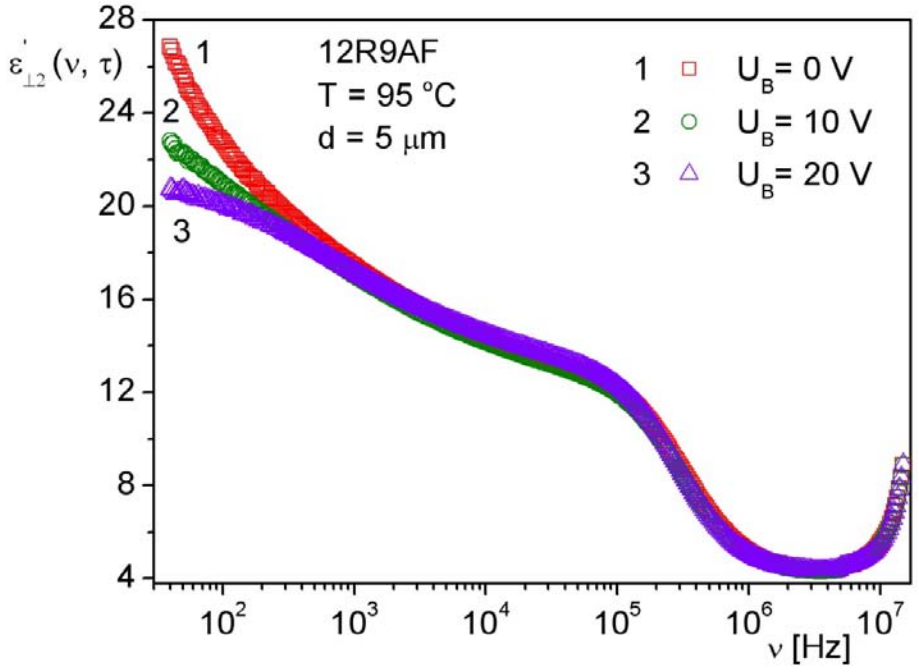

Fig. 4.58. (a) Bias field dependences of dispersion spectrum measured for B_2 phase of 12R9AF for positive voltages in the temperature of 95 °C

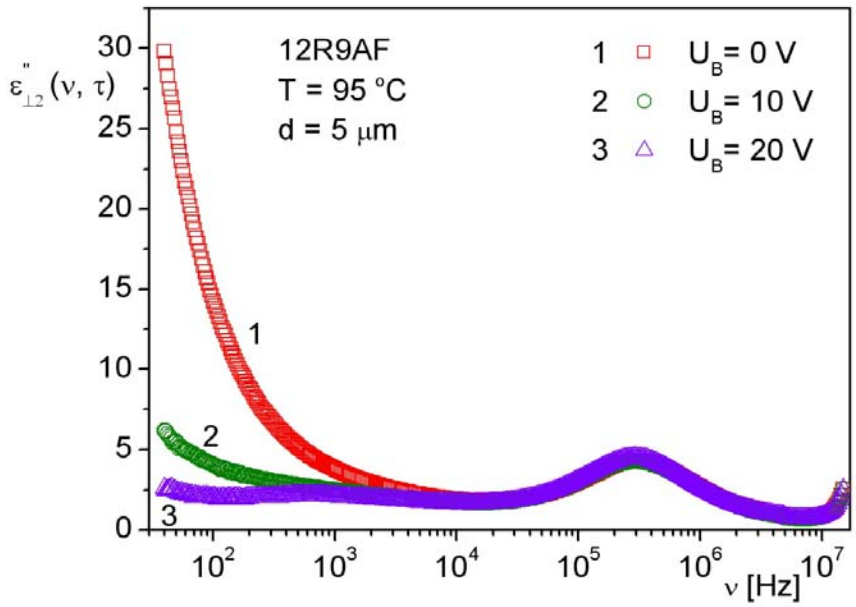

Fig. 4.58. (b) Bias field dependences of dispersion spectrum measured for B_2 phase of 12R9AF for positive voltages in the temperature of 95 °C

For B_2 phase of 12R9AF one can see from Figs. 4.58. only at low frequencies electrode polarization contribution to the dielectric permittivity (a) and the electrical ionic conductivity contribution to the dielectric loss (b) decreases with increase of the electric bias voltage.

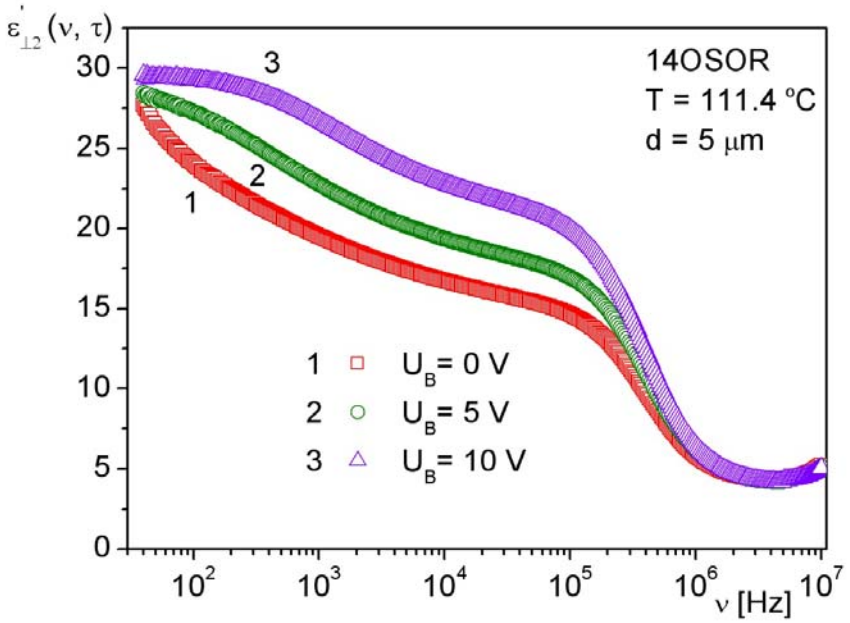

Fig. 4.59. (a) Bias field dependences of dispersion spectrum measured for B_2 phase of 14OSOR for positive voltages in the temperature of 111.4 °C

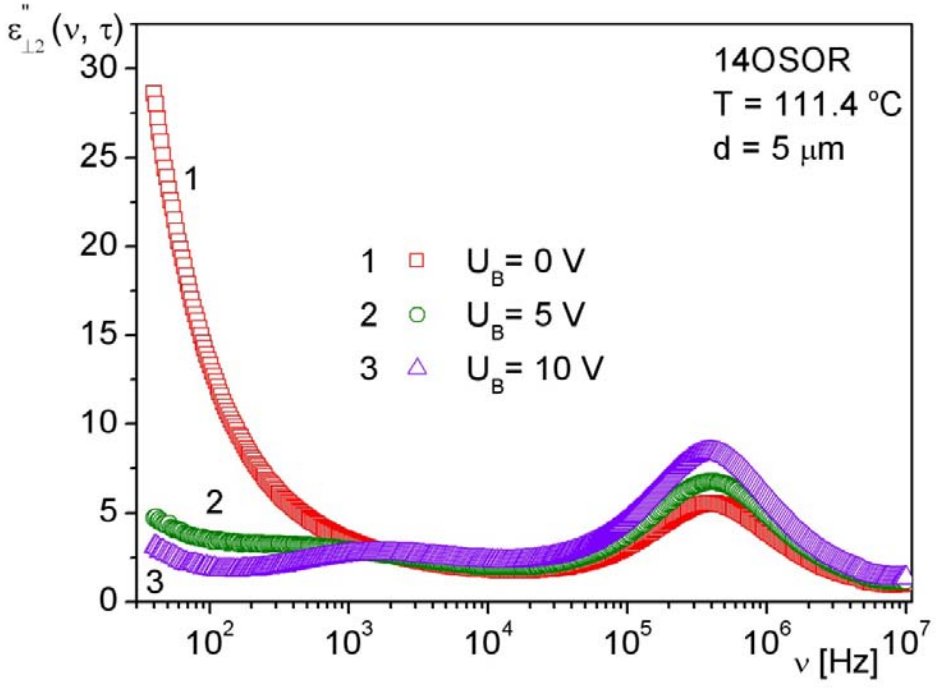

Fig. 4.59. (b) Bias field dependences of dispersion spectrum measured for B_2 phase of 14OSOR for positive voltages in the temperature of 111.4 ^oC

In 14OSOR compound dielectric dispersion and absorption are growing with electric bias voltage (Figs. 4.59 (a) and (b) but at low frequencies electrode polarization contribution to the dielectric permittivity (a) and the electrical ionic conductivity contribution to the dielectric loss (b) decreases with increase of the electric bias voltage.

4.5.2. Conductivity

Banana shaped thioesters studied in this work show distinctly lower conductivity in B_2 phase, than other similar compounds [28, 29, 30] studied up to now. Conductivity contribution to the dielectric spectrum of B_2 phase is complex and the M parameter shows a considerable difference between calamitic LCs and B phases.

Electric conductivity was calculated using A fitting parameter from 3.5 equation:

$$A = \frac{\sigma(\nu)}{(2\pi)^M}.$$

Figs. 4.60. – 4.63 show electric conductivity vs. temperature for 9OSOR, 12OSOR, 12R9AF and 14OSOR, respectively, measured in case when the electric bias field was turned off.

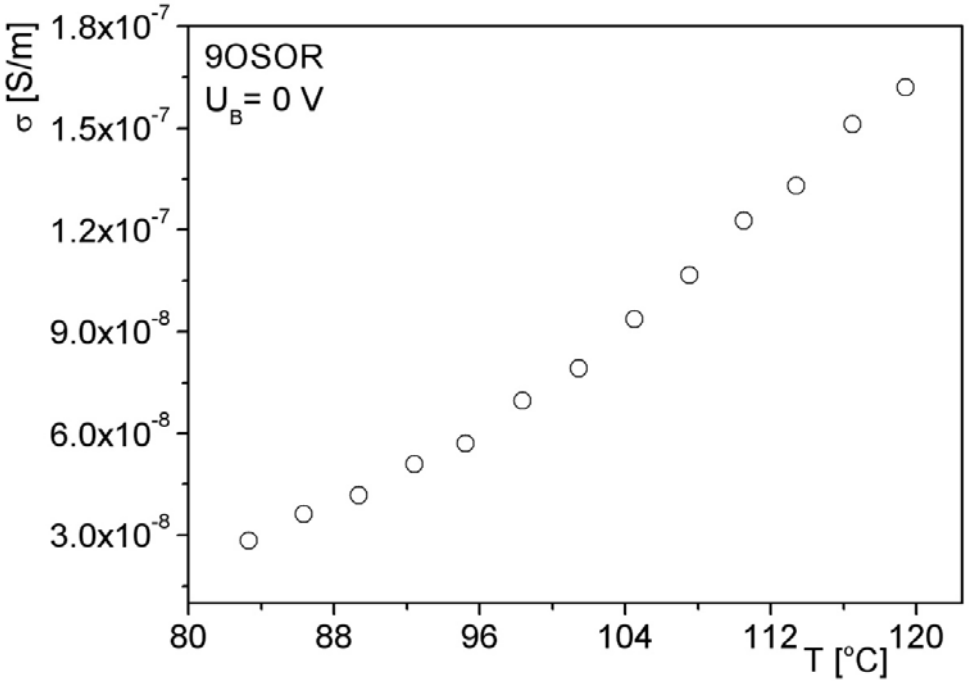

Fig. 4.60. Electric conductivity vs. temperature for B_1 phase of 9OSOR

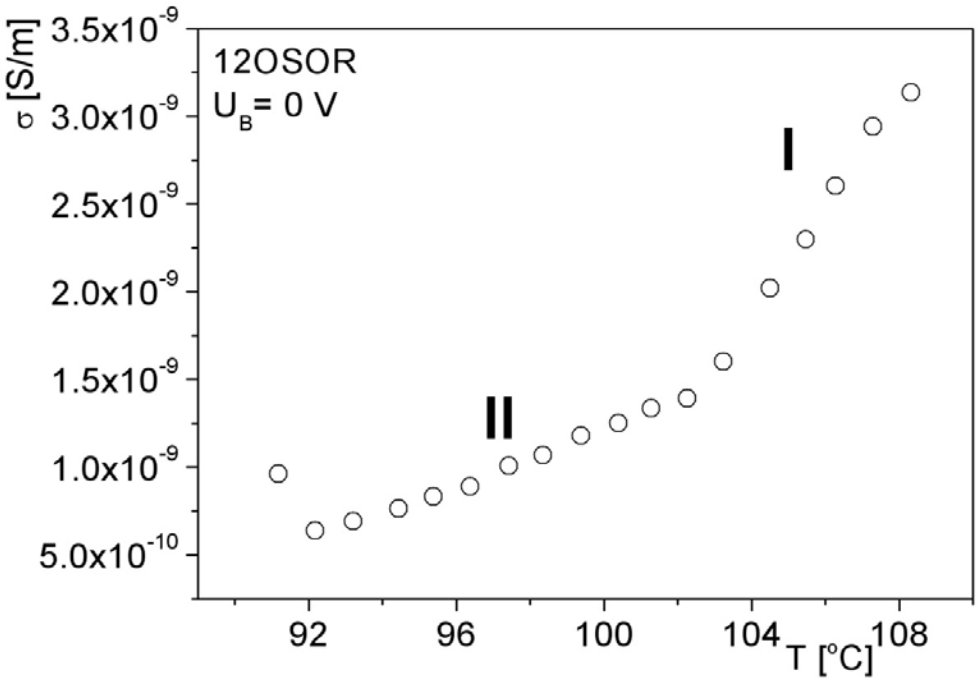

Fig. 4.61. Electric conductivity vs. temperature for B_2 phase of 12OSOR

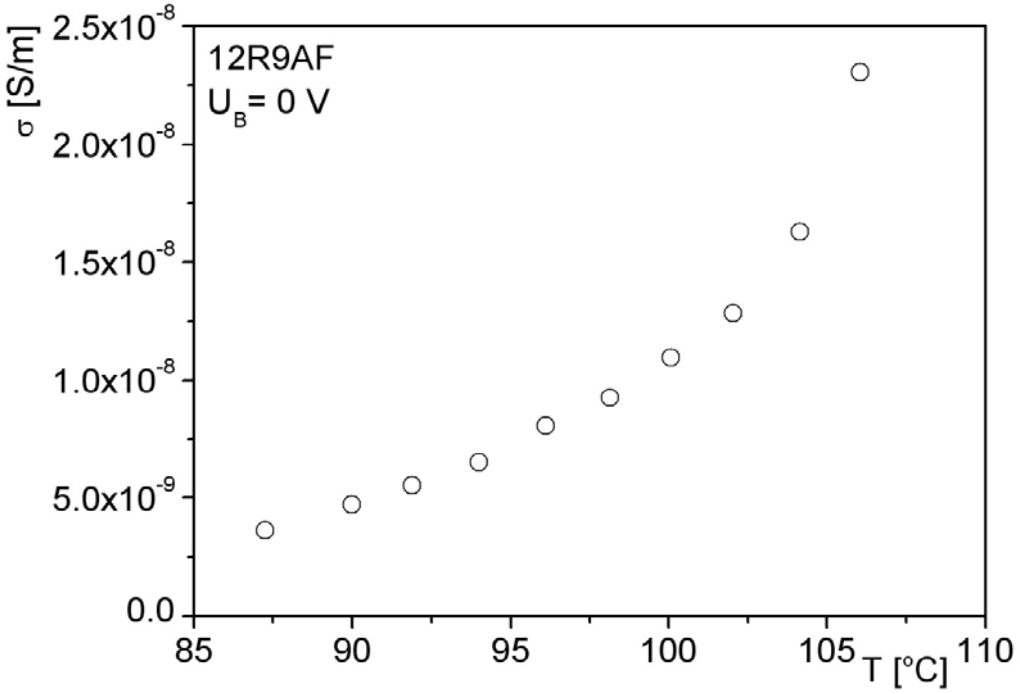

Fig. 4.62. Electric conductivity vs. temperature for B_2 phase of 12R9AF

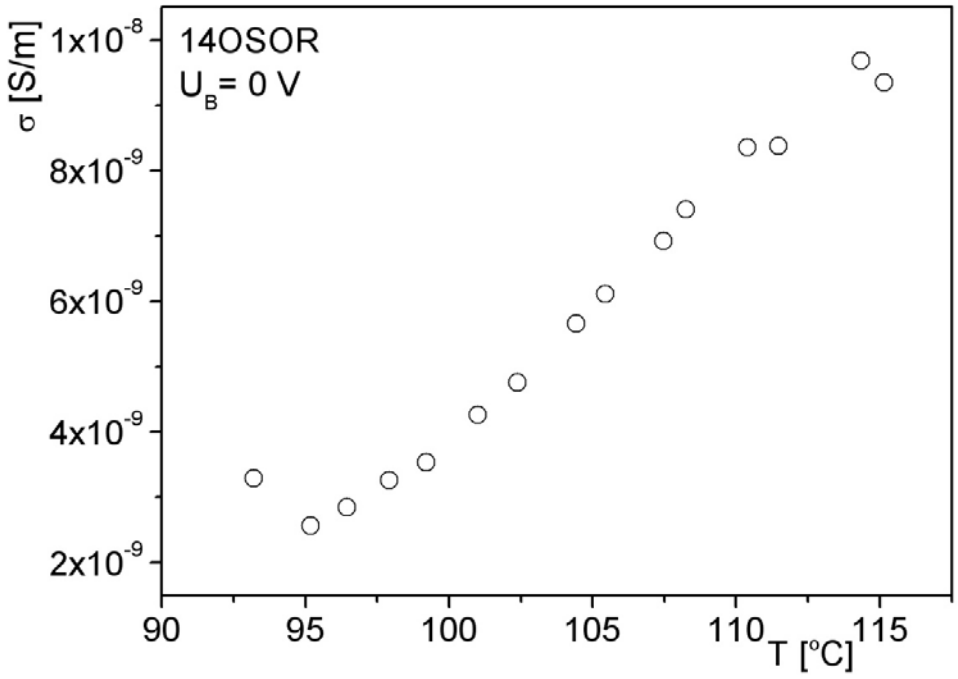

Fig. 4.63. Electric conductivity vs. temperature for B_2 phase of 14OSOR

For all materials electric conductivity increases with increasing temperature. In case of 12OSOR conductivity increases more for relaxation process connected with molecular reorientation around the short axes, than for molecular reorientation around the long axes.

5. Conclusions

The aim of present PhD Thesis was to investigate the electrooptic and dielectric properties and conductivity of B phases of banana-shaped homologues 9OSOR, 12OSOR, 14OSOR and a mixture 12R9AF.

DSC measurements and texture observations allowed to determine the transition temperatures and to identify phases appearing in materials investigated. 9OSOR compound shows banana-shaped ferroelectric B_1 phase, however 12OSOR, 14OSOR and 12R9AF mixture show antiferroelectric B_2 phase. Using thin AWAT cells with ITO electrodes it was possible to observe electro-optic switching between quasi-planar and quasi-homeotropic textures for B_2 phase of 12OSOR compound.

Spontaneous polarization measurements confirmed, that the B_1 phase of 9OSOR is a ferroelectric one – one broad peak was observed – and B_2 phase of 12OSOR, 12R9AF and 14OSOR is an antiferroelectric one – two well separated peaks were observed as a response current. Polarization for phase B_1 of 9OSOR is rather small and it's temperature dependence is unusual for ferroelectric liquid crystals – it increases with temperature. For B_2 phase of 12OSOR spontaneous polarization is very high, it is close to 600 nC/cm^2, it is larger than for 14OSOR (about 550 nC/cm^2) and for 12R9AF (about 500 nC/cm^2). The B_2 phase of 12R9AF is shifted to lower temperatures by about 10 ^{o}C in comparison to the pure compound.

The dielectric spectra measured for B_1 phase of 9OSOR with and without bias voltage showed only one dielectric relaxation process connected with molecular reorientation around the short axis. However, for B_2 phase of 12OSOR, 12R9AF and 14OSOR the dielectric spectra measured with bias voltage show two well separated relaxation processes. In low frequency range the relaxation process is connected with fluctuations of domains. In high frequency range – it is connected with reorientation around the long axis and it is also observed without bias field. For 12OSOR the dielectric relaxation process observed without bias field is complex: in the high temperature range of B_2 phase it is connected with molecular reorientation around the short molecular axis, whereas in the low temperature range – around the long axis.

Dielectric measurements showed also that at low frequencies there is an electrode polarization contribution to the dielectric permittivity and the electrical ionic conductivity contribution to the dielectric loss for all materials studied. The electric conductivity of these

banana-shaped thioesters is distinctly lower than for other similar compounds. The M parameter for all materials studied shows the difference between calamitic LCs and B phases.

6. Bibliography

[1]. D. Demus, J. W. Goodby, G. W. Gray, H.W. Spiess, V. Vill, *Handbook of Liquid Crystals,* Wiley-VCH, Verlag GmbH, Germany 1998

[2]. T. Noiri, T. Sekine, J. Watanabe, T. Furukawa and H. Takezoe, *J. Mater. Chem.*, **6,** 1231 (1996)

[3]. T. Sekine, Y. Takanishi, T. Noiri, J. Watanabe and H. Takezoe: *Jpn. J. Appl. Phys*. **36**, L1201 (1997)

[4]. L. Longa, G. Pająk and T. Wydro, *Phys. Rev. E*, **79**, 040701 (2009)

[5]. J. Dierking*, Textures of Liquid Crystals*, Wiley-VCH, Verlag GmbH & co. KGaA, Germany 2003, section 11.4.: *Bent-core Mesogens, "Banana" Liquid Crystal Phases*

[6]. J. Ortega, M. R. De la Fuente, J. Etxebarria, C. L. Folcia, S. Díez, J. A. Gallastegui, N. Gimeno, M. B. Ros and M. A. Pérez-Jubindo, *Phys. Rev. E*, **69**, 011703 (2004)

[7]. E. Górecka, D. Pociecha, section: „Polar mesophases formed by achiral bent-core materials", Edits.: W. Kuczyński, *Chiral Liquid Crystals*, Institute of Molecular Physics, Polish Academy of Sciences, Poznań 2005,

[8]. E. Górecka, D. Pociecha, J. Matraszek, J. Mieczkowski, Y. Shimbo, Y. Takanishi, H. Takezoe, *Phys. Rev. E,* **73**, 031704 (2006)

[9]. J.C. Rouillon, J.P. Marcerou, M. Laguerre, H.T. Nguyen, M.F. Achard, *J. Mater. Chem*., **11**, 2946 (2001)

[10]. P. Grzybowski, L. Longa, *Stability of Biaxial Nematic Phase in Model Bent-Core Systems*, presented at the International Symposium on Biaxial Nematic Liquid Crystals, Ohio, USA (2008)

[11]. Piotr Grzybowski, *PhD Thesis*, Jagiellonian University, Cracow (2008)

[12]. N. Vaupotič, *Ferroelectrics* **344**, 151 (2006)

[13]. Z. Vakhovskaya, W. Weissflog, R. Friedemann and H. Kresse, *Phase Transitions*, **80**, 705 (2007)

[14]. R. A. Reddy and C. Tschierske, *J. Mater. Chem.*, **16**, 907 (2006)

[15]. J. M. Janik, *Fizyka chemiczna*, PWN, Warszawa 1989

[16]. S. Urban, *Fizyczne metody badań w biologii, medycynie i ochronie środowiska*, section 10: „Spektroskopia dielektryczna", Edits.: A. Z. Hrynkiewicz, E. Rokita, PWN, Warszawa 1999

[17]. Marta Wierzejska, *Master's Thesis*, Jagiellonian University, Cracow (2006)

[18]. H. Kresse, *Relaxation Phenomena*, section 5.7.: „Dielectric behavior of phases formed by bent-shaped molecules", Edits.: W. Haase, S. Wróbel, Springer-Verlag Berlin Heidelberg, Germany 2003

[19]. W. Witko, *Komplementarne metody badań przemian fazowych*, section 10: „Mikroskopia polaryzacyjna", Edits.: E. Mikuli, A. Migdał - Mikuli, Wydawnictwo UJ, Kraków 2006

[20]. http://www.microscopyu.com/articles/polarized/polarizedintro.html

[21]. A. Adamczyk, Z. Strugalski, *Ciekłe kryształy*, WNT, Warszawa 1976.

[22]. H. Takezoe, „*Characterization of ferroelectric liquid crystals by different physical method*", w: Tutorials of 7th International Conference on Ferroelectric Liquid Crystals, Darmstadt 1999

[23]. A. Fąfara, *PhD Thesis*, Jagiellonian University, Cracow (2001)

[24]. M. Marzec, *PhD Thesis*, Jagiellonian University, Cracow (1997)

[25]. S.Wróbel, M.Marzec, *Komplementarne metody badań przemian fazowych*, section 2: „Różnicowa kalorymetria skaningowa", Edits.: E. Mikuli, A. Migdał - Mikuli, Wydawnictwo UJ, Kraków 2006

[26]. D. M. Ossowska-Chruściel, K. Kudłacz, A. Sikorska, J. Chruściel, M. Marzec, A. Mikułko, S. Wróbel, R. Douali and Ch. Legrand, *Phase Transit*. **80,** 781 (2007)

[27]. D. M. Ossowska-Chruściel, M. Wierzejska-Adamowicz, M. Marzec, A. Mikułko, R. Douali, Ch. Legrand, J. Chruściel, A. Sikorska and S. Wróbel, *Phase Transit.*, **82**, 889 (2009)

[28]. H. Schmalfuss, D. Shen, C. Tschierske and H. Kresse, *Liq. Crystals*, **26**, 1767 (1999)

[29]. G. Pelzl, S. Diele, S. Grande, A. Jakli, Ch. Lischka, H. Kresse, H. Schmalfuss, I. Wirth and W. Weissflog, *Liq. Crystals*, **26**, 401 (1999)

[30]. S. Wróbel, W. Haase, D. Kilian, L.-C .Chien and L. Chong-Kwang, *Ferroelectrics*, **243**, 277 (2000)

Appendix A: Publications

1. A. Mikułko, M. Marzec, M. Wierzejska, R. Douali, Ch. Legrand, S. Wróbel, R. Dąbrowski, W. Haase, *Phase Transition*, **79**, 585 (2006)

2. A. Mikułko, M. Wierzejska, M. Marzec, S. Wróbel, J. Przedmojski, W. Haase, *Mol. Cryst. Liq. Cryst.*, **477**, 185 (2007)

3. D. M. Ossowska-Chruściel, M. Wierzejska-Adamowicz, M. Marzec, A. Mikułko, R. Douali, Ch. Legrand, J. Chruściel, A. Sikorska and S. Wróbel, *Phase Transit.*, **82**, 889 (2009)

4. M. Wierzejska-Adamowicz, D. M. Ossowska-Chruściel, J. Chruściel, R. Douali, Ch. Legrand, M. Marzec, A. Mikułko, A. Sikorska and S. Wróbel, *Acta Physica Polonica A*, **117**, 333 (2010)

5. M. Wierzejska-Adamowicz, D. M. Ossowska-Chruściel, J. Czerwiec, R. Douali, Ch. Legrand, J. Chruściel, M. Marzec and S. Wróbel, *"Bias Field Influence on Dielectric Spectra of B Phases of Bent-Core Thioesters"*, submitted to *Opto-Electronic Review*

Appendix B: Conferences

1. V Katowicko - Krakowskie Seminarium Fazy Skondensowanej, 19-20 May 2006, Rychwałd, Poland, oral presentation: *„Badania elektrooptyczne własności substancji chiralnej z fazą de Vriesa”*

2. Polish - Czech Seminar, 22-26 May 2006, Znojmo, Czech Republic, poster A23: *„Highly ordered hexatic phases with large spontaneous polarization”*, A. Mikułko, M. Marzec, M. Wierzejska, R. Douali, Ch. Legrand, S. Wróbel, R. Dąbrowski, W. Haase, J. Przedmojski

3. 21st International Liquid Crystal Conference, 2-7 July 2006, Keystone, Colorado, poster: *„Ferroelectricity of hexatic phases”* S. Wróbel, A. Mikułko, M.Marzec, M. Wierzejska, J. Przedmojski, W. Haase

4. VI Katowicko - Krakowskie Seminarium Fazy Skondensowanej, 18-20 May 2007, Zakopane, Poland, oral presentation: *„Elektrooptyczne właściwości ciekłego kryształu 12OSOR o molekułach bananopodobnych”*

5. XVII Conference on Liquid Crystals – Chemistry, Physics and Applications, 17-22 September 2007, Augustów, Poland, poster: *“Planar-Homeotropic Transition Observed for B_2 Phase of Banana-Shaped Thioester”*, D. M. Ossowska-Chruściel, M. Wierzejska, M. Marzec, A. Mikułko, R. Douali, Ch. Legrand, J. Chruściel, S. Wróbel

6. VII Katowicko - Krakowskie Seminarium Fazy Skondensowanej, 16-17 June 2008 Rychwałd, Poland, oral presentation: *„Badania elektrooptyczne faz typu B w szeregu homologicznym nOSOR bananopodobnych tioestrów”*

7. 22nd International Liquid Crystal Conference, 29 June – 04 July 2008, Jeju, Korea, poster: *„Influence of Bias Field on Dielectric Spectra and Textures of Banana-shaped Thioester's B_2 Phase"* M. Wierzejska, M. Marzec, A. Mikułko, S. Wróbel, D. M. Ossowska-Chruściel, J. Chruściel, R. Douali, and Ch. Legrand

8. IX Polish – Ukrainian Meeting and XXIX International School on Ferroelectric Physics, 14-18 September 2008, Kraków, Poland, poster: *„Investigations of Antiferroelectric B_2 Phase Composed of Bent-Core Molecules"*, M. Wierzejska-Adamowicz, D. M. Ossowska-Chruściel, M. Marzec, A. Mikułko, J. Chruściel, R. Douali, Ch. Legrand and S. Wróbel

9. 10th European Conference on Liquid Crystals, 19-24 April 2009, Colmar, France, poster: "*Frustrated B_1 and antiferroelectric B_2 phases of bent-core thioesters studied by electro - optic methods"*, M. Wierzejska-Adamowicz, D. M. Ossowska-Chruściel, M. Marzec, A. Mikułko, J. Chruściel, R. Douali, Ch. Legrand and S. Wróbel

10. VIII Katowicko - Krakowskie Seminarium Fazy Skondensowanej, 8 maj 2009 Kraków, Poland, poster: *„Badania elektrooptyczne sfrustrowanej fazy typu B_1 i antyferroelektrycznej fazy typu B_2 bananopodobnych tioestrów"*, M. Wierzejska-Adamowicz, D. M. Ossowska-Chruściel, M. Marzec, A. Mikułko, J. Chruściel, R. Douali, Ch. Legrand and S. Wróbel

11. VI Ogólnopolska Konferencja "Rozpraszanie neutronów i metody komplementarne w badaniach faz skondensowanych", 14-18 June 2009, Chlewiska, Poland, oral presentation: *„Badania elektrooptyczne i dielektryczne sfrustrowanej fazy B_1 i antyferroelektrycznych faz B_2 banano-podobnych tioestrów"*

12. XVIII Conference on Liquid Crystals – Chemistry, Physics and Applications, 14-18 September 2009, Augustów, Poland, poster: *„Bias field influence on dielectric spectra of B phases of bent-core thioesters"*, M. Wierzejska-Adamowicz, D. M. Ossowska-Chruściel, M. Marzec, A. Mikułko, J. Chruściel, R. Douali, Ch. Legrand and S. Wróbel

13. 23rd International Liquid Crystal Conference, 11-16 July 2010, Kraków, Poland, poster: *„Textures, dielectric and electrooptic measurements of B phases of nOSOR compounds and 12R9AF mixture”*, M. Wierzejska-Adamowicz, D. M. Ossowska-Chruściel, M. Marzec, A. Mikułko, J. Chruściel, R. Douali, Ch. Legrand and S. Wróbel